UNIVERSITÀ DEGLI STUDI DI TRIESTE

XXVI Ciclo del Dottorato di Ricerca in Ingegneria dell'Informazione

TITRATION OF HIGH FREQUENCY PERCUSSIVE VENTILATION BY MEANS OF REAL-TIME MONITORING OF THE VISCOELASTIC RESPIRATORY SYSTEM PROPERTIES AND ENDOTRACHEAL TUBES PRESSURE DROP

Settore scientifico-disciplinare: ING-INF/06

DOTTORANDO
UMBERTO LUCANGELO

RESPONSABILE DOTTORATO DI RICERCA
CHIAR.MO PROF. WALTER UKOVICH
(UNIVERSITA' DEGLI STUDI DI TRIESTE)

SUPERVISORE
CHIAR.MO PROF. AGOSTINO ACCARDO
(UNIVERSITA' DEGLI STUDI DI TRIESTE)

ANNO ACCADEMICO 2012 / 2013

Alla mia famiglia senza la quale

nulla avrei potuto

e

alla Vita che

ha voluto concedermi

il privilegio della "Cura".

Index

Introduction

The use of High Frequency Percussive Ventilation (HFPV) is still debated although this type of non-conventional ventilation has proven effective and safe in patients with acute respiratory failure.

In the clinical practice, HFPV is not an intuitive ventilatory modality and the absence of real-time delivered volume monitoring produces disaffection among the physicians.

Avoiding the "volutrauma" is the cornerstone of the "protective ventilation strategy", which assumes a constant monitoring of inspiratory volume delivered to the patient. Currently the system capable of delivering HFPV is the VDR-4® (Volumetric Diffusive Respirator), which provides only analog airway pressure waveform and digital output of peak and the mean airway pressure. The latter is involved in the determination of oxygenation and hemodynamics, irrespective of the mode of ventilation. At the present time, the mean airway pressure, together with gas exchange analysis, are the only parameters that indirectly guide the physician in assessing the clinical effectiveness of HFPV. Till now, flow, volume and pressure curves generated by HFPV have never been studied in relation to the specific patients respiratory mechanics. The real-time examination of these parameters could allow the physicians to analyze and understand elements of respiratory system mechanics as compliance (Crs), resistance (Rrs), inertance (Irs) and of patient-ventilator interaction. The mechanical effects are complex and result from interactions between ventilator settings and patient's respiratory system impedance.

The aim of this doctoral thesis was to acquire and study volume and respiratory parameters during HFPV in order to explain this complex patients-machine interaction and transfer the results in clinical practice.

The first chapter defines the circuit and the basic principles of operation of the HFPV. It also describes the main theories of gas transportation under conditions of high frequency ventilation and the main clinical applications.

In the second chapter are described *in vitro* studies that characterize the intrinsic properties of HFPV at different mechanical loads. Moreover, these studies faithfully

describes the effect of load on the relationship between convective and diffusive volume delivery, representing the link from bench to a new bedside HFPV use.

A proper acquisition system for measurement of pressure, flow and volume during this particular ventilation strategy was developed and reported in third chapter. The suitable approaches for estimation of respiratory system compliance, resistance, inertance and endotracheal tube pressure drop were identified and proposed.

In vivo measurements and the main results of this study are reported in Chapter 4.

In Chapter 5 the results and interpretation of "mini recruitment maneuver" by means of pressure–volume curve model are discussed.

Finally, in Chapter 6 a decision support algorithm for the optimization of HFPV treatment, in severe hypoxemic patient, is proposed.

Chapter 1 – High Frequency Percussive Ventilation

The high-frequency percussive ventilation (High Frequency Percussive Ventilation, HFPV) is a ventilatory mode introduced in the early 80's by FM Bird and initially used for the treatment of patients with acute respiratory failure secondary to pulmonary injury from smoke inhalation and burns patients [1-7]. The introduction into clinical practice of high frequency ventilation dates back to the early seventies [8-12]. To date, there are many theories used to explain the transport of gas during this particular method of ventilation, although none of them, individually, is sufficiently explanatory [13-16].

The first proposal concerns the theory of direct alveolar ventilation, also known as bulk gas flow. This is the simplest example of alveolar ventilation, observable during spontaneous breathing and CMV. This mechanism seems to play a predominant role during HFPV.

The second theory concerns the facilitated diffusion. It suggests that the high frequency pulsations increase the kinetic energy of the oxygen molecules, promoting the diffusion of oxygen through the alveolar-capillary membrane.

The third hypothesis is commonly referred to as the Taylor dispersion that describes the dispersion that occurs with laminar and turbulent flows in an experimental model. In the presence of a turbulent flow, the formation of vortices occurs, resulting in an increase of the mixing of gases between the proximal and more peripheral airways. It has also been suggested that gas exchange occurs in the epithelium of the airways. In laminar flow conditions, using high-frequency oscillatory ventilation (HFO), the cyclic movement of the piston creates acceleration and deceleration phenomena. The return movement of the piston does not affect the inertia of the molecules that are moving to the periphery with a given axial velocity; consequently, the molecules continue to maintain their direction towards the periphery (out of phase respect to the piston), increasing the exchange of gases even in the presence of small tidal volumes.

The fourth theory relates to the asymmetric profiles of velocity. During HFPV ventilation, the inspiratory flow occupies the central part of the airways, while the expiratory moves along the peripheral zones. The result is the simultaneous movement of the inspiratory and expiratory flows.

The fifth mechanism specifically concerns the HFO and involves the exchange of gases between alveolar units with different time constants. During HFO ventilation, lung volume remains relatively constant. If the lung volume is maintained above the critical pressure of the alveolar opening, the distribution of the gas that is obtained is more homogeneous: this leads to a reduction of the risk of hyperinflation in high-compliance regions and of atelectasis in those of low-compliance. The increase of gas exchange is the result of a greater homogeneity of the lung due to a better ventilation/perfusion ratio and relative reduction of the shunt [17].

The last proposed theory regards the increase of the ventilation through the Kohn's pores and Lambert's channels, even if the amount of gas exchange between contiguous units remains unknown.

Among the many controversial aspects regarding high-frequency ventilation (HFV), one of these is the lack of a universally accepted classification and a precise nomenclature [18]. Depending on the frequencies used, we can distinguish:

• HFJV: high frequency jet ventilation,

• HFFI: high frequency flow interruption (variant of the previous),

• HFO: high frequency oscillation (60-2400 cycles/min),

• HFPPV: high frequency positive pressure ventilation (60-300 cycles/min).

Notwithstanding this premise, from technical point of view all modes of high frequency ventilation share at least three essential elements [19,20]:

• a generator of high pressure flow,

• a valve of interruption of flow,

• the connection circuit to the patient.

The HFPV can be defined as pneumatically powered, flow regulated and time cycled ventilation that determines a controlled pressure and delivers a combination of high-frequency subtidal volumes with low frequency breathing cycles.

The only system capable of delivering HFPV is the VDR-4® (Volumetric Diffusive Respirator), a pressure controlled and time cycled ventilator, provided with an high

frequency flow generator and associated with a device (phasitron) which represents the interface between the patient and the machine [20-22].

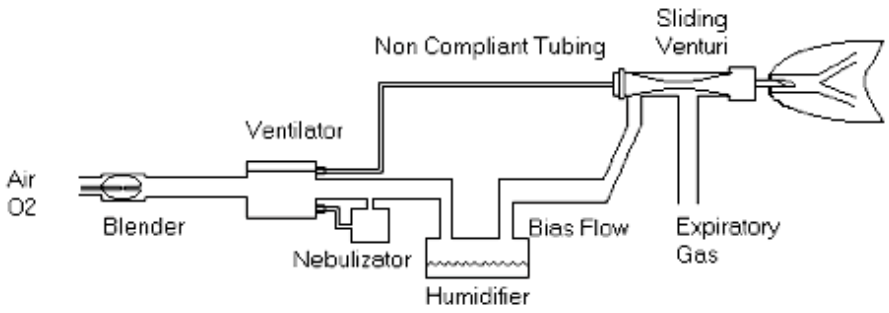

Figure 1.1 Schematic diagram of HFPV system. The high frequency circuit consists of non-compliant tubing while the low pressure circuit has a nebulizator and humidifier connected downstream from one another [22].

The ventilator is connected to a high-pressure pneumatic generator, powered by two normal sources of oxygen and air. From the ventilator two inspiratory circuits originate, a high-pressure and the other at low pressure; the low-pressure circuit is connected to the active humidification system and to nebulization. The two circuits are connected to the phasitron, which also includes the expiratory circuit. The phasitron is also equipped with a system for recording and real-time displaying the pressure delivered to the patient that is measured distal to the source of pulsatile high-pressure flow, which is located nearby the connection with the endotracheal tube.

The nebulization system is connected to a reservoir and served by an accessory line, which delivers a high-pressure flow synchronized with that connected to the phasitron.

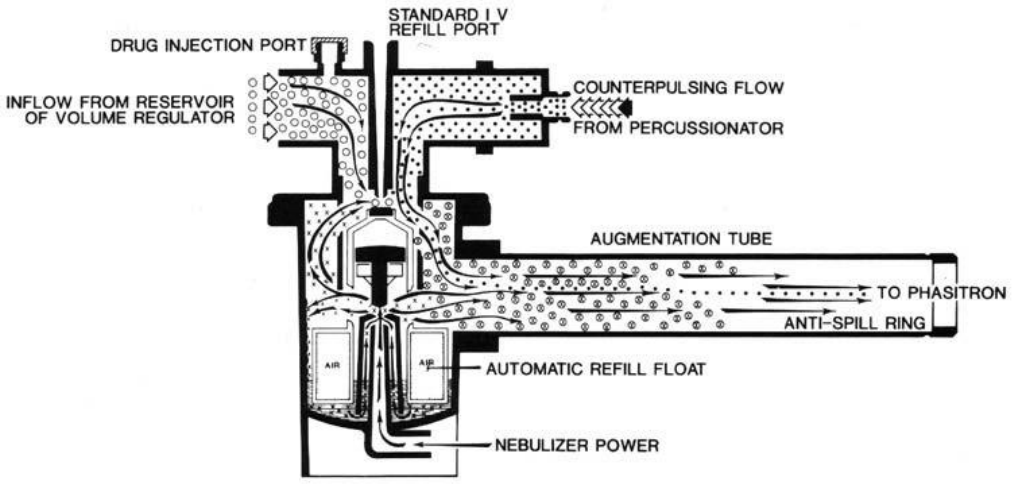

Figure 1.2 Nebulization system. Drug injection port: system for the delivery of drugs; Standard IV refill port: accessory line; Inflow from reservoir of regulators: connection to the reservoir; Counterpulsing flow from Percussionator: flow from the ventilator; Augmentation tube: low-pressure inspiratory flow; Automatic refill float: drugs containing reservoir; Nebulizer Power: accessory line (from FM Bird).

This system allows the administration as nebulized aerosol of bronchodilators and mucolytics, to reduce the forces of cohesion and adhesion of secretions and thus contributing to a more effective removal of secretions themselves. Together with the humidification system, the action of the nebulization system allows to provide to the inspiratory circuit a gaseous mixture heated with 100% humidity.

The phasitron is a device that consists of a cylinder, within which the airflow from the high-pressure circuit imparts a movement of "coming and going" to a coaxial piston, provided with a spring. According to the Venturi principle, the inspiratory circuit connected to the low-pressure humidification systems and the nebulizer contributes to the administration of the tidal volume with a value inversely proportional to the pressure reached at the respiratory airways. When the desired pressure level is approaching, the quote of air supplied is derived almost exclusively from the high-pressure circuit.

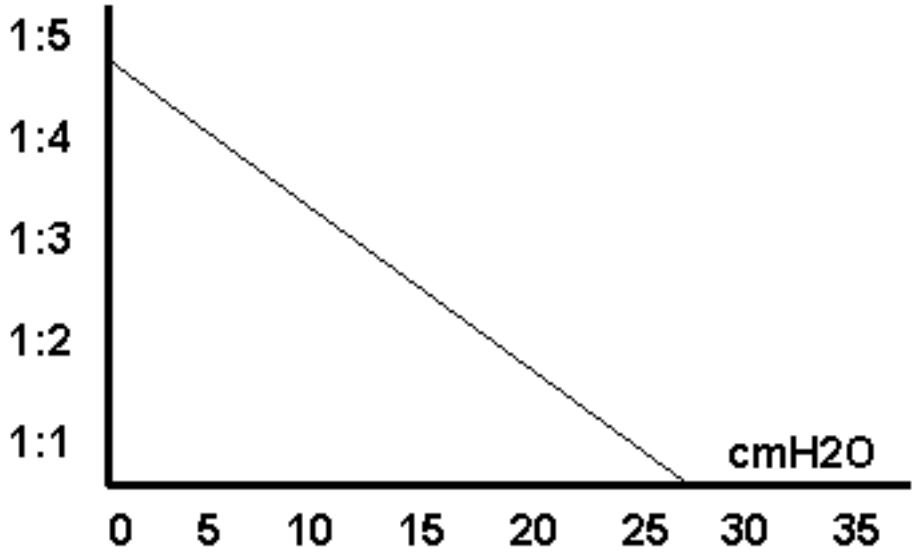

Figure 1.3 Relationship between the proportions of air coming from the high pressure and low-pressure systems (ordinate) and the airways pressure (abscissa). The increase of the latter corresponds to a reduction of the proportions of air coming from the high and low-pressure circuits. Once the set value is reached (40 cmH_2O), the plateau pressure is maintained mainly by the pulsatile system, which draws poorly by low-pressure circuit (from FM Bird).

The phasitron is equipped with two safety valves (an inspiratory and an expiratory), which allow to maintain the preset pressure; a third security expiratory valve is connected to the reservoir. Thus, the circuit is permanently open to the air and allows the patient to trigger during the entire ventilatory cycle, without adding supplementary pressure loads.

It is essential to highlight that the same circuit can either be applied both in neonatal and pediatric as in adult patients.

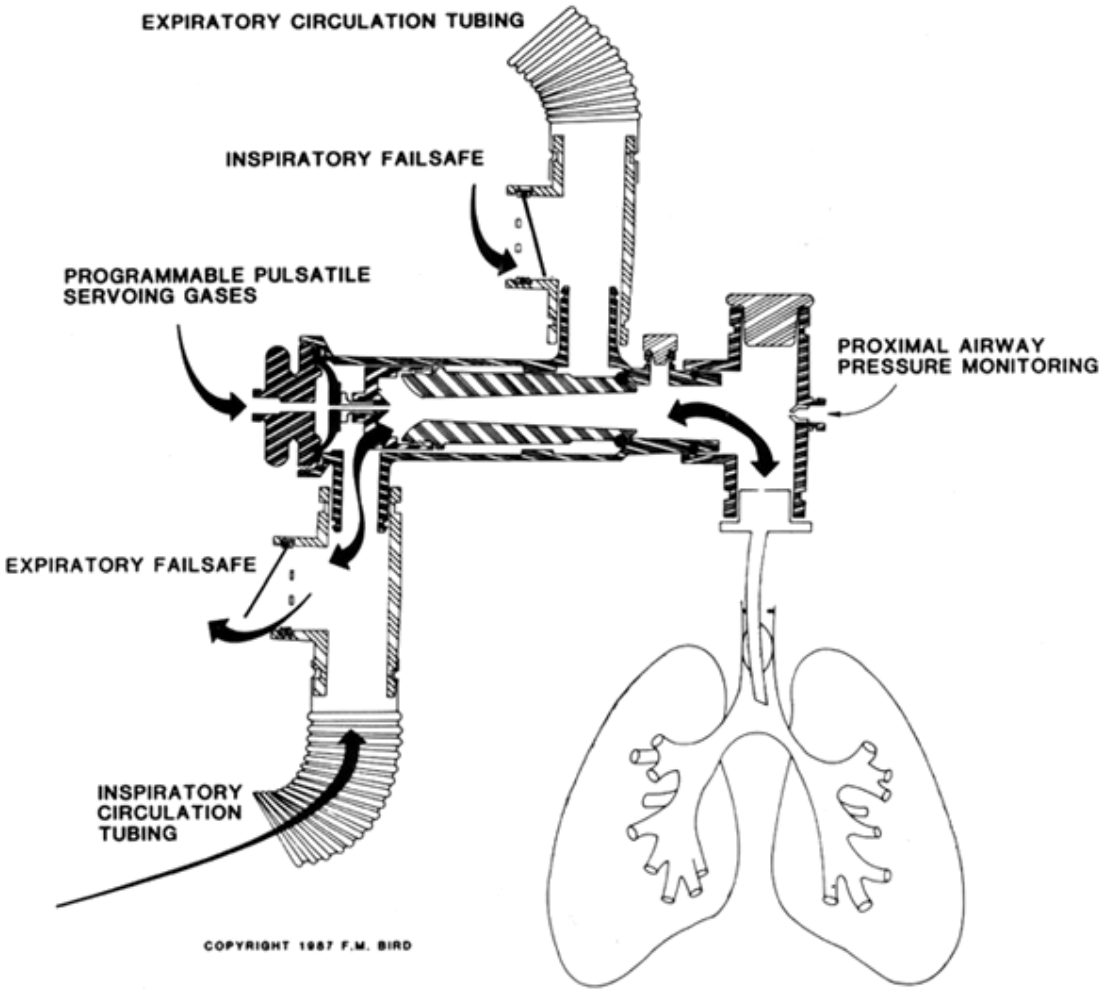

Figure 1.4 HFPV circuit. Programmable pulsatile servoing gases: inspiratory high-pressure circuit; Inspiratory circulation tubing: low-pressure inspiratory circuit, Inspiratory/Expiratory failsafe: inspiratory/expiratory safety valves; Proximal airway pressure monitoring: system for monitoring airway pressure (from FM Bird).

The Volumetric Diffusive Respirator allows to adjust:

• the flow ratio delivered, which generates the desired working pressure,

• inspiratory "I" and expiratory "E" times,

• the positive end-expiratory pressure "PEEP", linear rather than oscillatory,

• the percussion frequency.

Should there be an additional convective contribution, this can be administered in tele-inspiratory phase as an additional quota of oscillatory flow, which results in an increase of the pressure load.

Figure 1.5 VDR-4® ventilator (from FM Bird).

By acting on the inspiratory and expiratory times, it is possible to determine a respiratory rate equal to the conventional mechanical ventilation. Every breath is the result of an act of CMV with superimposed micro-volumes delivered at high frequency. These originate from the high-pressure inspiratory circuit and their progressive accumulation, with the portion of heated and humidified flow coming from the low-pressure system, allows to reach the desired pressure.

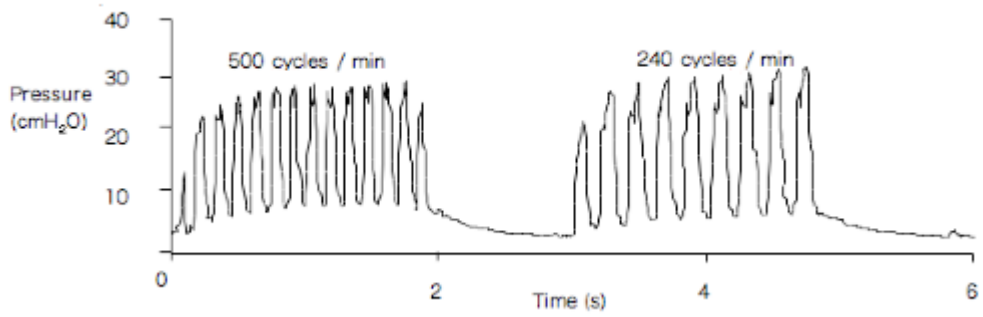

Figure 1.6 Pressure curves during HFPV with inspiratory time (I) equal to 2 seconds and expiratory time (E) of 1 second. The setting of the ventilator provides constant delivery of flow that generates the same pressure of work in both respiratory acts. These differ only in the percussion frequency and consequently the I/E ratio. In both acts the expiratory phase is passive. Note that between the delivery of a micro-volume and the next, the flow is interrupted and the pressure decreases to a value that depends on the mechanical characteristics of the thoraco-pulmonary system [22].

The percussion frequency can be set by the operator in a variable range between 200 and 1100 cycles/min.

Moreover, the magnitude of the pressure variation determined by the individual micro-volume is inversely proportional to the percussion frequency. Furthermore the wider pressure excursion determined by each gas mini-burst, the lower the percussion frequency. The pressure excursion is operator programmable by adjusting the inspiratory and expiratory times (i/e ratio) of the individual micro-volume delivered [22].

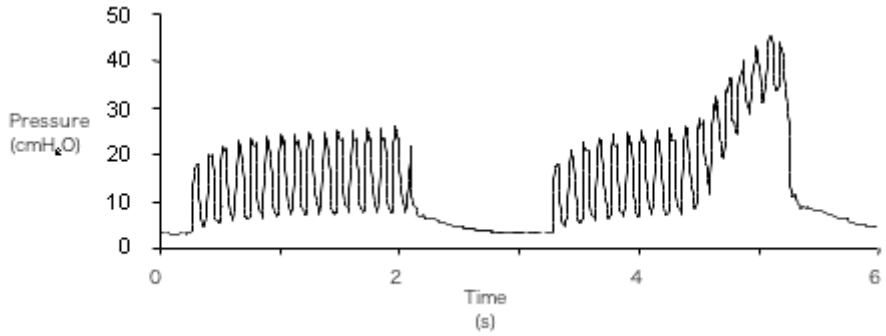

Figure 1.7 Pressure curves during HFPV. The tele-inspiratory phase of the second act has a pressure increase caused by a supplementary flow set by the operator. This option allows, for the same inspiratory time (I), an increase in the volume delivered due to convection [22].

The features of the phasitron and the breathing circuit allow some interesting considerations regarding the potential of the HFPV mode.

The phasitron permits to administer the tidal volume through a succession of micro-volumes, until the progressive attainment of a plateau pressure whose value and duration are chosen by the operator; moreover, due to the Venturi effect, the delivered flow is converted into pressure (and vice versa), depending on the thoraco-pulmonary impedance.

These factors allow the operator to:

• optimize the distribution of the flow, avoiding preferential ventilation,

• maintain constant values of mean airway pressure when resistive and elastic load of the respiratory system change, without modification of the parameters on the VDR-4®.

Moreover, since the circuit remains constantly open to the air, the risk of barotrauma and/or volotrauma is limited.

The percussion frequency is a critical factor in the management of hypoxia and hypercapnia. At low percussion frequencies (200-400 cycles/min) the convective phenomenon is prevalent, which results in an increased wash-out of CO_2 , whereas at high percussion frequencies (600-900 cycles/min) is more significant the diffusive

phenomenon; the latter is probably due to the increased kinetic energy of the oxygen molecules.

In the clinical experience of the Intensive Care Unit of the Cattinara Hospital, out of 24 patients with acute respiratory failure , the application of a percussion frequency of 500 cycles/min achieved the best combined effect on clearance of CO_2 and improvement of hypoxia [23].

Factors determining the mean airways pressure (Paw_m) and therefore able to change individually or in combination the gas exchange are the percussion frequency, inspiratory and expiratory times, the plateau pressure, PEEP and the I/E ratio.

Owing to the characteristics of the low-pressure inspiratory circuit and the activity of *pneumatic air hammer* determined by the micro-volumes, the administration of aerosolized bronchodilators and mucolytics allows to thin the secretions, reducing the forces of adhesion and cohesion and promoting their clearance.

The mobilization of secretions during HFPV is then due to three main factors :

1. the sequence of pressure peaks causes a vibration effect on the mucous membrane and bronchial secretions,
2. the variation of the percussion frequency generates turbulence at the respiratory Airways,
3. the high flow, combined with the percussion, promotes the mucociliary clearance.

The drainage of secretions and thus the recruitment of atelectasis is possible as a result of three additional key factors related to the intrinsic characteristics of the HFPV:

A) The high-flow aerosol coupled to the percussion allows an effective and adequate humidification of the airways,

B) the application of PEEP allows the maintenance of the atelectasis, recruited from high-frequency percussive mechanism of the VDR-4®,

C) the percussion micro-volumes and the high flow allow the overcoming of mucous plugs and their upward movement , due to the elastic return of the alveoli.

Several authors have reported their experience with HFPV in neonates with hyaline membrane disease [24,25], in patients with neuromuscular disease [26] and in those with acute respiratory failure following chest trauma [27]. In a pilot study on patients with cystic fibrosis, Natale et al. [28] compared the effects of HFPV with those of conventional chest physiotherapy. HFPV has also been studied in patients with post-traumatic

intracranial pressure [29,30]. Gallagher et al. [31] compared techniques of CMV and HFPV in patients with respiratory failure following sepsis and trauma. Further studies have shown improvement in lung gas exchange at equal airway peak pressure and FiO_2. Moreover the application of HFPV was capable to maintain normocapnia, without causing hemodynamic alterations. In 2008 Allardet-Servet et al. [32] provides new evidence to consider HFPV as an effective protective ventilation strategy, attenuating lung injury in a rabbit model of gastric juice aspiration.

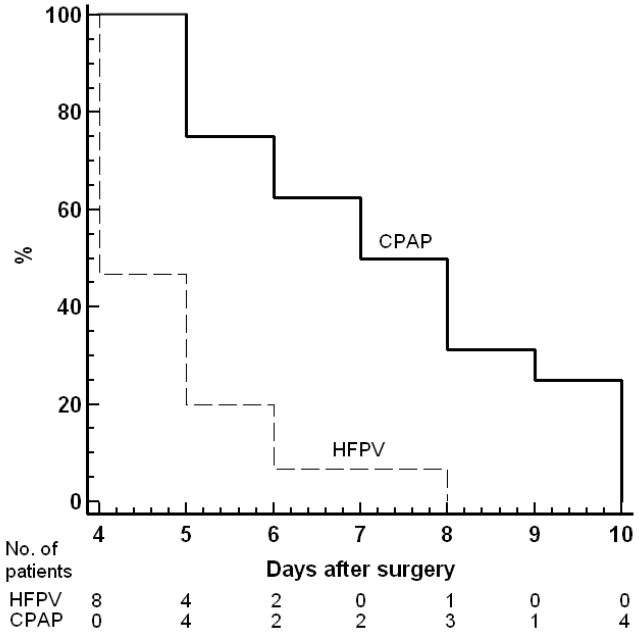

Figure 1.8 Probability of patients discharge as a function of postoperative days. Patients treated with high frequency percussive ventilation (*HFPV, solid line*) had a 3.14-fold larger chance of being discharged earlier than those under continuous positive airway pressure (*CPAP, dotted line*), $p = 0.0007$ [34].

HFPV was demonstrated also applicable during surgery; to maintain gas exchange during surgical bronchial repair in a patient with one lung [33] and to improve perioperatively clinical evolution in pulmonary resection [34]. In the latter study 40 patients were randomized to be treated with CPAP or HFPV during surgery and in the group treated with the HFPV gas exchange was improved, the premature mobilization of endobronchial secretions and their elimination were promoted and finally HFPV promote a premature discharge, reducing money costs and the risk of development of nosocomial complications.

Recently HFPV has been inserted between the ventilatory strategies to apply in severe hypoxemic respiratory failure [35] and in 2012 the earl short-term application of

HFPV was proven to be effective in improving gas exchange in hypoxemic patients [36]. In particular, HFPV applied during 12h to severe hypoxemic patients with different pulmonary diseases was able to significantly increase their gas exchange. Furthermore, this finding remained unaltered from the cessation of HFPV until 12 h under subsequent CV when the study ended.

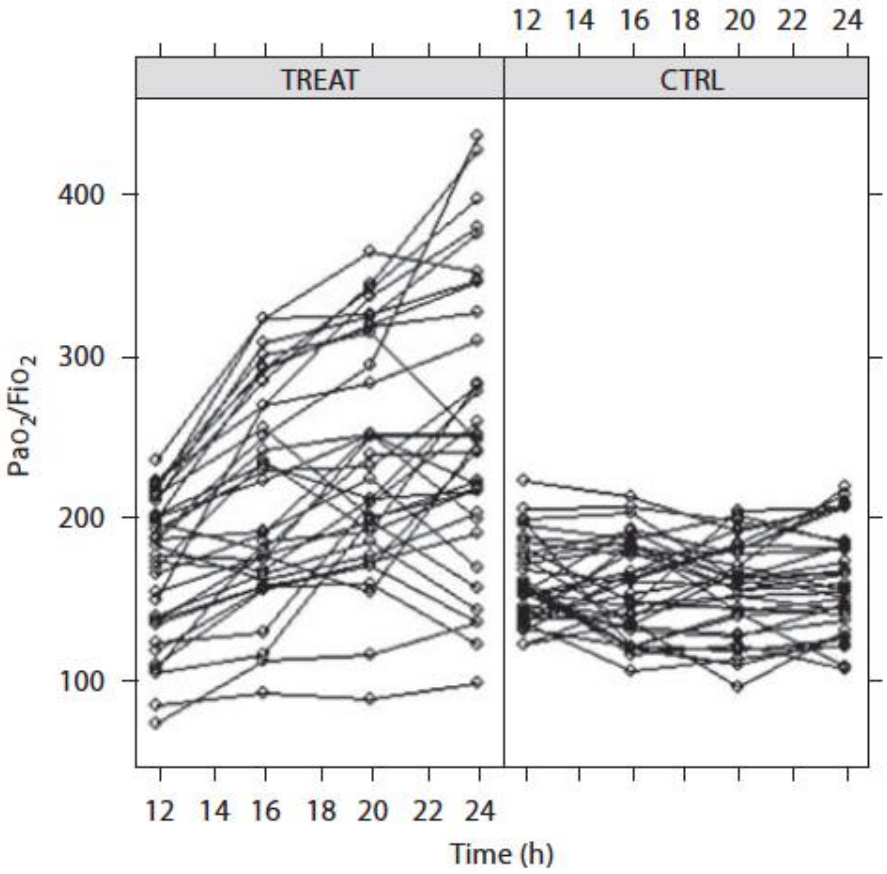

Figure 1.9 PaO_2/FiO_2 versus time in hypoxemic patients. At 12 h [baseline, conventional (volume- or pressure-controlled ventilation, CV)] the patients were either switched to HFPV (left panel, n = 35, TREAT group) or left under CV (right panel, n = 35, CTRL group). Pa O 2 /Fi O 2 increased in TREAT patients while it remained unaltered in CTRL [36].

Chapter 2 - From Bench to Bedside

The purpose of this chapter is to describe the previous studies that are on the base of this doctoral thesis.

The knowledge gained from the previous bench and clinical investigations was a fundamental prerequisite to focus on the development of a new electronic system able to calculate the viscoelastic properties of the respiratory system during HFPV.

High frequency percussive ventilation has been commercially available in Europe in early 1999 and probably, clinically used, as the first time in Italy, at the Department of Perioperative Medicine, Intensive Care and Emergency, Cattinara Hospital, University of Trieste. At that time only "twelve" publications were available (Pub Med selection of research from 1980 to 1999), and only one had mentioned the respiratory system compliance as a term of comparison between HFPV and conventional mechanical ventilation. In this study the respiratory system compiance (Crs) was calculated through the use of a simple data acquisition system (flow and pressure transducers with a sampling frequency of 50 Hz)[37]. It is also important to remember that neither in this, nor in other work available at that time was taken into consideration the volume curve during HFPV. All studies of the considered period, including the current instruction manual of VDR-4® (Volumetric Diffusive Respirator), report the airway pressure curve exclusively.

Flow, volume and pressure curves generated by HFPV have been critically studied in relation to a single-compartment lung simulator with varying elastic and resistive loads only in the year 2004 [38].

In this context, the clinical use of HFPV appeared to be extremely unintuitive and in the larger part of the cases was used as a lifesaving technique. The majority of physicians required a careful monitoring system that was able to describe the mechanical response of the respiratory system during HFPV.

2.1 Effects of mechanical load on flow, volume and pressure delivered by high-frequency percussive ventilation

As aforementioned, in 2004 for the first time was evaluated how inspiratory flow, volume and pressure curves generated by HFPV change in the face of imposed mechanical loads [38]. For this purpose, a single-compartment lung simulator with varying elastic and resistive loads (without viscous resistance) was used, maintaining the pre-selected ventilatory setting in the HFPV generator.

The highest positive value of pulse flow during inspiration, inspiratory positive peak flow (IPPF), was measured, as well as the corresponding lowest negative pulse flow, inspiratory negative peak flow (INPF). Volume was obtained by digital integration (trapezoidal rule) of the flow signal. The highest Paw inspiratory value Pawpeak was determined. Mean airway pressure (Pawmean) was calculated by dividing the integral of Paw as a function of time by the duration of the respiratory cycle (I + E). The baseline pattern was: E = 20 cmH_2O/L, R = 0 $cmH_2O/L/s$. The flow required to establish baseline pattern was kept constant throughout the experiment, as well as pulse frequency (500 cycles/min during inspiration, i/e ratio of 1:2.75), and convective respiratory frequency (10 breaths/min, I/E ratio of 1:1.25). Expiration was passive in all conditions, with exhalation to ambient air through the Phasitron® exhalation valve gate. The load combinations and mechanical parameter are reported in table 2.1.

Experimental settings	Paw_m (cmH_2O)	Paw_{peak} (cmH_2O)	ΔPaw (cmH_2O)	Inspiratory positive peak flow (l/s)	Inspiratory negative peak flow (l/s)	Volume (l)
$E = 20, R = 0$	6.91	26.68	19.24	1.59	−1.03	0.465
$E = 50, R = 0$	7.09	26.55	18.64	1.54	−1.03	0.269
$E = 100, R = 0$	7.17	26.54	18.12	1.54	−1.03	0.163
$E = 20, R = 5$	7.57	29.22	23.15	1.21	−0.78	0.470
$E = 50, R = 5$	7.63	29.82	23.64	1.23	−0.79	0.258
$E = 100, R = 5$	7.75	28.90	22.83	1.22	−0.83	0.141
$E = 20, R = 20$	8.23	34.36	29.91	0.87	−0.53	0.437
$E = 50, R = 20$	8.26	34.75	30.05	0.88	−0.56	0.215
$E = 100, R = 20$	8.32	34.49	29.68	0.88	−0.59	0.129
$E = 20, R = 50$	8.60	39.06	35.27	0.56	−0.32	0.257
$E = 50, R = 50$	8.87	39.72	36.15	0.57	−0.37	0.162
$E = 100, R = 50$	8.83	39.75	35.69	0.57	−0.41	0.096
$E = 20, R = 200$	9.27	44.84	40.73	0.33	−0.16	0.205
$E = 50, R = 200$	9.34	45.43	41.57	0.34	−0.19	0.164
$E = 100, R = 200$	9.43	45.43	41.02	0.34	−0.23	0.115

Table 2.1 Pressure and flow values for different loads. R ($cmH_2O/L/s$) and E (cmH_2O/L) are resistive and elastic loads, respectively; Pawm, Pawpeak, and ΔPaw are mean, peak, and mini-burst airway pressures, respectively. Inspiratory positive and negative peak flows are the maximum and minimum values of flow during inspiration [38].

The main results demonstrated that all the measured parameters were sensitive to resistive loading, while elastic loading affected solely tidal volume. Although very high impedance values were used in the model, the highest pressure amounted solely to 45.4 cmH_2O when E = 100 cmH_2O/L and R = 200 cmH_2O/L/s. Increases in Pawpeak amounting to 18.75 cmH_2O correspond to a rise in Pawm levels of only 2.52 cmH_2O going from the control to the highest impedance (E = 100 cmH_2O/L, R = 200 cmH_2O/L/s) conditions.

These data reveal how the average Pawm values are stable under all experimental configurations, due to the physical characteristics of the Phasitron® design. Even though the VDR-4 flow generation setting remains unchanged, the Phasitron® near instantaneously varies the velocity of inspiratory and expiratory oscillatory peak flows at all resistance values.

Pawpeak and Pawmean, (Figures. 2.1, 2.2 respectively) augmented with increasing R, but were practically insensible to the variations in E. In all instances a curvilinear relationship with an upward convexity was found between pressures and R.

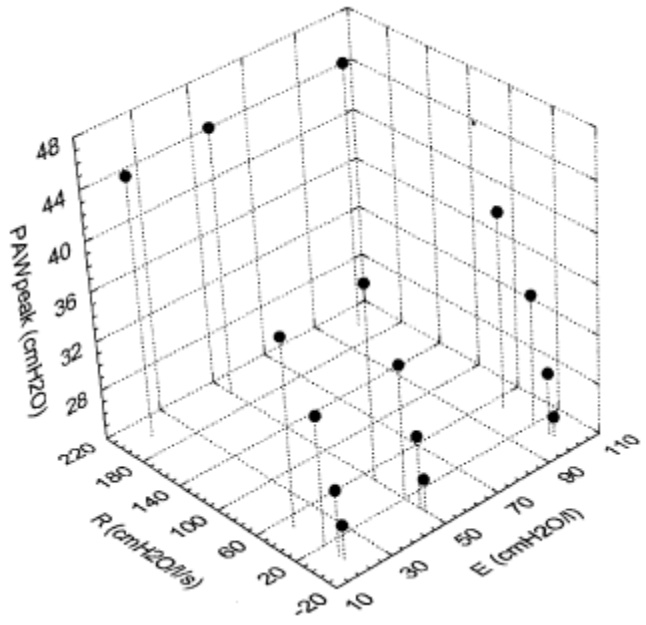

Figure 2.1. Peak airway pressure (Pawpeak) plotted against added elastic (E) and resistive (R) loads. Peak airway pressure increases when R increases, but is almost unaffected by changes in E. For the same E a curvilinear relationship (with an upward convexity) between Pawpeak and R was found [38].

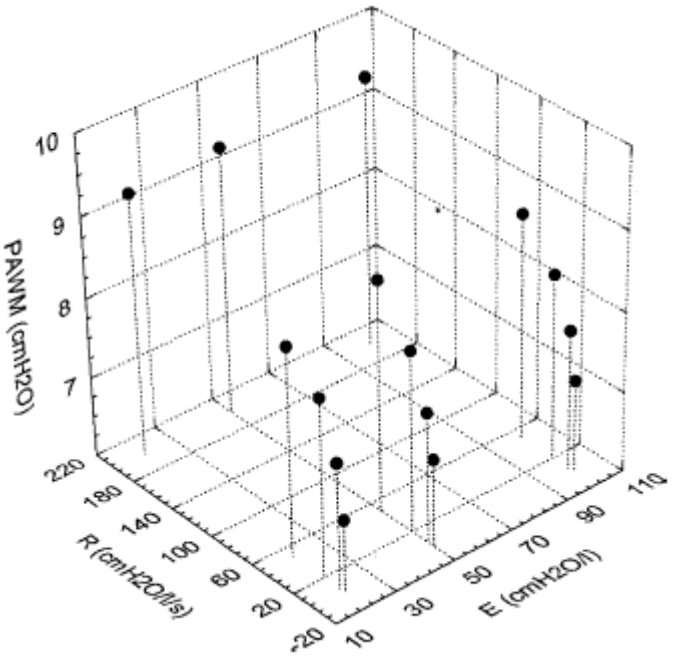

Figure 2.2. Mean airway pressure (Pawm) plotted against added elastic (E) and resistive (R) loads. Mean airway pressure increases with R increment, but is almost unaffected by changes in E. For the same E a curvilinear relationship (with an upward convexity) between Pawm and R was found [38].

Tidal volume decreased with increasing R and E (figure 2.3). Indeed, in the face of the association of the highest R and E tidal volume fell to 24.7% of its control value.

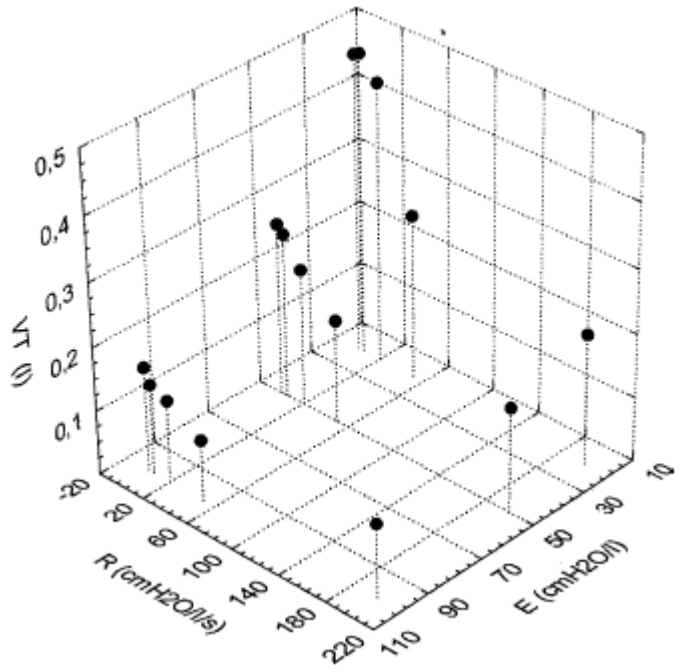

Figure 2.3. Tidal volume (VT) plotted as a function of elastic (E) and resistive (R) loads. Volume decreased with increasing E and R [38].

Figure 2.4 shows flow, volume, and Paw tracings (one breath) under four different loading patterns; in panels A–D the values of E and R are, respectively: 20 cmH_2O/l and 0 $cmH_2O/l/s$, 20 cmH_2O/l and 20 $cmH_2O/l/s$,100 cmH_2O/l and 0 $cmH_2O/l/s$, and 100 cmH_2O/l and 200 $cmH_2O/l/s$. The volume curve shown in figure 2.4A presents progressively lower increases in micro-burts, which tended to become stable at end-expiration. This phenomenon occurs much earlier in figure 2.4C, where a plateau extends for most of the inspiration time. The volume curve in figure 2.4B presents a smaller micro-burst and this characteristic was even more marked in figure 2.4D (higher R values).

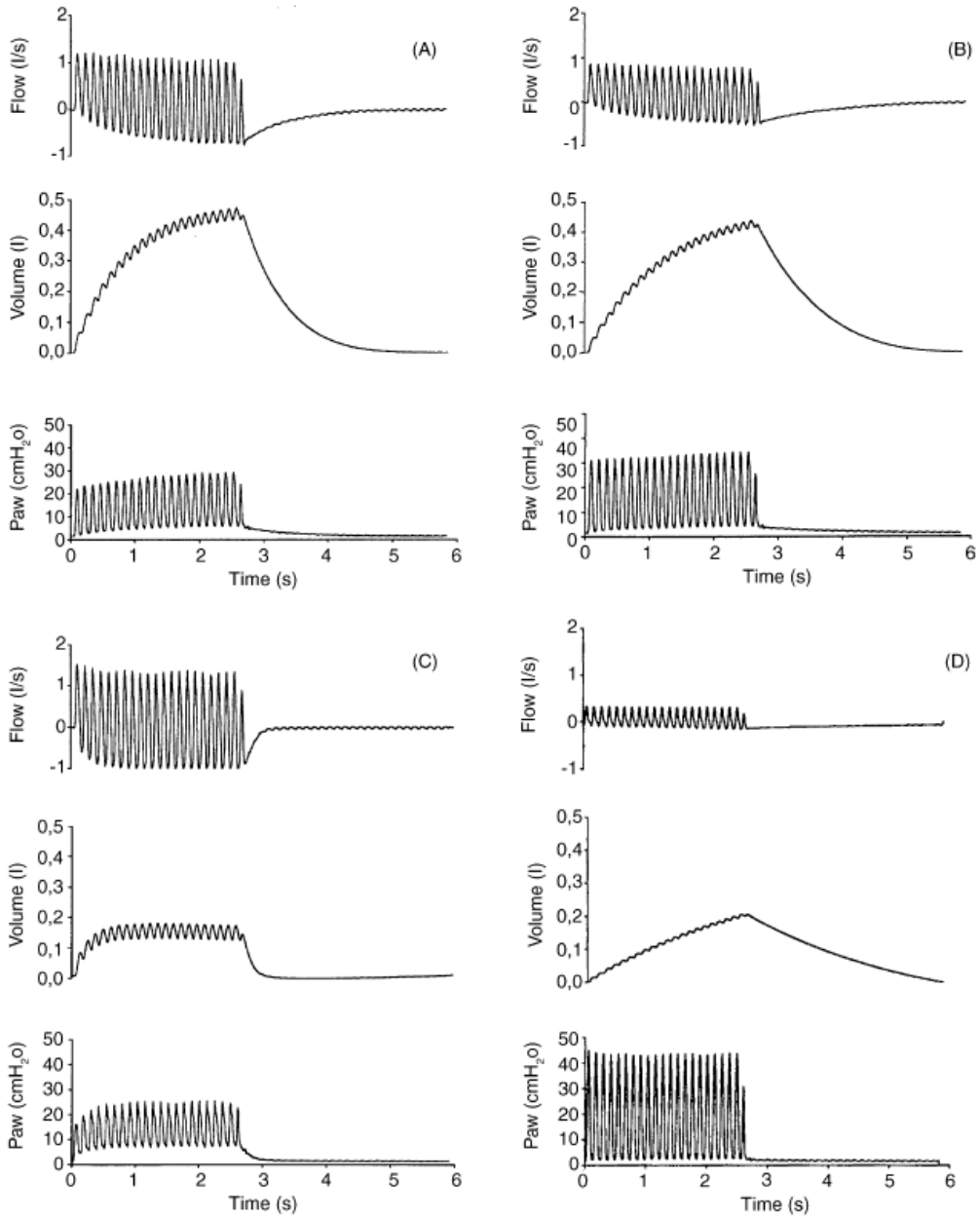

Figure 2.4. Flow, volume, and airway (Paw) pressures tracings (one breath) under four different loading patterns; in panels A–D the values of E and R are, respectively: 20 cmH_2O/l and 0 $cmH_2O/l/s$, 20 cmH_2O/l

and 20 $cmH_2O/l/s$, 100 cmH_2O/l and 0 $cmH_2O/l/s$, and 100 cmH_2O/l and 200 $cmH_2O/l/s$. At end-expiration in 2.4D, expiratory flow does not reach zero, generating auto-PEEP [38].

As displayed in figure 2.4A, during early part of inspiration the positive peak flow is definitely higher than the negative. This finding indicates that the quantity of air introduced into the system is greater than the volume washed out of it. In the same figure it may be seen that at end inspiration the absolute values of the positive and the negative peak flows are almost identical, and the net flow approaches zero. When this phase is reached, a plateau is evident on the corresponding volume curve, which is the same as the generated volume. Oscillations during this phase may be useful for gas exchange, but they do not increase the inspired volume. In figure 2.4C, the phase with positive and negative peaks having the same width is reached much earlier during inspiration (greater duration of the plateau phase in the volume curve). Under the extreme conditions displayed in figure 2.4D, flow oscillations are definitely low in amplitude, and flow generation may occur with a minimum gas requirement by the low-pressure circuit, delivering small mixing sub tidal volumes during the entire physiological period of exhalation.

In conclusion this study demonstrated:

1) Flow, volume and pressure values depended fundamentally on the value of R, but their shapes were modified by R and E. Although peak Paw increased 70.3% in relation to control value, mean Paw augmented solely 36.5% under the same circumstances (maximum of 9.4 cmH_2O). Intrinsic properties of the HFPV device may explain this results. As retrogressive intrapulmonary pressures increase, the venturi system, due to its fluidic entrainment characteristics, may progressively reduce the quantity of entrainment gases until the quantity of flow generated by the high-pressure circuit is prevailing, which is demonstrated by the fall in inspiratory peak flow from 1.6 to 0.33 l/s as resistance rises from 0 to 200 cmH_2O/l s.

2) A simple morphological analysis of flow, volume and pressure curves may provide useful information about the mechanical loading of a lung simulator driven by HFPV. These signals reveal the physical effect of the imposed loads on the output of the ventilatory device, secondary to constant alterations in pulmonary dynamics.

These curves were shown to result from mechanical characteristics of the model, as well as from properties inherent to the ventilator itself.

2.2 Mechanical loads modulate tidal volume and lung washout during high-frequency percussive ventilation

Latter in 2006 were evaluated the effects of mechanical loading on the tidal volume and lung washout during HFPV [33].

In the previous study was reported the elastance and resistance dependence of flow, volume and pressure curves generated during HFPV. Nevertheless, considering that the HFPV device generates a tidal volume based on intermittent positive pressure ventilation associated with a superimposed continuous pulmonary washout of gas by means of high-frequency pulsatile mini-volumes, further analysis of the responses of these ventilation waveforms to imposed loads is still wanted. Therefore, was important from the clinical point of view, to evaluate the effects of mechanical resistive and elastic loading on tidal volume and lung washout during HFPV.

Tidal volume and lung washout were determined as described below: for each inspiration, the flow signal was divided into a positive component with oscillation peaks above the zero-flow reference value, and a negative component with oscillation peaks below this value. As shown in figure 2.5, the mathematical integration of the positive component as a function of time yielded the cumulative pulsatile in-volume (Vin), while the integration of the negative component provided the cumulative pulsatile out-volume (Vout). Tidal volume (VT) resulted from Vin $-V$out. We defined as total cumulative pulsatile volume (Vtot) the sum of Vin and Vout. Since the study was performed under a constant inspiration time (TI), the ratio VT/Vtot indicates the percentage of the pulsatile volume used to expand the model during inspiration in all instances.

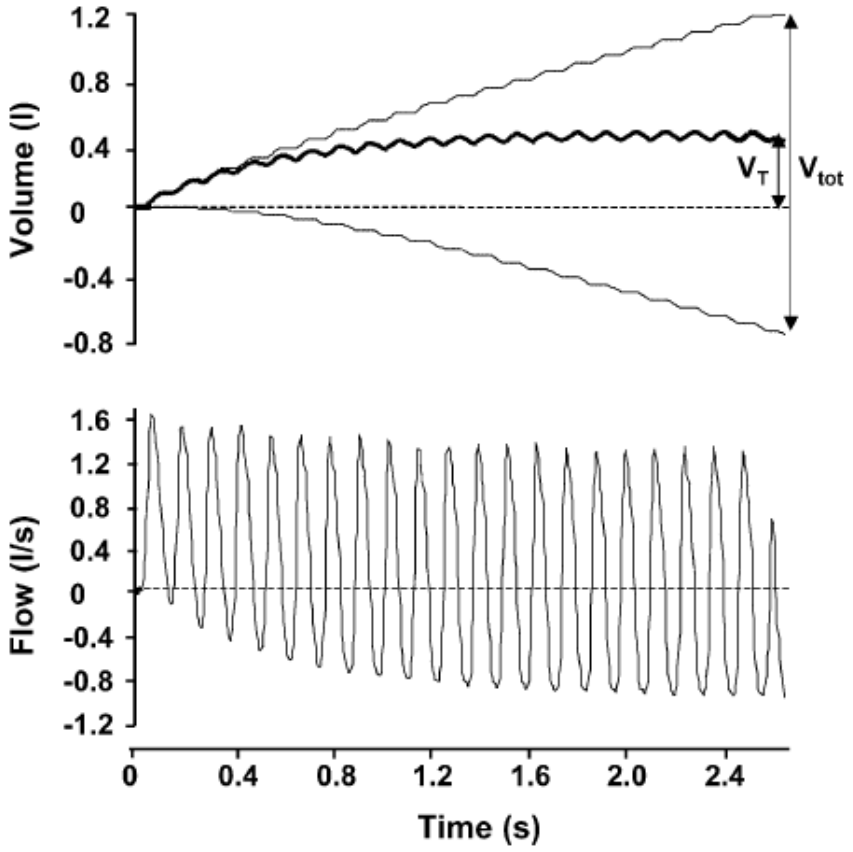

Figure 2.5 Volume and flow during inspiration modelled using resistance equal to 0 cmH_2O/l s and elastance of 20 cmH_2O/l. The flow signal was divided into a positive component with oscillation peaks above the zero-flow reference value and a negative component with oscillation peaks below this value (lower panel). Upper panel: the mathematical integration of the positive component as a function of time yielded the cumulative pulsatile in-volume (*V*in) (upper thin line), while the integration of the negative component provided the cumulative pulsatile out-volume (*V*out) (lower thin line).Tidal volume (*V*T) resulted from *V*in −*V*out (thick line). In both panels the interrupted lines represent zero values. *V*tot, total cumulative pulsatile volume (=*V*in + *V*out). Lower panel: at the beginning of inspiration, flow is mainly inspiratory (above zero), but as inhalation progresses it develops a progressively higher expiratory component (below zero) [33].

A peculiar mechanism involved in the lung ventilation by HFPV is related to its high turnover of gas in the lung: figure 2.5 shows that tidal volume (0.465 l, Table 2.2) corresponds to 25.6% of the total cumulative percussive volume (*V*tot). In other words, 1.82 l are pumped in and expired off the lung during percussive ventilation, washing CO_2 out of it and moving O_2 in. The balance between the in-volume and the out-volume (*V*T) remains in the lung (Table 2.2). This could be an important mechanism when the time allowed for diffusive ventilation is short.

Experimental settings	V_{in} (l)	V_{out} (l)	V_{tot} (l)	V_T (l)	V_T/V_{tot} (%)	$T_{plateau}/T_I$ (%)	Paw_m (cmH_2O)	Paw_{peak} (cmH_2O)
$E=20$, $R=0$	1.14	0.676	1.82	0.465	25.6	20.6	6.91	26.68
$E=50$, $R=0$	1.04	0.774	1.82	0.269	14.8	35.9	7.09	26.55
$E=100$, $R=0$	1.01	0.848	1.86	0.163	8.7	63.1	7.17	26.54
$E=20$, $R=5$	0.92	0.454	1.38	0.470	34.1	12.3	7.57	29.22
$E=50$, $R=5$	0.87	0.611	1.48	0.258	17.4	37.4	7.63	29.82
$E=100$, $R=5$	0.80	0.663	1.47	0.141	9.6	58.8	7.75	28.90
$E=20$, $R=20$	0.68	0.317	1.0	0.363	36.3	0	8.23	34.36
$E=50$, $R=20$	0.61	0.339	1.03	0.215	20.9	36.6	8.26	34.75
$E=100$, $R=20$	0.57	0.445	1.02	0.129	12.6	54.8	8.32	34.49
$E=20$, $R=50$	0.43	0.174	0.61	0.257	42.5	0	8.60	39.06
$E=50$, $R=50$	0.40	0.238	0.64	0.162	25.4	32.5	8.87	39.72
$E=100$, $R=50$	0.40	0.305	0.71	0.096	13.6	46	8.83	39.75

Table 2.2 Mechanical parameters and load combination during high-frequency percussive ventilation. Values are means of three determinations in each condition. S.D. was negligible. R (cmH_2O/l/s) and E (cmH_2O/l) are resistive and elastic loads; Vin, Vout and Vtot are in, out, and total cumulative pulsatile volumes, respectively; VT, tidal volume; TI, duration of inspiration; Tplateau, duration of constant lung volume at end-inspiration; Pawm, Pawpeak are mean and peak pressures, respectively [33].

Figure 2.6 summarizes the effects of R and E on VT/Vtot, which increases with R but falls with E. Indeed, it can be seen in Fig. 3 that the smallest values of VT/Vtot (8.7%) were found when R = 0 and E = 100 cmH_2O/l.

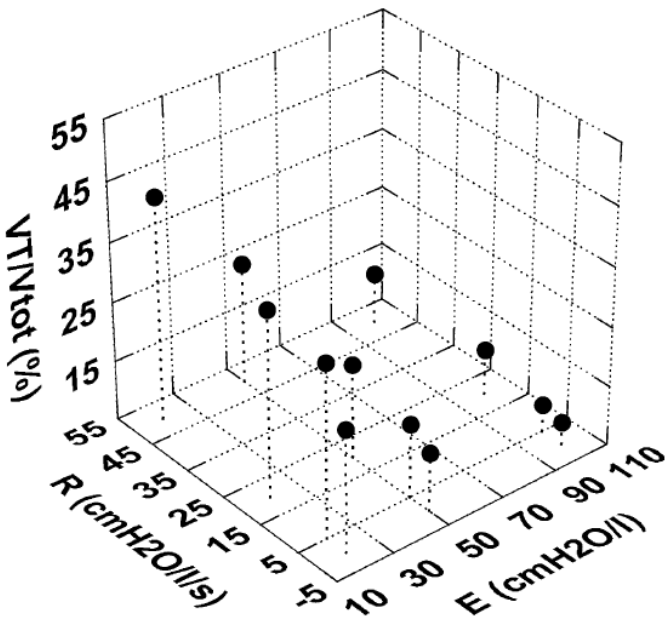

Fig. 2.6. Effects of resistive and elastic loads (R and E, respectively) on the ratio tidal volume/total cumulative pulsatile volume (VT/Vtot).The ratio increases with R but falls with E [33].

In figure 2.7A iso-elastance (E=20 cmH_2O/l) volume curves are displayed as a function of inspiratory time. From top to bottom R corresponded to 0, 5, 20, and 50 cmH_2O/l/s. A tele-inspiratory plateau was reached in the first two conditions only, as shown in Table 2.2. One can also see in figure 2.7A and Table 2.2 that VT is preserved in

the first three conditions, while *V*tot decreases progressively down to approximately one-third of the baseline condition as *R* increases. Under iso-elastance conditions, and for any of tested *R* values, both *V*in and *V*out fell with augmenting *R* (Table 2.2). In Fig. 2.7B iso-resistance (*R* = nil) volume curves are plotted against inspiratory time. From top to bottom *E* amounted to 20, 50 and 100 cmH_2O/l. Tidal volume decreased with increasing *E*, but *T*plateau/*T*I increased and *V*T/*V*tot decreased (Table 2.2). Under these conditions, and for any value of *R*, Table2.2 also shows that *V*in falls and *V*out augments with increasing *E*.

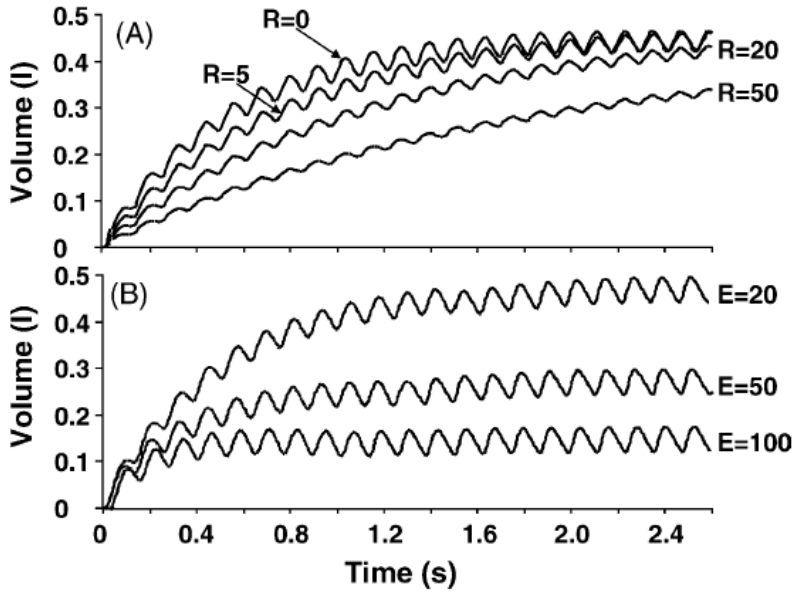

Figure 2.7. PanelA shows iso-elastance (*E*=20 cmH_2O/l) volume curves displayed as a function of inspiratory time. From top to bottom *R* corresponds to 0, 5, 20, and 50 cmH_2O/l s. In panel B iso-resistance (*R* = 0 cmH_2O) volume curves are plotted against inspiratory time. From top to bottom *E* amounted to 20, 50 and 100 cmH_2O/l [33].

In figure 2.8 it may be seen that Pawpeak is inversely proportional to *V*tot (Pawpeak = 46.07−11.12 *V*tot; $r = -0.985$, $p < 0.0001$), whereas Fig. 2.9 shows that Pawm is also related to *V*tot (Pawm = 9.703−1.42*V*tot; $r = -0.981$, $p<10-6$), even though the gentle slope indicates a substantially stable Pawm under the present experimental conditions

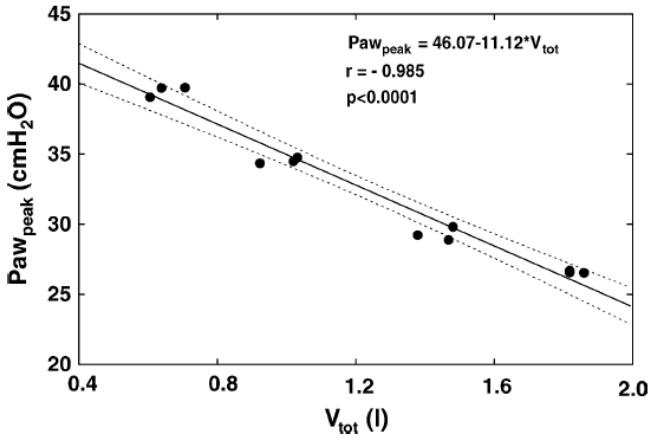

Figure 2.8. Linear regression between pressure in the model and cumulative pulsatile volume (*V*tot) for the 12 experimental conditions (solid circles). Peak pressure in the model (Pawpeak) is inversely proportional to *V*tot. Solid line, regression line; broken lines, 95% interval of confidence; *r*, regression coefficient

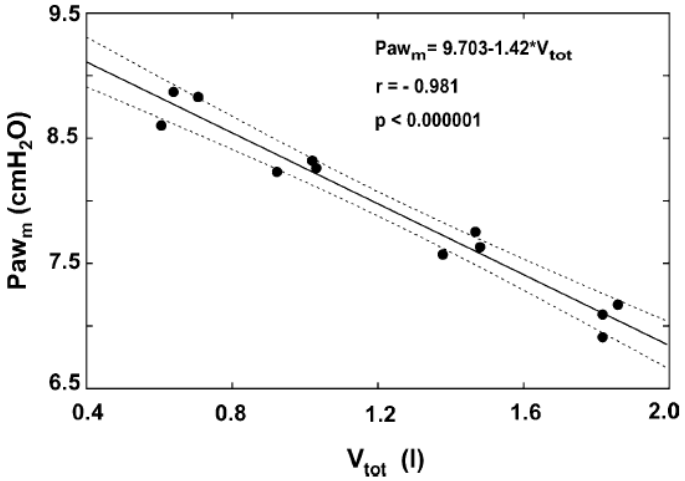

Figure 2.9. Linear regression between pressure in the model and cumulative pulsatile volume (*V*tot) for the 12 experimental conditions (solid circles). Mean pressure in the model (Pawm) is shown to be inversely related to *V*tot. Solid line, regression line; broken lines, 95% interval of confidence; *r*, regression coefficient [33].

In conclusion this study demonstrated:

1. The elastic or resistive loading modulates the mechanical characteristics of the HFPV device but in such a way that washout volume and time allowed for diffusive ventilation vary agonistically.
2. A peculiar mechanism involved in the lung ventilation by HFPV is related to its high turnover of gas in the lung.
3. Peak and mean airway pressures are inversely related to *V*tot, although the latter to a lesser extent (slopes = 11.12 and 1.42 cmH_2O/l, respectively).

Actually, we know that high-frequency percussive ventilation provides tidal volume as the difference between its pulsatile in- and out-volumes. Clearly, some amount of gas is washed out of the lungs throughout inspiration. Thus, HFPV would improve gas exchange as a result of both convective and diffusive mechanisms. Volutrauma phenomena is close related to convective volume delivered to the lung (VT). Tidal volume (VT) generation under HFPV is sensitive to loading but its changes are more important than those in Vtot. As a result, VT/Vtot decreases with increasing E and decreasing R. As a consequence, performance of the HFPV device vary according to the physiological/physical feedback of the model (or patient), but the interaction between loads, ventilator and Vt is poorly detectable by pressure monitoring.

The figures 2.10 and 2.11 describe a poor correlation between VT and Peak and mean airway pressures (r = - 0.47 and r = - 0.54, respectively).

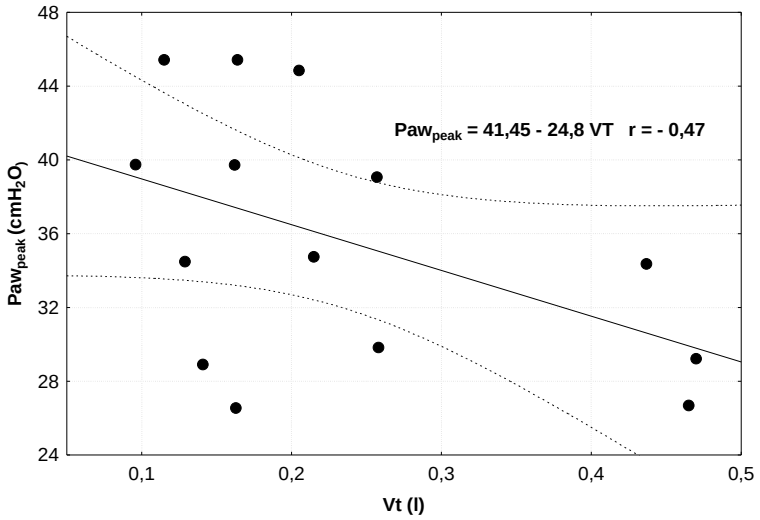

Fig. 2.10. Linear regression between pressure in the model and Tidal volume (*V*T) for the 12 experimental conditions (solid circles). Peak pressure in the model (Pawpeak) is scarcely proportional to *V*T. Solid line, regression line; broken lines, 95% interval of confidence; *r*, regression coefficient.

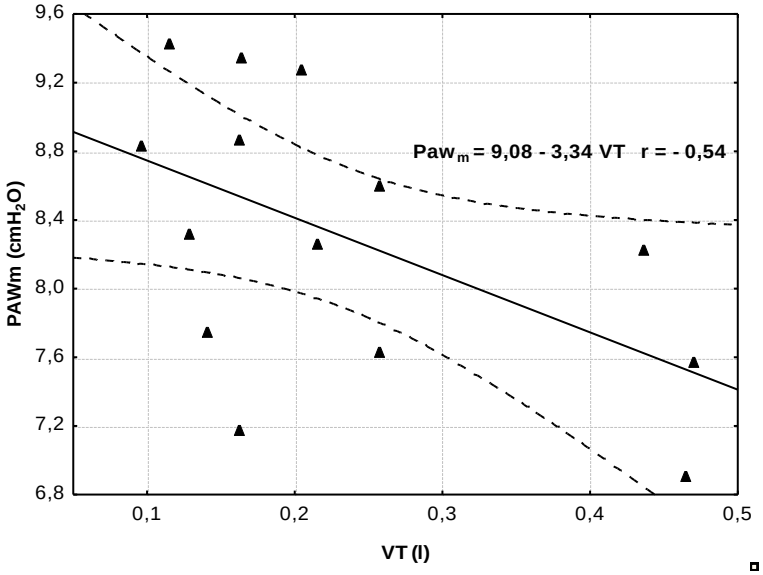

Fig. 2.11. Linear regression between pressure in the model and Tidal volume (*V*T) for the 12 experimental conditions (solid circles). Mean airway pressure in the model (Pawm) is scarcely proportional to *V*T. Solid line, regression line; broken lines, 95% interval of confidence; *r*, regression coefficient.

Considering the three dimensional graph (figure 2.12) it can be seen that in a range of 8.2-8.3 and 34.4-34.5 cmH_2O for PAWm and Ppeak respectively, VT varies from 0.437 to 0.129 litres. These volume variations depend on changes in resistive and elastic mechanical loads. This figure clearly demonstrated the intrinsic limits of PAWm and Ppeak monitoring.

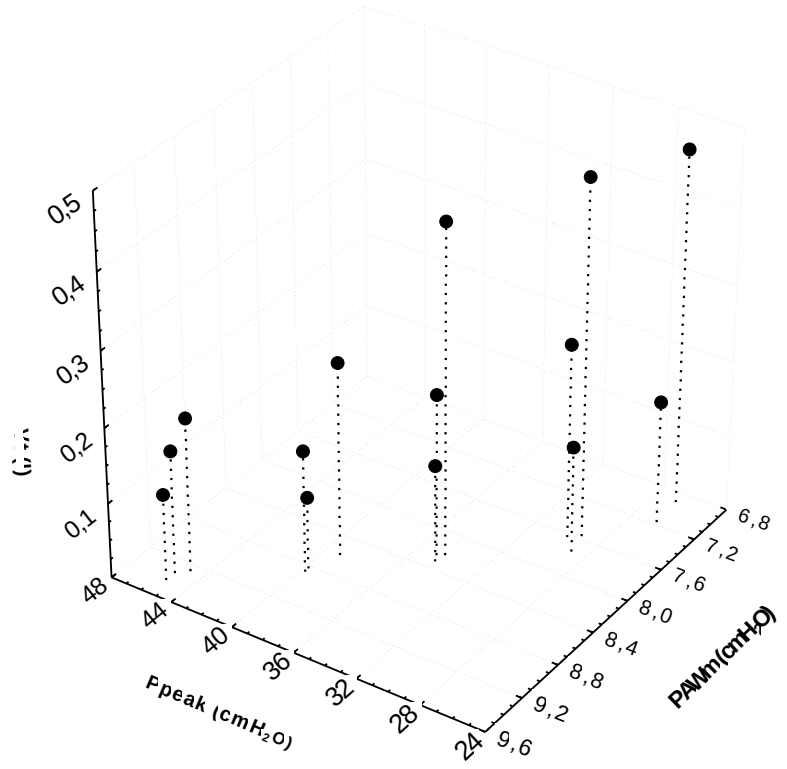

Figure 2.12. Tidal Volume (VT) plotted against Peak (Ppeak) and Mean airway pressure (PAWm) for the total experimental conditions. Tidal Volume is poorly affected by pressures. In a small range of peak and mean pressures a significant variation of VT was found.

Chapter 3 - Measurements during HFPV

The respiratory parameters during the high frequency percussive ventilation (HFPV) are determined by high frequency pulsatile oscillations of pressure and flow respiratory signals. The present measuring devices widely used during low frequency conventional mechanical ventilation are not designed for monitoring of respiratory parameters undergoing this particular high frequency ventilation. In this case the conventional devices may not be accurate enough especially due to transducer response time and low sampling frequency. In clinical practice, HFPV is not an intuitive ventilatory modality and the absence of real-time delivered volume monitoring, in the era of low-volume protective ventilatory strategy, produces disaffection among physicians.

In order to carry out a more reliable online characterization and monitoring of HFPV it is necessary to increase sensitivity and response time of the measuring system to overcome the fast variation of the respiratory parameters. For this reason innovative acquisition and elaboration systems, suitable for this particular ventilation modality, were developed. These systems are based on the use of pressure transducers of new generation with high sensitivity and reduced response time and acquisition and elaboration DSP systems with large bandwidth and high resolution.

3.1 Pressure, flow and volume measurement during HFPV

The absolute value of pressure in the upper respiratory tract of the patient, with a magnitude of some tens of H_2O centimeters, is measured by unipolar pressure transducer. This measure is not critical and it is performed using suitable conditioned transducer. Firstly the pressure was measured with (142PC05D, Honeywell, USA), while in later applications has been used a higher range transducer (ASCX01DN, Honeywell, USA) (figure 3.1). The ASCX01DN transducer measures pressure in the range of 0-70 cmH_2O and has a response time of 0.1 ms.

Figure 3.1 The ASCX01DN differential and gauge pressure transducer.

The flow is quantified by using a Fleisch pneumotachograph (figure 3.2), which converts the flow in a differential pressure, subsequently measured by high sensibility differential pressure transducer. The typical values of flow, expressed as a liter per second, are converted by pneumotachograph in a differential pressure measured in centimeters of H_2O. The pneumotachograph used in all applications was Fleisch (Type 2, Switzerland) with following characteristics:

Type	Maximum flow	Advisable flow	Inside diameter	Length	Dead space
2	3 L/s	2,5 L/s	28 mm	60mm	35mm

Table 3.1Technical characteristics of Fleisch pneumotachograph

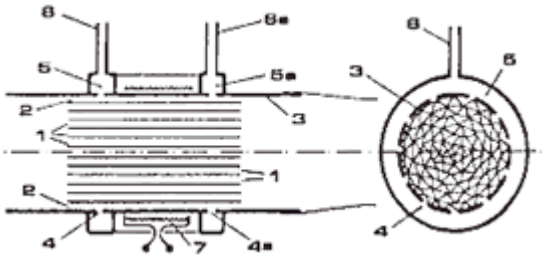

Figure 3.2 Schematics of cross sections of Fleisch pneumotachograph

The choice of pressure transducer was based on the features comparison of different amplified differential low pressure sensors (Table 3.2).

Manufacturer	Model	Pressure Range	Response Time
Sensym	ASDX001D44D	±70 cmH_2O	2.73 – 1.11 ms
Sensirion	SDP1000-L025	±0.25 cmH_2O	40 ms
Sensor Technics	HCLA02X5DB	±2.5 cmH_2O	0.5 ms
All Sensors	0.25INCH-D-4V	±0.63 cmH_2O	0.5 ms

Table 3.2 Comparison of differential pressure transducers

High sensitivity, low pressure range and fast response transducer 0.25INCH–D-4V (ALL SENSORS, USA) was chosen for this application. The amplified line of this low pressure sensor is based upon a proprietary technology able to reduce all output offset or common mode errors. This model provides a ratiometric 4 volt output with superior output offset characteristics. Output offset errors, due to temperature changes, as well as position sensitivity and stability to warm-up and to long time period, are all significantly improved when compared to conventional compensation methods. The sensor uses silicon, micromachined, stress concentration enhanced structure which provides a very linear output to measured pressure.

Figure3.3 Low differential pressure transducer 0.25INCH–D-4V

The reliability of new acquisition device based on proposed sensors and DSP system with 12 bit resolution 200 kHz A/D converter was verified and results were compared with device commonly used in conventional mechanical ventilation Gas Flow Analyzer VT+ (BIO-TEK, USA) [39]. The block diagram (Figure 3.4) illustrates the structure of the new acquisition device.

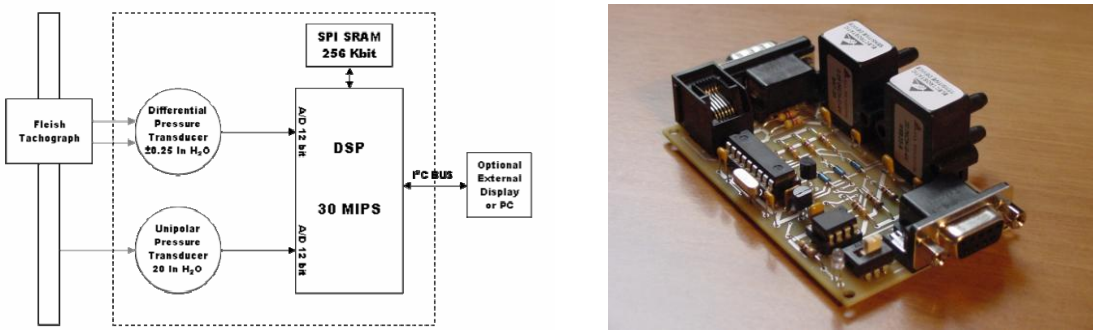

Figure 3.4 Block diagram (left) and prototype (right) of the DSP-based acquisition device [39].

In order to verify the reliability of the new device a procedure was established for measuring the volume. This procedure employed a 3-litre calibrating syringe (Fukuda Sangyo, Japan) and a manually simulated respiratory cycle of approximately 12 acts per minute for 120 seconds. The volume was calculated by integrating the flow; this operation,

described in [40] introduced a maximum error of 3% that can be considered satisfactory and within the accuracy of the employed instruments.

After the verification of the device reliability, a test bench was set up. The flow output of the high frequency percussive ventilator (VDR-4®, Percussionaire Corporation, USA) was connected through a laboratory measurement system Gas Flow Analyzer VT+ and a Fleisch pneumotacograph (Type 2, Lausanne, Switzerland) to the lung-simulator (SMS, Medishield, UK) with variable resistive and elastic loads. The pressure and flow measurements were carried out for 240 seconds, setting up on the VDR-4® a respiratory frequency of 15 cycles $minute^{-1}$ with I/E 1:1 and a percussive frequency of 800 cycles $minute^{-1}$ with working pressure of 25 cmH_2O. Mechanical resistance of 0 $cmH_2O\ L^{-1}$ s and compliance of 20 mL cmH_2O^{-1} was set on the lung-simulator. The acquired data was digitally filtered with a low-pass third order Butterworth IIR filter with a cut-off frequency of 400 Hz. The laboratory measurement system VT+ supplies directly the measured volume, while the volume measured by the new instrument was calculated by integration of the flow signal. The measured signals were evaluated considering a single respiratory act.

The acquired values of pressure (figure 3.5), flow (figure 3.6), and calculated volume (figure 3.7) are depicted in figures 3.5, 3.6 and 3.7, respectively. The figures show that the sampling frequency of VT+ 50Hz is not adequate in the case of high frequency percussive ventilation, while the sampling frequency of new device also based of new generation sensors produces better results. Moreover, VT+ generates an unacceptable error in volume measurement (figure 3.7). Therefore, for a correct assessment of the respiratory parameters and the volumes exchanged in the high-frequency percussive ventilation, is required a wide bandwidth measurement system.

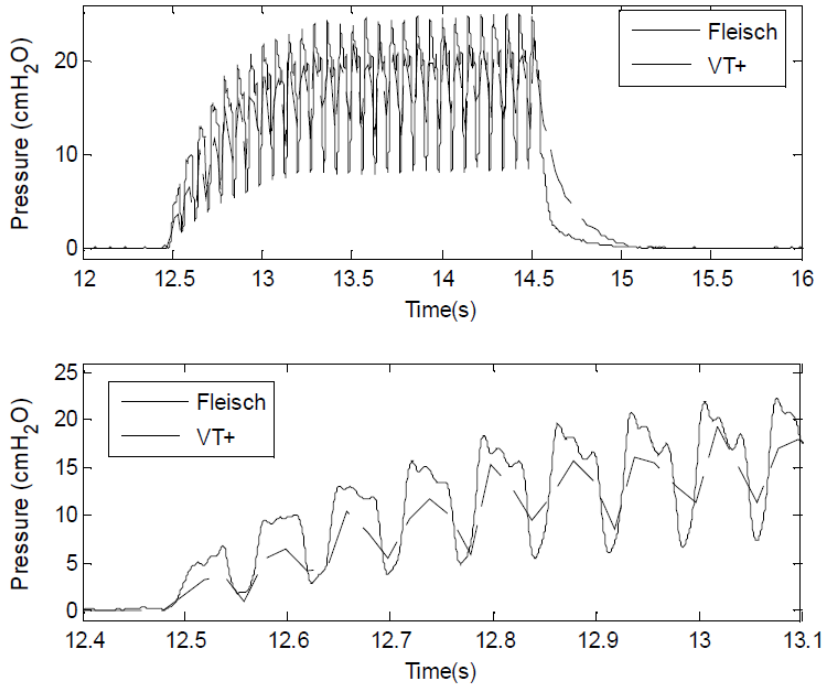

Figure 3.5 Pressure signal measured with new device (full line) and VT+ device (dotted line), during one respiratory cycle (top panel) and a particular (bottom panel) [39].

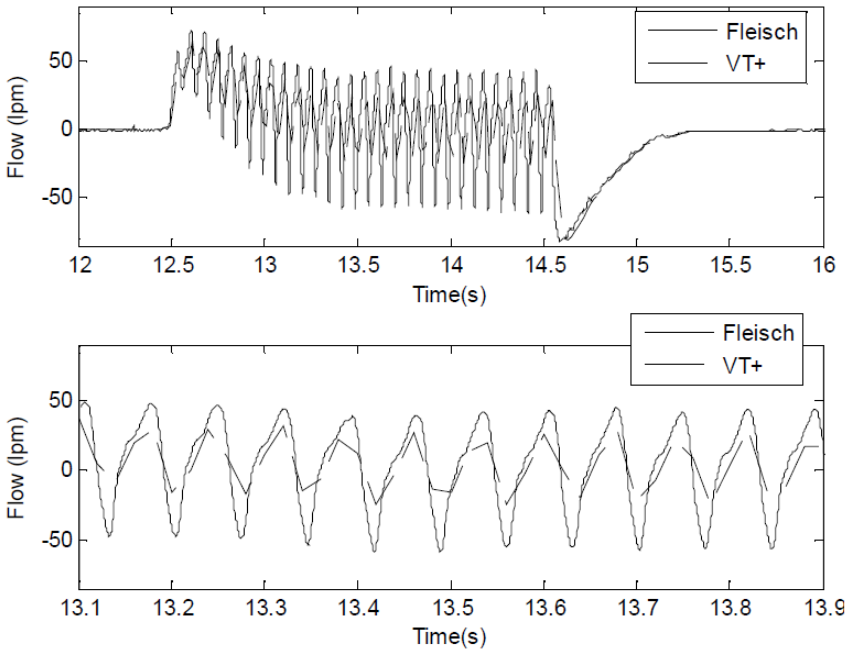

Figure 3.6 Flow signal measured with new device (full line) and VT+ device (dotted line), during one respiratory cycle (top panel) and a particular (bottom panel) [39].

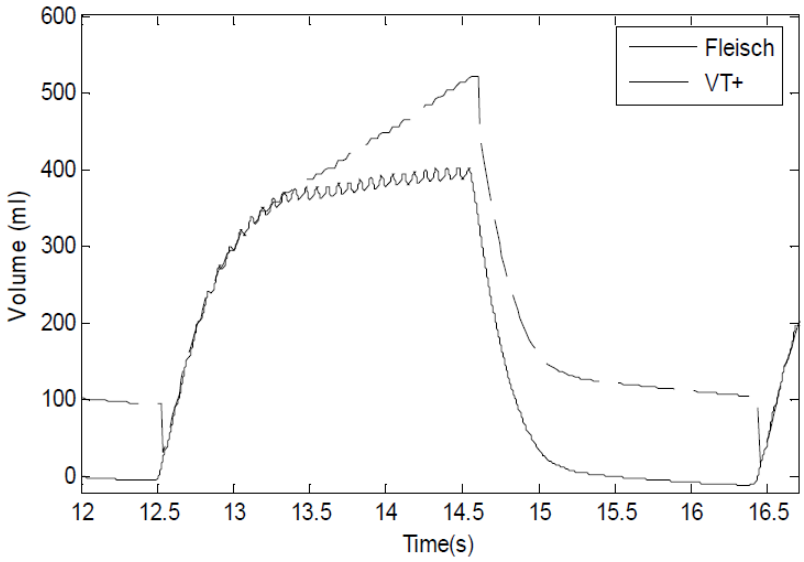

Figure 3.7 Volume measured with new device (full line) and VT+ device (dotted line), during one respiratory cycle under high frequency percussive ventilation [39].

3.2 *In vitro* measurements of respiratory mechanics during HFPV

Respiratory mechanics describes the mechanical behavior of the respiratory system exposed to pressure, flow and volume variations induced by respiratory muscles or by mechanical ventilation support. The simple three element Dorkin model is used every day clinical practice to describe respiratory mechanics, because of immediate physiological interpretation of its parameters and its sensitivity to changes in lung mechanics. This model can be applied both during conventional and high frequency ventilation. Dorkin's model approximates the respiratory mechanics function by the following motion equation [41]:

$$P_{aw} = E \cdot V + R \cdot \dot{V} + I \cdot \ddot{V} + P_0$$

where P_{aw} is the pressure applied to the respiratory system, V is the pulmonary volume, $\dot{V}$ is the airflow and $\ddot{V}$ is volume acceleration; P_0 represents the mouth pressure when V, $\dot{V}$ and $\ddot{V}$ are zero. The resistance R, elastance E and inertance I parameters describe respectively the viscous, elastic and inertial mechanical properties of respiratory system. The $E \cdot V$ term corresponds to the pressure necessary to balance elastic forces, the $R \cdot \dot{V}$

term corresponds to the pressure necessary to overcame the frictional forces, while the product $I \cdot \ddot{V}$ corresponds to the pressure necessary to overcome the system's inertia (i.e. the inertance of the respiratory system). Finally, P_{aw} - P_0 represents to the sum of the resistive, elastic and inertial pressure drops of the respiratory system.

P_{aw} and $\dot{V}$ may be measured directly at the patient's mouth with a pressure and flow transducer, respectively. Volume and volume acceleration can be calculated by integration and derivation of the airflow signal, respectively. On the other hand, E (elastance), R (resistance) and I (inertance) are not directly measurable.

The estimation of resistive and elastic parameters of the respiratory system during mechanical ventilation is of great importance to detect lung dysfunctions and to evaluate the effect of treatment [42-43]. The end inflation occlusion method is commonly used for the estimation of respiratory mechanics parameters, in patients undergoing conventional mechanical ventilation with constant inspiratory flow [42-43]. This method requires a constant flow, resulting inapplicable during HFPV, characterized by high frequency pulsatile flow. An alternative method is the parametric identification based on non-invasive measurements of flow and pressure signals with a three elements Dorkin model. Therefore, in order estimate these parameters parametric identification approach was applied in vitro both on conventional and high frequency percussive ventilation [44]. The parameters were estimated in different ventilator and experimental setups, starting from measured pressure and flow signals.

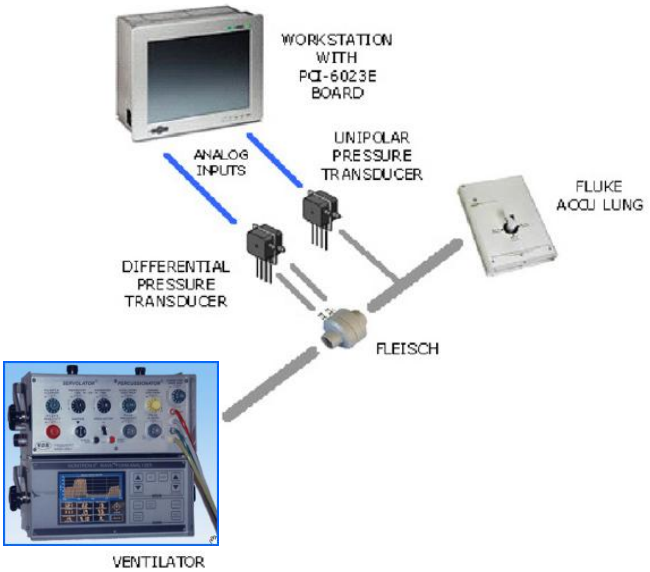

Figure 3.8 Schematic diagram of the experimental setup [44].

The schematic diagram of experimental setup is shown in figure 3.8. The high frequency percussive ventilation was provided by (VDR-4®, Percussionaire, USA), while conventional ventilation was provided by (SERVO-i®, Maquet, Germany). The flow output of the ventilator was connected to a lung simulator (ACCU LUNG, Fluke Biomedical, USA) through a Fleisch pneumotachograph (Type 2, Lausanne, Switzerland) linked to a differential pressure transducer (0.25 INCH-D-4V, All Sensors, USA) for the measurement of airflow. The pressure measurement was performed by (ASCX01DN, Honeywell, USA) transducer. In order to interface pressure transducers, appropriate conditioning boards were designed and produced at Biomedical Instrumentation and Signal Processing Laboratory at University of Trieste. Each conditioning board mounts a pressure transducer and an eighth-order Butterworth low-pass filter (Maxim MAX291), with programmable −3 dB cut-off frequency (from 62 Hz to 100 kHz). The low-pass filter allows us to reduce the high-frequency noise that mainly affects the flow signal. The noise generated by turbulence in the pneumotachograph may introduce error in the volume estimation, as a result of the integration of noisy signal. However, low pass filtering with cut-off frequency in aforementioned range does not affect the percussive signal. The highest percussive frequency is 15 Hz (equal to 900 cycles min^{-1}). A connector block connects the conditioning boards to a data acquisition board PCI-6023E (National Instruments, Austin, USA). The acquisition board gets up to 200 kHz sampling and 12 bit resolution on eight differential analogue inputs. The integrated pulse generator is used to set the cut-off frequency of the on-board low-pass filter in conditioning boards. Pressure and flow measurements for each experimental setting were carried out for 60 s, while the sampling frequency was 2 kHz.

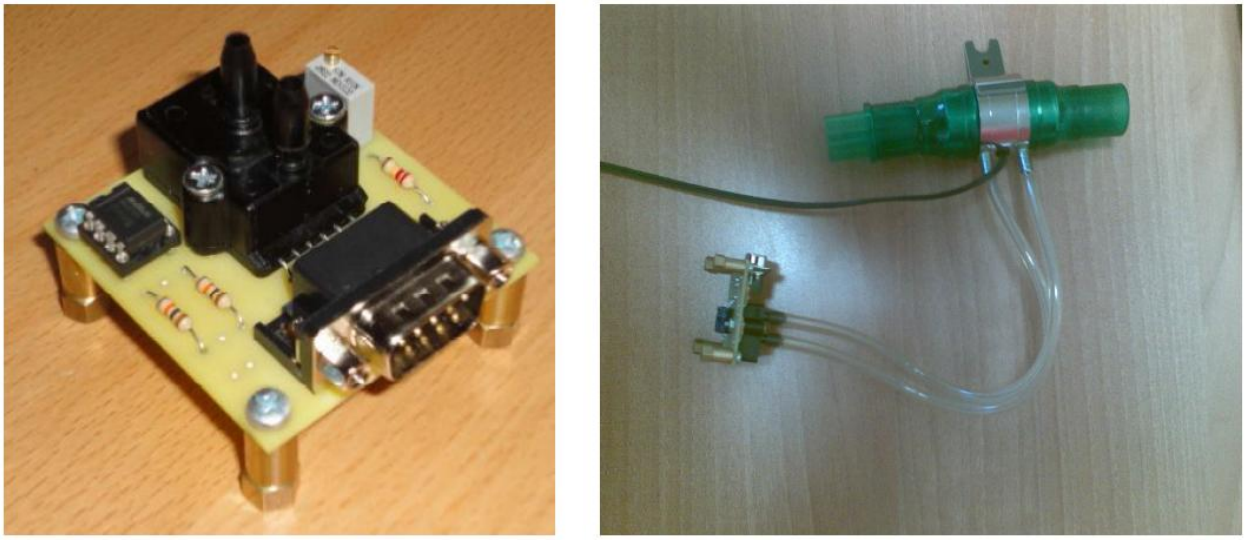

Figure 3.9 Pressure transducer (left panel) and Fleisch pneumotachograph linked to the differential pressure transducer (right panel), with corresponding conditioning boards.

The lung simulator was set up according all possible combinations of mechanical resistance (R) of 5, 20 and 50 $cmH_2O\ L^{-1}\ s$ and compliance (C) of 10, 20 and 50 mL cmH_2O^{-1} (corresponding to elastance values of 100, 50 and 20 $cmH_2O\ L^{-1}$, respectively). The lung simulator presents an inertance which can be considered negligible. The accuracy of the fixed resistance was 20% up to 2 $L\ s^{-1}$, and the accuracy of the fixed compliance was 10% up to 500 mL of tidal volume.

The SERVO-i® ventilator respiratory frequency was set up to 12 cycles min^{-1} with I/E 1:1 and the working pressure was set up to 30 cmH_2O with positive end-expiratory pressure (PEEP) = 0. During SERVO-i® measurements selected cut-off frequency of the on-board low-pass Butterworth filter was 125 Hz.

The HFPV ventilator VDR-4® was set up to respiratory frequency of 12 breaths min^{-1} with *I/E* 1:1 while the percussive frequency was progressively increased from 300 to 900 cycles min^{-1}. The working pressure was 20 cmH_2O with PEEP = 0. The expiratory phase was completely passive. The selected cut-off frequency of the on-board low-pass Butterworth filter was of 500 Hz.

In order to monitor pressure, flow and volume signals and estimate respiratory parameters a suitable elaboration system was developed and implemented in software which performs the following operations: The pressure and flow signals are acquired during a respiratory cycle and the exchanged volume within the cycle is calculated by integrating the flow with a trapezoidal rule. The computation of flow acceleration is

performed by the modified smooth noise Lanczos differentiator described by the following equation:

$$\ddot{V}_{n+1} = \frac{f_s}{28}(16 \cdot \dot{V}_n + \dot{V}_{n-1} - 10 \cdot \dot{V}_{n-3} - 6 \cdot \dot{V}_{n-4} + 9 \cdot \dot{V}_{n-5})$$

A single respiratory cycle is determined by three characteristic points identified on the pressure curve: a pressure-rise trigger point, a flow inversion point that demarks the transition between inspiratory and expiratory phase and a pressure-fall trigger point. The breath cycle is identified by considering the samples in the period from m_r samples before the pressure-rise trigger until m_f samples after the pressure-fall trigger. The respiratory mechanic parameters of previously described Dorkin model are estimated by applying the multiple linear regression (MLR) approach [45] on data acquired during the inspiratory phase of the analyzed respiratory cycle. The N acquired flow samples $\dot{V}$ together with corresponding volume V and volume acceleration $\ddot{V}$ are used to build the first three columns of an [N × 4] matrix A, while fourth column is composed of 1's. The corresponding N acquired samples of pressure P_{aw} are used to create an [N x 1] vector B. The estimation of the parameter vector θ was defined as:

$$\theta = \left(A^T \times A\right)^{-1} \times A^T \times B$$

with

$$\theta = \begin{bmatrix} E \\ R \\ I \\ P_0 \end{bmatrix}$$

$$A = \begin{bmatrix} V_1 & \dot{V}_1 & \ddot{V}_1 & 1 \\ V_2 & \dot{V}_2 & \ddot{V}_2 & 1 \\ \vdots & \vdots & \vdots & \vdots \\ V_{N-1} & \dot{V}_{N-1} & \ddot{V}_{N-1} & 1 \\ V_N & \dot{V}_N & \ddot{V}_N & 1 \end{bmatrix}$$

$$B = \begin{bmatrix} P_1 \\ P_2 \\ \vdots \\ P_{N-1} \\ P_N \end{bmatrix}$$

The computation time for the estimation of mechanical parameters is less than 1 s. The estimated values are calculated during expiratory phase and displayed on graphical user interface alongside pressure, flow and volume curves. Moreover, by implementing the estimated parameters to aforementioned motion equation the estimated pressure curve was constructed and superimposed onto the measured one. The mean square error is between the measured and the modeled pressure curve was calculated in order to verify the validity of the model. These operations are repeated for each respiratory cycle. Figure 3.9 shows the graphical user interface with the acquired pressure, flow and volume curves together with the estimated respiratory mechanic parameters during a single respiratory cycle.

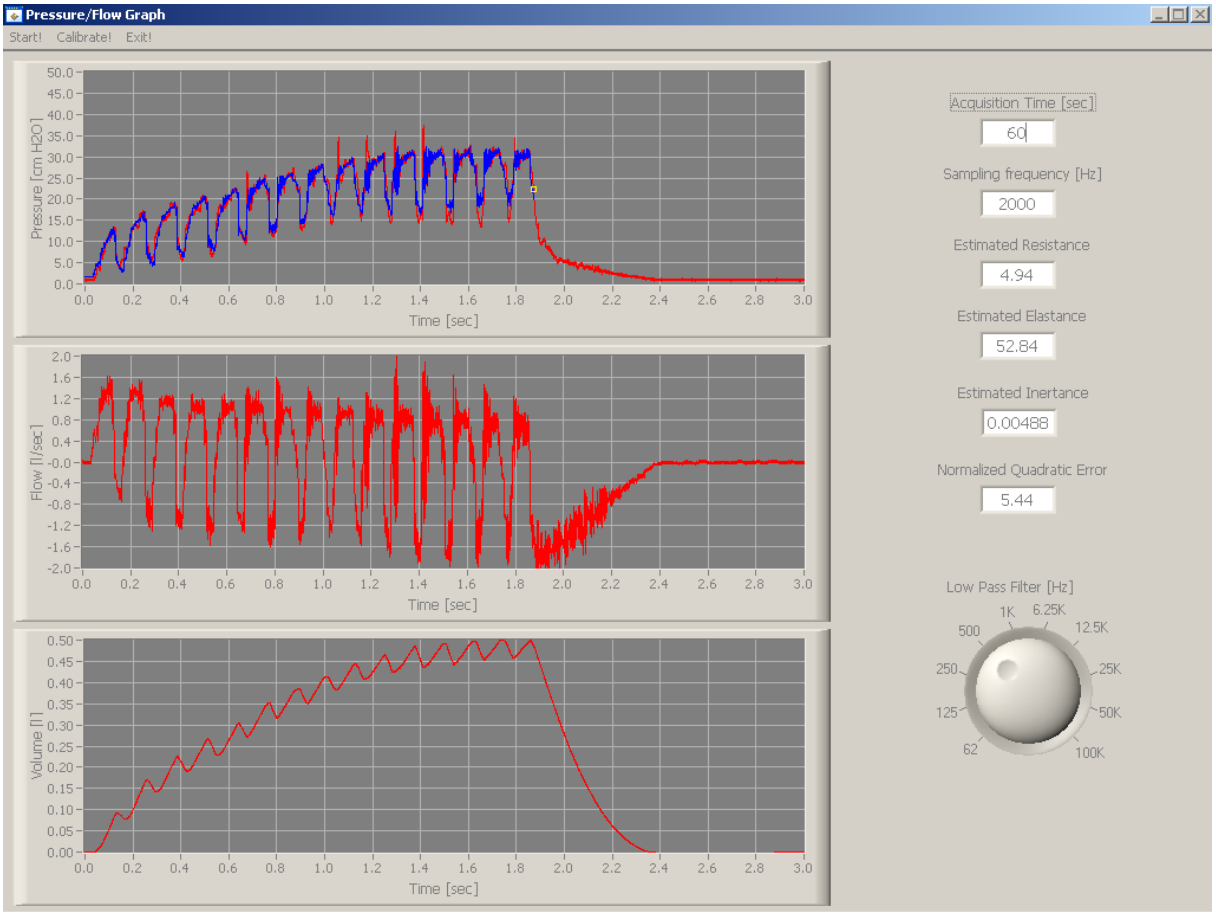

Figure 3.9 Graphical user interface with the acquired pressure, flow and volume curves together with the estimated respiratory mechanic parameters during a single respiratory cycle. From to bootom: measured pressure (red) superimposed on estimated pressure (blue) curve, measured flow and computed volume during a single high-frequency percussive respiration cycle [44].

Table 3.3 reports the mean and SD of estimated resistance R and elastance E values, undergoing conventional ventilation, together with corresponding % relative estimation errors (ΔR% and ΔE%) and normalized mean square error (NMSE) between the measured and the estimated pressure. The obtained estimated inertance I values were negligible. The mean and SD values were calculated over 12 successive respiratory cycles.

$R_{test\ lung}$ ($cmH_2O\ L^{-1}\ s$)	$E_{test\ lung}$ ($cmH_2O\ L^{-1}$)	$R_{estimated}$ mean ± 1SD ($cmH_2O\ L^{-1}\ s$)	ΔR %	$E_{estimated}$ mean ± 1SD ($cmH_2O\ L^{-1}$)	ΔE %	NMSE
5	20	5.9 ± 0.02	18.9%	24.4 ± 0.07	22.0%	0.03
20	20	22.2 ± 0.25	11.1%	19.9 ± 0.06	−0.2%	0.12
50	20	67.1 ± 0.83	34.2%	18.6 ± 0.14	−7.1%	0.94
5	50	5.1 ± 0.04	2.3%	60.1 ± 0.12	20.2%	0.09
20	50	17.4 ± 0.04	−13.2%	58.5 ± 0.12	17.0%	0.18
50	50	60.5 ± 0.75	21.0%	51.2 ± 0.28	2.3%	1.02
5	100	3.4 ± 0.09	−33.0%	125.7 ± 0.31	25.7%	0.22
20	100	14.6 ± 0.11	−26.8%	118.7 ± 0.64	18.7%	0.23
50	100	46.4 ± 0.10	−7.2%	111.2 ± 0.35	11.2%	0.38

Table 3.3 Resistance and elastance values estimated during conventional ventilation provided by the SERVO-i® ventilator. Pressure and flow measurements were carried out for 60 s (mean and SD values were calculated over 12 successive respiratory cycles) [44].

The values of estimated parameters during the conventional mechanical ventilation are very similar to the values set on the lung simulator. The lows standard deviation values indicate the good repeatability of this indirect measurement. Moreover, low NMSE shows that the model adequately estimates the behavior of the lung simulator. Jackson *et al.* obtained a similar level of accuracy (i.e. 20% of set values) during the measurement of respiratory mechanics compared to the known values of a neonatal lung simulator [46]. The results of resistance and compliance estimation of a lung model using the occlusion technique has also been reported (worst case −22% for compliance and +189% for resistance) [47].

In Table 3.4 are reported the mean and SD values of estimated resistance R and elastance E, during HFPV ventilation, together with corresponding % relative estimation errors (ΔR% and ΔE%) and normalized mean square error (NMSE). Also in this case the estimated inertance I values were negligible. The mean and SD values were calculated over 12 successive respiratory cycles.

$R_{test\ lung}$ ($cmH_2O\ L^{-1}\ s$)	$E_{test\ lung}$ ($cmH_2O\ L^{-1}$)	$R_{estimated}$ mean ± 1SD ($cmH_2O\ L^{-1}\ s$)	ΔR %	$E_{estimated}$ mean ± 1SD ($cmH_2O\ L^{-1}$)	ΔE %	NMSE
5	20	4.9 ± 0.16	−1.3%	21.9 ± 0.19	9.4%	2.8
20	20	13.7 ± 0.16	−31.7%	23.6 ± 0.51	18.0%	4.7
50	20	37.2 ± 0.56	−25.7%	31.7 ± 1.42	58.6%	22.9
5	50	5.0 ± 0.07	−0.70%	54.8 ± 1.66	9.6%	5.9
20	50	14.7 ± 0.26	−26.4%	52.1 ± 0.78	4.2%	10.0
50	50	42.2 ± 0.70	−15.6%	62.1 ± 1.45	24.1%	37.8
5	100	4.9 ± 0.06	−1.4%	116.4 ± 5.37	16.4%	5.3
20	100	13.2 ± 0.15	−33.7%	116.9 ± 4.27	16.9%	9.9
50	100	41.2 ± 0.63	−17.6%	109.8 ± 1.84	9.8%	36.5

Table 3.4 Resistance and compliance values estimated during HFPV provided by the VDR-4® percussive ventilator (f_p= 450 cycles min^{-1}). Pressure and flow measurements were carried out for 60 s (mean and SD values were calculated over 12 successive respiratory cycles) [44].

The estimation errors of the nominal resistance and elastance values within 20% range are retained acceptable in respiratory mechanics measurements [46].

Analyzing the estimation results, it is possible to make a distinction between three different cases:

- R= 5 $cmH_2O\ L^{-1}s$;
- R= 20 $cmH_2O\ L^{-1}s$
- R= 50 $cmH_2O\ L^{-1}s$

In the first case, referring to the mean frequency of 450 cycles min^{-1} (table 3.4), the mean square errors were low and the resistance and elastance estimation presented acceptable errors, smaller than 1.4% and 16.4% of their nominal values, respectively.

In the case of R= 20 $cmH_2O\ L^{-1}s$, the R and E estimation errors were higher than those in case of R= 5 $cmH_2O\ L^{-1}s$, < 33.7% and <18.0%, respectively.

On the other hand, in the case of 50 $cmH_2O\ L^{-1}s$, the mean square errors between measured and model estimated pressure were significantly higher. This fact indicates difficulty for used the model to reproduce experimental data in these conditions.

The comparison between the lung simulator set parameters and the corresponding estimated parameters at four different percussive frequencies (300, 500, 700 and 900 cycles min^{-1}) is reported in the figure 3.10. The results showed the clear dependence of estimated parameters on percussive frequency.

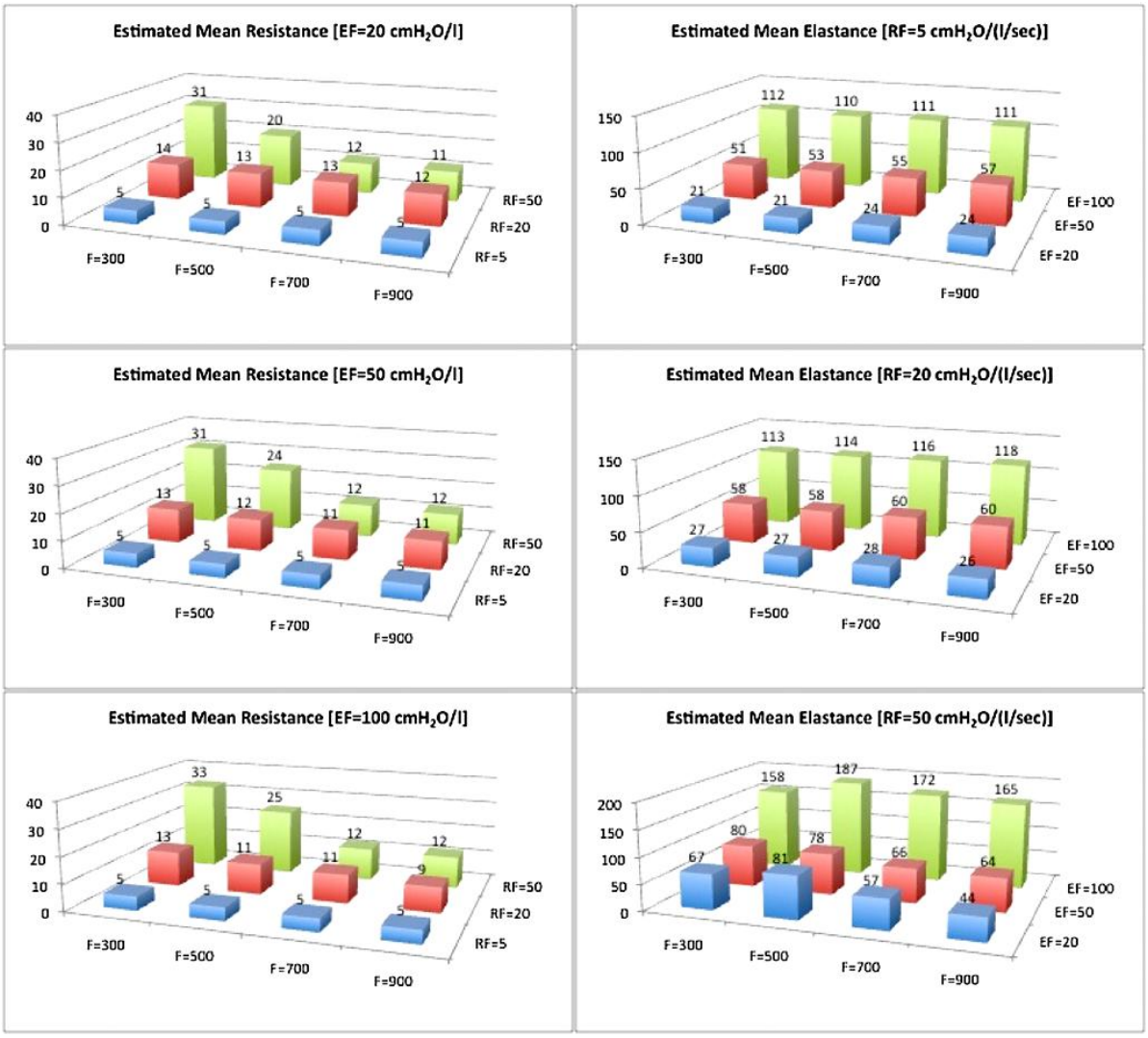

Figure 3.10 VDR-4: *R* mean and *E* mean values at different percussive frequencies [44].

Even if the results are probably affected by the intrinsic limit of the lung model, as frequency dependence and a nonlinear behavior at the highest resistance, the possibility to have real-time respiratory parameter monitoring is useful from the clinical point of view. It is important to point out that the lung elastance is the main factor to avoid volutrauma during pressure controlled ventilation logic [48]. For this reason the accurate estimation of elastance obtained by the computerized system is very important to correctly set the ventilator. In the present investigation, our mathematical model constantly overestimates the elastance, avoiding the hazard of hyperinflation during HFPV. On the other hand, the resistance underestimation seems to have a limited impact on volume delivery.

3.3 *In vitro* estimation of endotracheal tube pressure drop

Endotracheal tube (ETT) is routinely used in clinical practice to connect the artificial ventilator to the airway of a patient undergoing mechanical ventilation (figure 3.11).

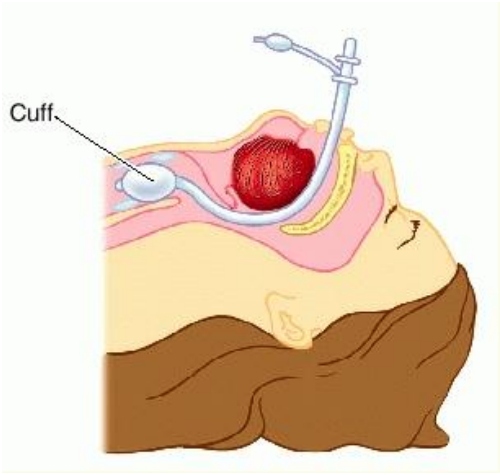

Figure 3.11 Endotracheal tube (from Medical dictionary)

However, its presence contributes an extra mechanical burden to the respiratory system [49-50]. The airway pressure supplied by ventilator represents the sum of the endotracheal tube pressure drop (ΔP_{TT}) and the pressure dissipated to inflate lung. From the clinical point of view, it is of paramount importance to take into account the real amount of pressure dissipated by endotracheal tube to avoid baro and volutrauma [51].

Several approaches have been developed to estimate the mechanical characteristics of the various kinds of endotracheal tubes. Under certain conditions, e.g., laminar low flow, the pressure-flow relationship characterizing endotracheal tubes may be considered linear [52-53], and the pressure drop can be calculate by following equation:

$$\Delta P_{TT}(t) = R_{tube} \cdot \dot{V}(t)$$

where $\dot{V}(t)$ is airflow while R_{tube} represents linear tube resistance.

However, in most cases a non-linear pressure-flow relationship has been found. In such cases this relationship has been generally described as:

$$\Delta P_{TT}(t) = K_1 \cdot \dot{V}(t) + K_2 \cdot \dot{V}^2(t)$$

or

$$\Delta P_{TT}(t) = a \cdot \dot{V}^{b}(t)$$

where $\dot{V}(t)$ represents flow, K_1 and K_2 are the Rohrer's constants [54], and a and b are constants that define the power function [51][55-57].

Moreover, another approach to estimate in vitro adult and neonatal ΔP_{TT} was proposed by Blasius that suggested a formula for circular tubes P_{TT} [58-59]:

$$\Delta P_{TT}(t) = K_b \cdot \dot{V}^{1.75}(t)$$

where, $\dot{V}(t)$ represents the flow and K_b is the constant that depends on the inner geometry of the tube and the physical properties of the gas [58-59].

During high frequency ventilation (HFV) the aforementioned approaches do not properly describe the pressure-flow relationship in endotracheal tubes possibly because of the turbulence and the presence of mechanical inertance (I). In fact, the latter was taken into consideration under high-frequency oscillatory ventilation (HFOV) [60]. The pressure drop due to inertial effects can be defined as follows:

$$\Delta P_{TI}(t) = I \cdot \ddot{V}(t)$$

where $\ddot{V}$ represents the volume acceleration.

In order to characterize in vitro the mechanical behavior of endotracheal tubes under HFPV, the modelling of pressure-flow relationship under different working pressures, percussive frequencies, and added mechanical loads was performed [61].

3.3.1. Material and methods

The experimental setup used in this study [61] is shown in figure 3.12. A physical model of respiratory system was provided by a single-compartment lung simulator (ACCU

LUNG, Fluke Biomedical, Everett, WA, USA). In our measurements the lung simulator was set according to all the combinations of resistive loads (R), namely, 5 and 20 cmH_2O L^{-1} s and elastic loads (E): 20, 50, and 100 cmH_2O L^{-1}.

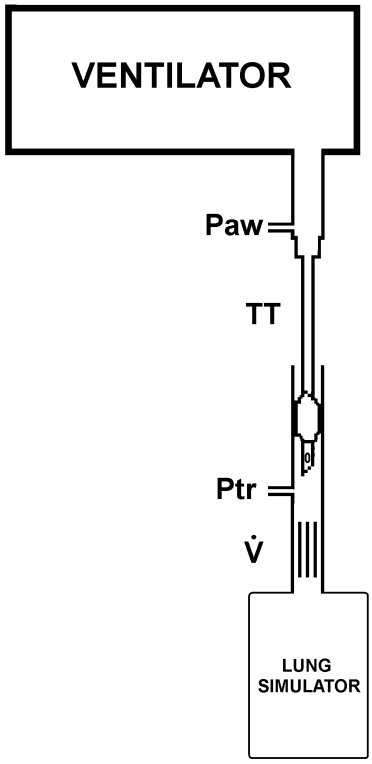

Figure 3.12 Experimental set-up. Paw and Ptr pressures measured before and after the endotracheal tube (TT), respectively. V̇, pneumotachograph [61].

The lung simulator was connected to a no. 2 Fleisch pneumotachograph (Lausanne, Switzerland) linked to a differential pressure transducer (0.25 INCH-D-4V, All Sensors, Morgan Hill, CA, USA) for the measurement of airflow. Its other extremity was attached to a tube with a sideport for the measurement of endotracheal pressure (Ptr) by means of a differential pressure transducer (ASCX01DN, Honeywell, Morristown, NJ, USA). Endotracheal tube sizes 6.5, 7.5 and 8 (Rusch, Milan, Italy) were indwelled into the artificial trachea. Their cuffs were inflated to avoid leaks. These tubes sizes were chosen because they are the most frequently used in adolescent and adult patients. Another differential pressure transducer followed (ASCX01DN, Honeywell, Morristown, NJ, USA) for the measurement of airway pressure (Paw). Finally, a high-frequency percussive ventilator (VDR-4®, Percussionaire Corporation, Sandpoint, ID, USA) was linked to the circuit.

The VDR-4® ventilator was set to deliver a pulse inspiratory/expiratory (i/e) duration

ratio of 1:1, and inspiratory and expiratory duration (TIn and TEx) ratio of 1:1 [33][38]. The tele-inspiratory work pressure (P_{Work}), i.e., peak inspiratory pressure measured by the VDR-4® ventilator, was progressively increased in 5-cmH_2O steps from 20 to 45 cmH_2O, resulting in different airflow rates. The percussive frequency was set to 300, 500 and 700 cycles/min. Measurements were performed for all 108 possible combinations of loads, frequencies, and work pressures for each ETT size. Each measurement setting included three respiratory cycles. The signals were sampled at 2 kHz by a 12-bit acquisition board (PCI-6023E, National Instruments, Austin, TX, USA) and fed into a low-pass second order Butterworth filter (cut-off frequency 35 Hz).

Volume acceleration ($\ddot{V}$) was calculated by numerical differentiation of the air flow using low-noise Lanczos differentiator. ΔP_{TT} was calculated by subtracting Ptr from Paw during the inspiratory phase exclusively.

The endotracheal pressure drop was characterized during the inspiratory phase of the breathing cycle by parametric identification of coefficients pertaining to the three proposed models, defined according to the following equations:

Model 1: $\Delta P_{TT}(t) = R_{tube} \cdot \dot{V}(t) + I \cdot \ddot{V}(t)$

Model 2: $\Delta P_{TT}(t) = K_1 \cdot \dot{V}(t) + K_2 \cdot \dot{V}^2(t) + I \cdot \ddot{V}(t)$

Model 3: $\Delta P_{TT}(t) = K_b \cdot \dot{V}^{1.75}(t) + I \cdot \ddot{V}(t)$

Model 1 is characterized by linear resistive [$R_{tube} \cdot \dot{V}(t)$] and inertial [$I \cdot \ddot{V}(t)$] terms. Model 2 takes into consideration Rohrer's approach [$K_1 \cdot \dot{V}(t) + K_2 \cdot \dot{V}^2(t)$] and inertance [$I \cdot \ddot{V}(t)$]. In Model 3 the pressure drop caused by friction is represented by the non-linear Blasius component [$K_b \cdot \dot{V}^{1.75}(t)$] and the inertial term [$I \cdot \ddot{V}(t)$]. In this study we assumed that coefficients include both distributed and concentrated pressure drops. The latter takes into account the connectors and the effect of abrupt changes in cross sectional area [62-63]. The least squares method was used to estimate the coefficients pertaining to the different models. The estimation of the parameter vectors θ_1, θ_2 and θ_3 for the three Models was defined as:

$$\theta_i = \left(A^T \times A\right)^{-1} \times A^T \times B \quad i=1,2,3$$

with

$$\theta_1 = \begin{bmatrix} R_{tube} \\ I \end{bmatrix} \qquad \theta_2 = \begin{bmatrix} K_1 \\ K_2 \\ I \end{bmatrix} \qquad \theta_2 = \begin{bmatrix} K_b \\ I \end{bmatrix}$$

$$A_1 = \begin{bmatrix} \dot{V}_1 & \ddot{V}_1 \\ \dot{V}_1 & \ddot{V}_2 \\ \vdots & \vdots \\ \dot{V}_N & \ddot{V}_N \end{bmatrix}$$

$$A_1 = \begin{bmatrix} \dot{V}_1 & \dot{V}_1^{\,2} & \ddot{V}_1 \\ \dot{V}_1 & \dot{V}_2^{\,2} & \ddot{V}_2 \\ \vdots & \vdots & \vdots \\ \dot{V}_N & \dot{V}_N^{\,2} & \ddot{V}_N \end{bmatrix}$$

$$A_1 = \begin{bmatrix} \dot{V}_1^{1.75} & \ddot{V}_1 \\ \dot{V}_2^{1.75} & \ddot{V}_2 \\ \vdots & \vdots \\ \dot{V}_N^{1.75} & \ddot{V}_N \end{bmatrix}$$

$$B = \begin{bmatrix} \Delta P_1 \\ \Delta P_2 \\ \vdots \\ \Delta P_N \end{bmatrix}$$

The matrix elements $\dot{V}_n$, $\ddot{V}_n$, ΔP_{TTn}, where n = 1,2, … N is the sample index , N is the number of acquired samples for each experimental setting and tube.

As indicator of the adequacy of the model used to describe the measured system, the residual root mean square error (RMSE) was calculated:

$$\mathrm{RMSE} = \sqrt{\frac{\sum_{k=0}^{N-1}\left[\Delta P_{TTm}(kT) - \Delta P_{TTe}(kT)\right]^2}{N}}$$

where ΔP_{TTm} and ΔP_{TTe} represent the measured and estimated ΔP_{TT}, respectively, N is the number of samples, and T represents the sampling period.

Endotracheal tubes display an inertial fluid dynamic component proportional to the volume acceleration ($\ddot{V}$), particularly evident during HFV, which also consumes energy in

terms of pressure drop. In addition to the estimated inertance with aforementioned method, its theoretical value based on fluid dynamics laws was also calculated:

$$I = \rho L\ A^{-1}$$

where ρ is the gas density, L the tube length and A the cross-sectional area [64].

The RMSE and inertance pertaining to the three models were compared. The normal distribution of the data and the homogeneity of the variances were assured by the Kolmogorov-Smirnov (with Lilliefors' correction) and Levene median tests, respectively. One-way ANOVA was then applied and since statistically significant values were found, Bonferroni's post hoc test was used to assess differences among the three models. $\alpha = 5\%$. Statistical analysis was performed using Statistica 6.1 software (StatSoft, Vigonza, Italy).

3.3.2 Results and Discussion

Three measurements were done in each condition (108 for each model). The reproducibility of the estimated parameters was assessed as the median and range of the corresponding coefficients of variation, as listed in table 1. Model 2 presented the broadest range of variability, whereas model 3 displayed the narrowest range. Inertance data were similar in the three models.

Constants	Tube 8		Tube 7.5		Tube 6.5	
			Model 1			
R ($cmH_2O\ L^{-1}\ s$)	0.0065	(0.0003-0.0662)	0.0055	(0.00001-0.046)	0.0034	(0.0002-0.0560)
I ($cmH_2O\ L^{-1}\ s^2$)	0.0106	(0.0001-0.2016)	0.0055	(0.0003-0.217)	0.0105	(0.00045-0.215)
			Model 2			
K_1 ($cmH_2O\ L^{-1}\ s$)	0.0827	(0.0058-6.8510)	0.1004	(0.0002-11.62)	0.0871	(0.0023-10.0)
K_2 ($cmH_2O\ L^{-2}\ s^2$)	0.0445	(0.0048-0.8230)	0.0263	(0.0002-4.456)	0.0229	(0.0001-5.110)
I ($cmH_2O\ L^{-1}\ s^2$)	0.0105	(0.00001-0.2011)	0.0055	(0.0006-0.2157)	0.0106	(0.0003-0.214)
			Model 3			
K_b ($cmH_2O\ L^{-1.75}\ s^{1.75}$)	0.0065	(0.0004-0.0300)	0.006	(0.0001-0.060)	0.0034	(0.0001-0.0588)
I ($cmH_2O\ L^{-1}\ s^2$)	0.0105	(0.00001-0.2012)	0.0055	(0.0006-0.2160)	0.0106	(0.0003-0.214)

Table 3.5 Reproducibility of the estimated parameters. Values are expressed as median and (range) of coefficients of variation of the measurements of three consecutive breaths for each model considering the possible 108 settings in each one. R, resistance. I, inertance. K_1 and K_2, are Rohrer's constants. K_b, Blasius' constant. [61]

RMSE was measured in all 108 possible combinations of loads, frequencies, work pressures for each ETT sizes. In all instances model 1 presented RMSE values significantly higher than those in models 2 and 3 (table 2), and no significant difference was detected between models 2 and 3. Correlation coefficients between gathered curves and fitted data are very similar among the three methods.

Model	Tube 8	Tube 7.5	Tube 6.5
	RMSE (cmH_2O)		
1	1.097±0.38	1.661±0.57	1.720±0.57
2	0.915±0.29	1.330±0.35	1.330±0.30
	$P = 0.00011$	$P < 0.00001$	$P < 0.00001$
3	0.933±0.28	1.400±0.38	1.038±0.32
	$P = 0.00062$	$P = 0.00007$	$P < 0.00001$
	Correlation coefficient		
1	0.964 (0.895 - 0.994)	0.958 (0.886 - 0.990)	0.970 (0.911 - 0.991)
2	0.974 (0.906 - 0.995)	0.969 (0.893 - 0.993)	0.980 (0.916 - 0.994)
3	0.973 (0.906 - 0.995)	0.970 (0.895 - 0.993)	0.981 (0.914 - 0.995)

Table 3.6 Root mean square errors and correlation coefficients between experimental and fitted curves. Mean ± SD of 108 different experimental conditions (three measurements per condition) of root mean square errors (RMSE) and median (range) of correlation coefficients. Model 1 assumes a linear relationship between pressure and flow; model 2 introduces a flow-dependent quadratic equation; and model 3 incorporates the term $\dot{V}^{1.75}$. *P* values describe difference between models 2 and 3 versus model 1. No significant difference was detected between models 2 and 3. [61]

Figure 3.13 depicts the mean and standard deviations of estimated inertance in the three models plotted against P_{Work} obtained for all 108 possible combinations of loads and frequencies. Inertances (I) were similar in the three models [0.081 ± 0.005, 0.096 ± 0.0006 and 0.095 ± 0.0007 $cmH_2O\ L^{-1}\ s^2$ (mean ± SD) for tubes 8, 7.5 and 6.5, respectively], but significantly different among tube sizes ($P < 0.002$). Furthermore they were very close to I calculated based on fluid dynamics, i.e., 0.081, 0.097 and 0.111 $cmH_2O\ L^{-1}\ s^2$ for tubes 8, 7.5 and 6.5, respectively.

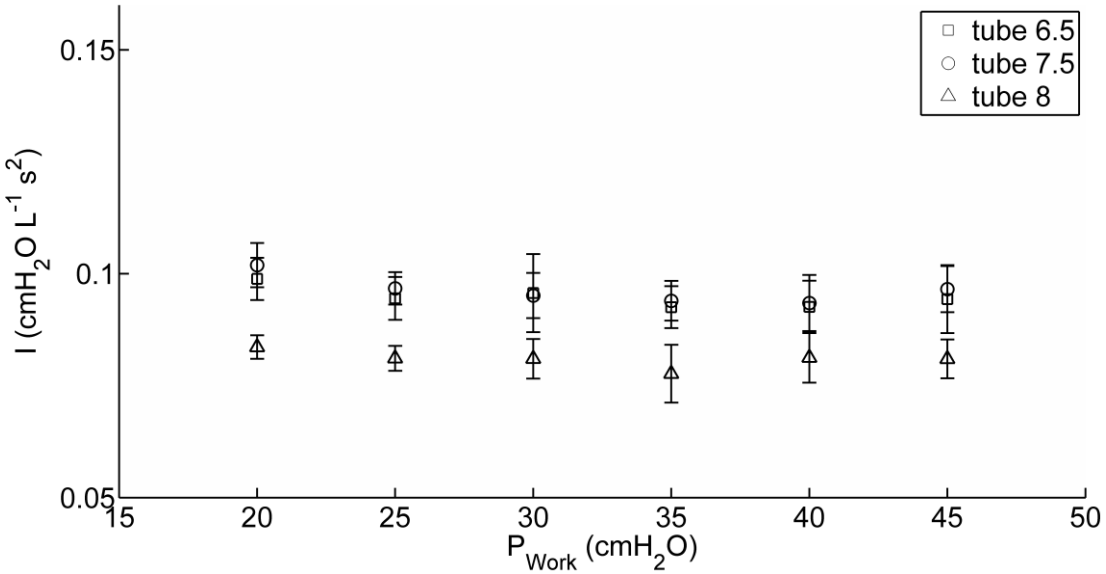

Figure 3.13 Inertance (I) plotted versus working pressures for different endotracheal tubes. Each data point is the average of 18 estimated model constants encompassing two and three resistive and elastic loads, respectively, and 3 percussive frequencies. Bars, ±SD. Open squared, circles and triangles represent tubes 6.5, 7.5, and 8.0, respectively.

Figure 3.14 shows the mean and standard deviations of the estimated parameters pertaining to the three proposed models plotted against P_{Work} obtained for all 108 possible combinations of loads and frequencies. The results obtained for the three endotracheal tubes are depicted. $R_{tube,}$ K_1 and K_2 values depended on P_{Work}, which was not the case for the K_b value. Furthermore, $R_{tube,}$ K_1 and K_2 values presented higher variabilities than the K_b parameter.

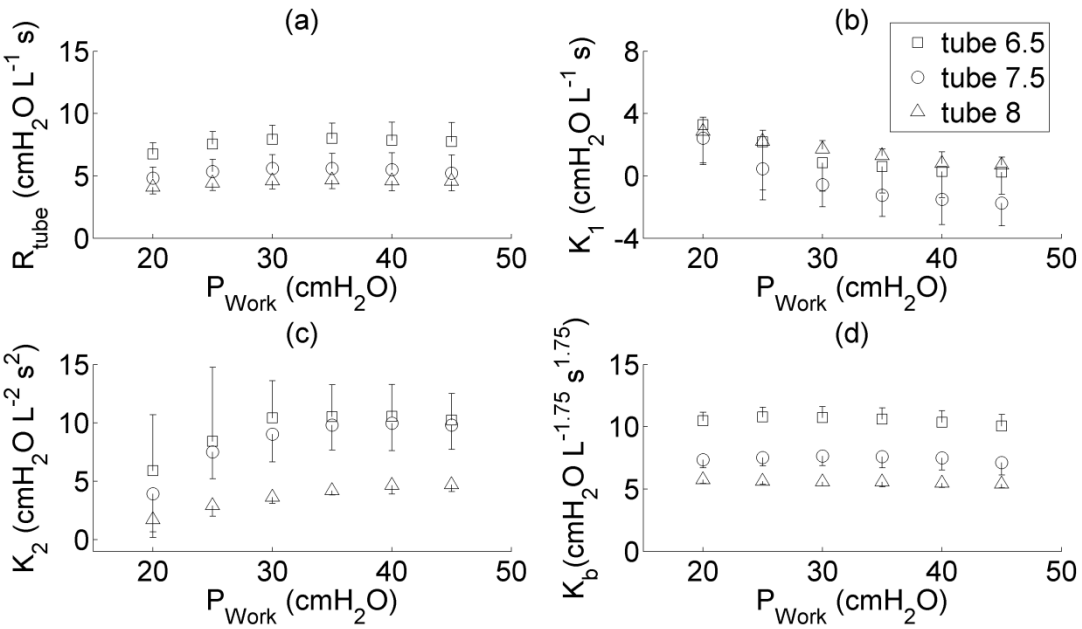

Figure 3.14 Estimated model constants plotted against working pressure (P_{Work}). (a) linear model (#1), R_{tube}, Newtonian flow resistance. (b and c) model #2, K_1 and K_2, Rohrer's coefficients. (d) Blasius' constant, K_b (model #3). Each data point is the average of 18 estimated model constants encompassing two and three resistive and elastic loads, respectively, and 3 percussive frequencies. Bars, + or – SD. Open squares, circles and triangles represent tubes 6.5, 7.5, and 8.0, respectively. [61]

In Figure 3.15 pulsatile flow, Paw, Ptr and ΔP_{TT} (= Paw - Ptr) tracings during one inspiration (R = 5 $cmH_2O\ L^{-1}$ s; E = 50 $cmH_2O\ L^{-1}$; percussive frequency = 300 cycles/min; P_{Work} = 25 cmH_2O and tube size = 8) are shown. ΔP_{TT} is represented as measured and also calculated with models 1, 2 and 3. To facilitate identification of the four ΔP_{TT} curves one mini-burst (identified in the third tracing from top to bottom was expanded and depicted as a fourth tracing). It can be seen that models 2 and 3 closely fitted the experimentally registered ΔP_{TT} curve.

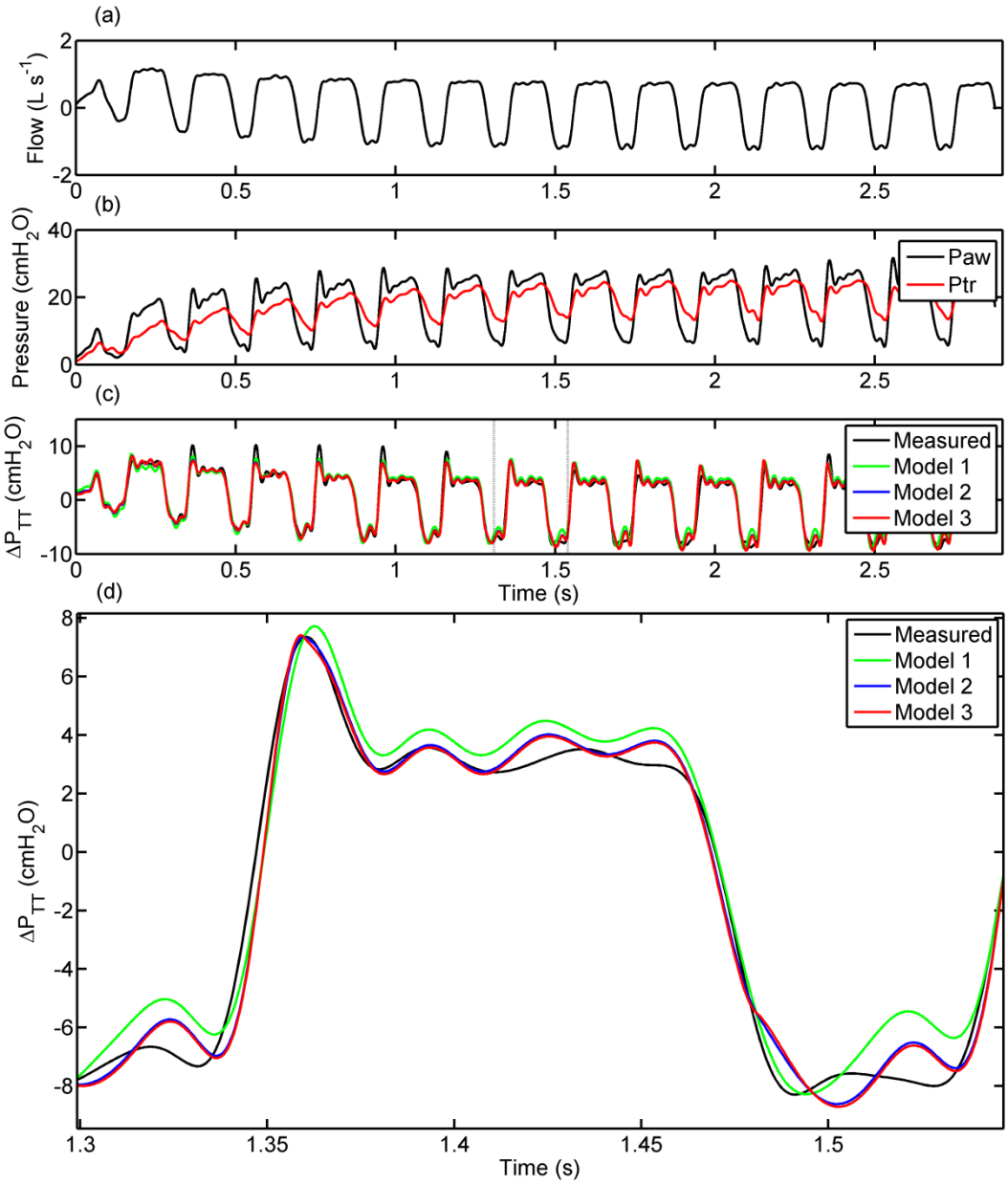

Figure 3.15 Flow and pressures tracings during one inspiration under high-frequency percussive ventilation. Panel (a) shows pulsatile flow; panel (b) displays Paw (black) and Ptr (red); in panel (c) ΔP_{TT} is represented as the measured curve (black) and also calculated with models 1 (green), 2 (blue) and 3 (red); panel (d) shows one ΔP_{TT} mini-burst identified in panel (c). [61]

Medians and ranges of the 108 measured pressure drops across each tube (ΔP_{TT}) during the inspiratory phase of the mini-bursts were also calculated: 9.28 (4.95-12.93), 9.48 (5.05-13.47), and 10.04 (5.62-16.97) cmH_2O for tubes 8, 7.5 and 6.5, respectively.

From the clinical point of view the real time estimation of endotracheal tube contribution to pressure losses within the breathing system is of paramount importance.

Frequently the physician can only assess the pressure delivered by the ventilator, usually measured before the tubing ensemble (endotracheal tube included) linking the ventilator to the patient. This pressure does not represent that actually delivered to the patient. If the latter pressure is too high, barotraumas may ensue [65]. Thus, a tool that can provide information about the endotracheal tube flow-dependent resistance during HFPV and that could also be implemented in future monitoring systems is wanted.

Three simple common models relating ΔP_{TT} and flow were tested. Model 1 assumes a linear relationship between pressure and flow; model 2 introduces a flow-dependent quadratic equation; and model 3 incorporates the term $\dot{V}^{1.75}$. Inertance is included in all three models since the ventilatory mode is based on high-frequency pulsatile flow. Using two and three diverse resistive and elastic loads, respectively, three percussive pressures, and six working pressures, 108 different combinations were generated, and three breathing cycles were measured in each one of them. The smallest variability among the measurements of the estimated parameters was presented by model 3, while model 2 depicted the broadest range of results (Table 3.5).

To the experimental pressure and flow curves the three aforementioned models were fitted using the least square method. The similarity between the correlation coefficients (Table 3.6) would suggest that the three models adequately fitted the experimental data. However, considering that RMSE is a measure of the differences between values estimated by a model and the values actually observed in an experiment, we used it to evaluate the goodness of our fittings. Table 3.6 shows that Model 1 presented significantly higher RMSE than Models 2 and 3, and that the latter did not differ between them. Thus, the former is not as accurate as the latter, possibly due to turbulence, a term not included in Model 1, as previously reported [58-59] [64]. Furthermore, Models 2 and 3 seem to present the same predictive power. Following the parsimony principle we have to consider Model 3 more convenient than Model 2 [66]. Model 2 is frequently used in respiratory physiology to describe pressure-flow relationships. Blasius' formula was used to determine the effect of mucus deposition on the effective diameter of endotracheal tubes in patients [59], and to calculate in vitro the pressure drop along pediatric endotracheal tubes under constant flow [58]. The latter study reports that a linear model can adequately describe flow-pressure relationship under laminar flow, but when turbulence ensues, Blasius' formula represents a better descriptor of the system [58]. On the other hand, in a pediatric study with high-

frequency oscillation, Blasius' and Rohrer's formulas resulted inaccurate to calculate pressure drop across endotracheal tubes based on measured flows [60]. Hence, our study fitted experimentally generated pressure and flow signals with a linear and two non-linear models and estimated R_{tube} K_1, K_2, K_b and I.

The estimated coefficients are plotted against P_{Work} (figure 3.16). The wider the tube the smaller is the SD in all instances and the smaller are the estimated coefficients, except for K_1. The large variability of estimated Rohrer's coefficients has also been previously reported [60]. Additionally, K_b does not depend on P_{Work}, in opposition to the other coefficients. Finally, K_b presents the smallest SD. Indeed, the overall means±SDs were 5.57±0.34, 7.46±0.84; and 10.51±0.87 $cmH_2O\ L^{-1.75}\ s^{1.75}$ for tubes 8.0, 7.5 and 6.5, respectively. The corresponding coefficients of variation were 0.061, 0.11, 0.08. The median values did not differ appreciably from the means. It should be stressed that each point represents data collected with two resistive and three and elastic loads, and three pulsatile frequencies, i.e., each point is a lumped value. Taken together these results strongly suggest that estimated K_b is the most robust resistance-related coefficient calculated in our study.

Other models [57] under conventional mechanical ventilation take into consideration the asymmetry between inspiratory and expiratory phases, expressed by their exponents K2. In HFPV each inspiration comprises many mini-bursts, which in our case presented frequencies amounting to 300, 500 and 700 cycles/min. Each mini-burst represents one mini-inspiration and a mini-expiration [33][38]. In their study [57] the results are expressed considering inspiration and expiration separately. In our case, we have inspiratory and expiratory phases in each mini-burst plus the whole cycle inspiration and expiration, which would result in a series of values possibly difficult to be handled and understood in clinical practice. Furthermore, the aforementioned models do not take into consideration inertance, which represents an important mechanical component in high-frequency ventilation, as seen in Figure 4.

Because inertial forces are negligible during tidal breathing they are usually disregarded in curve fitting [67]. However inertance may became important during fast breathing, which is the case in HFPV. For this reason we included an inertial term in our models, as also reported in other studies [44][60][64][68-69]. In figure 3.16 the measured ΔP_{TT} was split into its inertance-dependent ($\Delta P_{TT}I$) and resistive-dependent ($\Delta P_{TT}R$)

components. The former plays a major role during rapid changes in ΔP_{TT}, whereas the latter responds for the slower variations in ΔP_{TT}, corresponding to the phases where gas accelerations are high and small, respectively. Once again there is no single value for the contributions of either I or R to $\Delta P_{TT.}$ This finding applies to all settings.

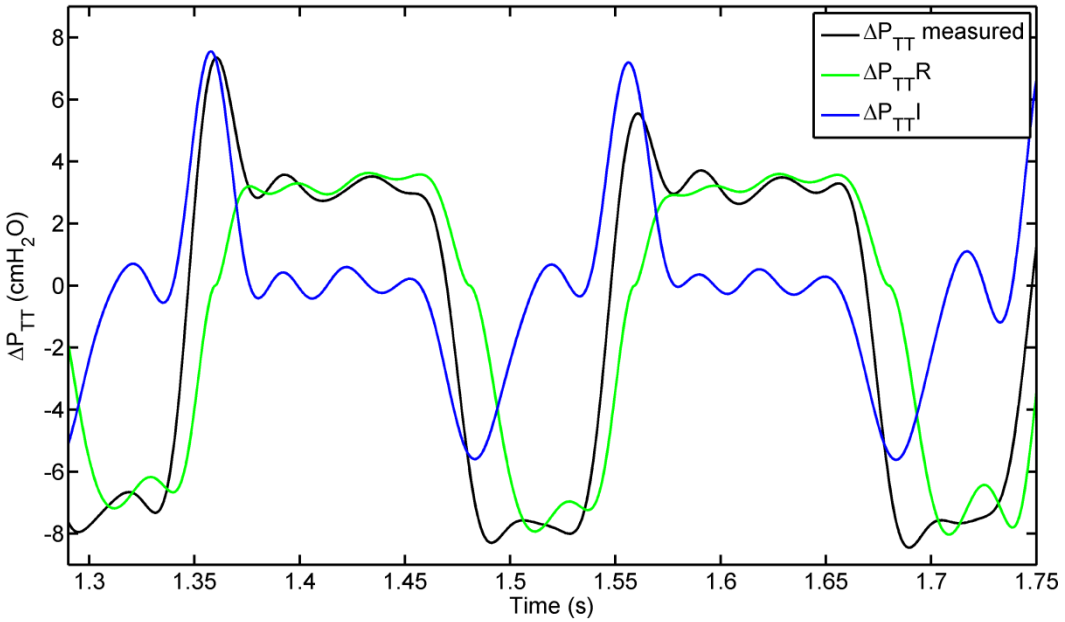

Figure 3.16 The measured ΔP_{TT} (black line) and its inertance-dependent (blue line $\Delta P_{TT}I$) and resistive-dependent (green line $\Delta P_{TT}R$) components are shown for two complete mini-bursts (R = 5 $cmH_2O\ L^{-1}$ s; E = 50 $cmH_2O\ L^{-1}$; percussive frequency = 300 cycles/min; P_{Work} = 25 cmH_2O and tube size = 8). [61]

In the present study the estimated inertances did not vary among the models, thus rendering inertia not responsible for the differences in fitting the models to the experimental data using the same tube. However, possibly due to geometric factors [64][68-69], inertance varied in the present work according to tube size.

Considering that for each tube size only Model 3 is characterized by two constant coefficients (resistance- and inertia-dependent), it may be very useful for the clinician: using two constants and the flow value he/she may be able to estimate the average pressure lost owing to the endotracheal tube as:

$\Delta P_{TT}(t) = 5.57\ \dot{V}^{1.75}(t) + 0.081\ \ddot{V}(t)$ (tube 8)

$\Delta P_{TT}(t) = 7.46\ \dot{V}^{1.75}(t) + 0.096\ \ddot{V}(t)$ (tube 7.5)

$\Delta P_{TT}(t) = 10.51\ \dot{V}^{1.75}(t) + 0.095\ \ddot{V}(t)$ (tube 6.5)

This study present some limitations: (a) results were gathered under HFPV; (b) resistive and elastic loads, pulsatile frequency were constrained within specific ranges; (c) clinical limitations may also arise: curvature of the tube, its partial blockage due to mucus and/or condensed water vapour, and connectors.

3.4 *In vivo* data acquisition system during HFPV

The measurements on patients undergoing HFPV were performed with a device suitably designed for bedside measurements during this particular high frequency modality. The flow and pressure measurements were performed with aforementioned transducers: Fleisch pneumotachograph (Type 2, Lausanne, Switzerland) linked to a differential pressure transducer (0.25 INCH-D-4V, All Sensors, USA) for the measurement of airflow and pressure transducer (ASCX01DN, Honeywell, USA) for pressure measurement. The volume and volume acceleration were calculated by numerical integration and differentiation of flow, respectively. In order to interface transducers new conditioning boards were designed and produced at Biomedical Instrumentation and Signal Processing Laboratory at University of Trieste. Conditioning boards in addition to transducers mount a DC/DC converter for power supply of sensors and a second-order Butterworth low-pass filter. The filters were designed using Sallen-Key configuration and the cut-off frequency was 300Hz. The acquisition board NI USB-6009 (National Instruments, Austin, USA) connected to PC notebook was used for analogue to digital conversion of pressure and flow signals. The signals were sampled at 2kHz with 14-bit resolution. The visualisation and registration of acquired data was managed by suitable graphical user interface. The acquisition device was supplied using power supply output on NI-USB-6009 which was supplied by PC notebook battery. Thus, there was no risk of electrical injury.

The VDR-4® output was connected to endotracheal tube of intubated patient trough a Fleisch pneumotachograph and a sideport for pressure measurement. To prevent water vapour condensation in the duct system, the apparatus was heated for five minutes before and during use, by small heating element built round the pneumotachograph apparatus.

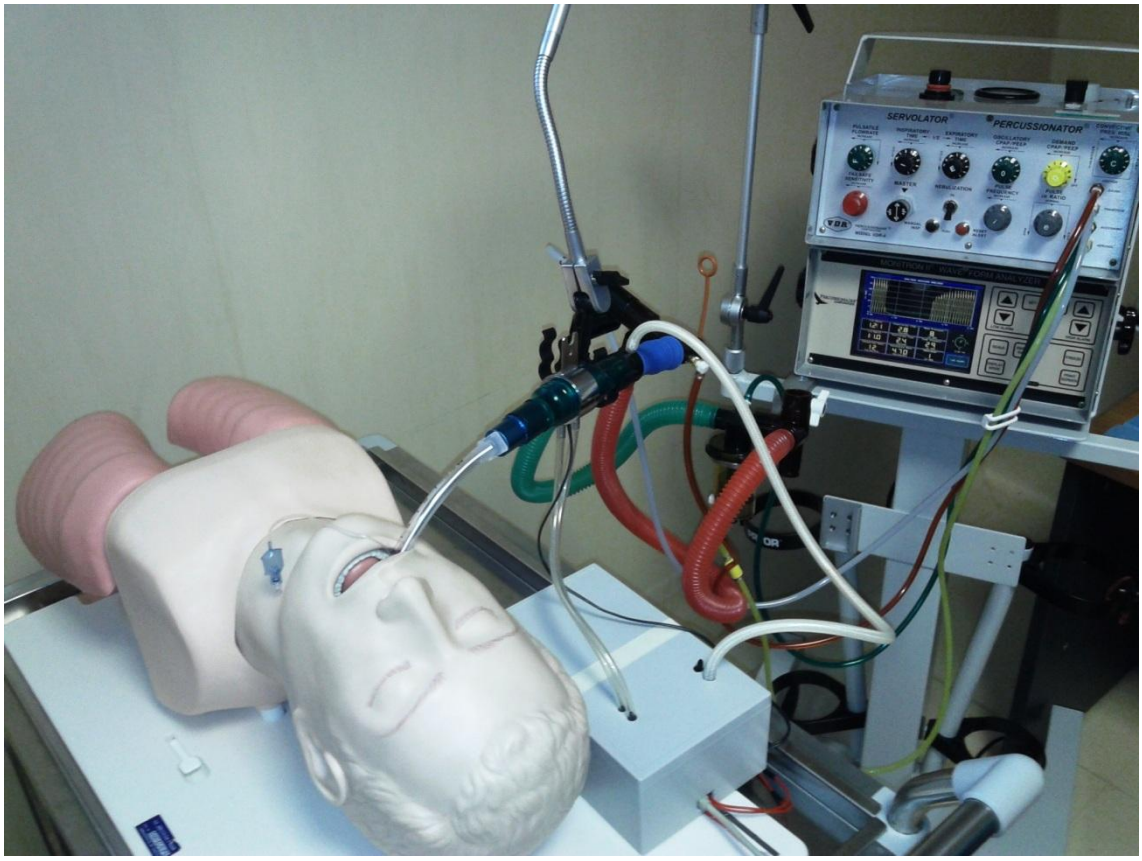

Figure 3.17 The final prototype of bedside acquisition system. In respect to a patient privacy, in this figure the application is represented on anatomical simulator.

Chapter 4 - *In vivo* measurements during High Frequency Percussive Ventilation

4.1 Material and methods

The HFPV treatment was applied in patients admitted to the Intensive Care Unit of the Department of Perioperative Medicine, Intensive Care and Emergency, Cattinara Hospital, University of Trieste.

During the first 12 h after admission to the Intensive Care Unit (ICU) the patients underwent conventional mechanical ventilation in volume controlled mode (VCM).This conventional ventilatory modality is based on preselected VT delivery that in accordance to protective ventilatory strategy is limited to 6-8 ml/kg predicted body weight (PBW). The predicted body weight was calculated using the equations suggested by "The Acute Respiratory Distress Syndrome Network" [70]:

For males PBW = 50 + 0.91 · (centimeters of height -15.4)

For female PBW = 45.5 + 0.91 · (centimeters of height -152.4)

During VCM the PEEP and FiO_2 were selected to obtain arterial oxygen saturation (SaO_2) of 90% or more.

After 12 hours of VCM arterial blood gas was analyzed and the patients that present PaO_2/FiO_2 of 200 or less or greater than 200 but with an increase below 20% in relation to the admission value were shifted to HFPV, as non-responders to VCM.

4.4.1 High Frequency Percussive Ventilation protocol

HFPV was substituted for VCM in non-responder patients and has been applied for 12 hours. HFPV was set up similarly to VCM i.e. inspiratory:expiratory time (I:E) ratios, Pawmean and PEEP were equaled. To obtain the same Pawmean, the following adjustments were made on a VDR-4®: during inspiration a pulsatile flow with a percussive frequency of 500 cycles min^{-1} and a pulse inspiratory and expiratory ratio (i and e respectively) of 1 was used.

After 10 minutes stabilization period the acquisition system was connected in order to measure pressure, flow and volume.

The first aim was to verify if the tidal volumes were similar in both ventilatory strategy, at the same mean airway pressure. In case of violation of protective ventilatory strategy (i.e. 6-8 mL/Kg_{PBW}) tidal volume was modified accordingly by acting on VDR-4® flow knob. After that a safety $VTmL/Kg_{PBW}$ was reached the respiratory parameters were measured by acquisition system. At the present time, the mean airway pressure is the only parameter that allows an indirect comparison between VCM and HFPV treatment set up [36][71].

Beside the airway pressure, flow and volume measurements, the Rrs, Crs, Irs and endotracheal pressure drop ΔP_{TT} values were also estimated by using the aforementioned MLR approach on RCI Dorkin model and Blasius equation, respectively.

Since the flow is the dependent variable, it changes as the features of the respiratory system change: the HFPV will constantly adjust flow as resistance or compliance change, with the hazard of uncontrolled tidal volume delivery. Respiratory resistance and compliance changes occur stochastically during the treatment. The airway resistance mainly depends on the presence of secretions. The mobilization of secretions is a recognized, but not immediate, feature of HFPV. On the other side, the elastic properties can suddenly change when alveolar recruitment or de-recruitment occur. From a clinical point of view alveolar de-recruitment must be avoided and frequently recruitment maneuver are necessary to keep the lung open. Presently it is not possible to evaluate the intrinsic recruitment effect during HFPV. Thus second aim of the thesis was to produce a respiratory system perturbation as “mini recruitment maneuver” and verify respiratory system response. To avoid arbitrary pressure increment was used for each patient the own ΔP_{TT} value.

After optimization of tidal volume was performed a pressure perturbation as a mini recruitment maneuver. The effects of this pressure increment on the respiratory system are referred to measured initial conditions. The perturbation pressure input was performed by acting on pulsatile flow rate (F-knob) present on VDR-4®. As a consequence a working peak pressure increased by ΔP_{TT} value. At this point, a novel estimated VT', Crs', Rrs', Irs' and $\Delta P_{TT'}$ parameters were recorded and compared with the corresponding starting point values.

During the following 12 hours the patients were ventilated under these conditions and every 4 hours blood samples were collected for gas analysis. Intermediate gas analysis samples were available at the discretion of the physician in charge of the patient. At the end of 12 hours of HFPV treatment a new measurement of respiratory parameters was performed. After this recording the protocol ends and the patients returned to CVM.

This study was performed during a standardized HFPV clinical protocol without interfering with patients care and under the supervision of a physician not involved in the study. The information obtained by the data acquisition and the consequent ventilator set up variations were applied in agreement with the physician. The study posed no added risk to the patient and did not interfere with usual patient care.

Thus, 10 patients (8 male) aged between 60 and 83 years were prospectively studied. The VCM was setup as reported in table 4.1. The tidal volume per predicted body weight (VT/PBW), positive end-expiratory pressure (PEEP), respiratory system compliance (Crs), and Paw_{mean} were also determined 10 minutes before changing to HFPV using the same acquisition device used for further HFPV measurements.

The group encompassed patients presenting chest trauma (n = 2), sepsis (n = 3), bacterial pneumonia (n = 4), neurogenic pulmonary edema (n = 1).

Patient	Age (years)	VT/PBW mL/Kg	PEEP (cmH_2O)	Crs (mL/cmH_2O)	Paw_{mean} (cmH_2O)
1	65	7,33	6	22,9	10
2	74	6,25	5	32	14
3	75	7,18	5	43,5	15
4	77	6,43	7	42,0	12
5	66	5,97	5	30	12
6	83	5,56	6	29,0	11
7	72	6,50	12	46,9	17
8	60	6,13	8	27	10
9	75	6,14	13	27,0	9
10	69	6,41	12	50,0	15
Median (1^{st}-3^{rd} IQT)	73 (66-75)	6.33 (6.13-6.50)	6.5 (5-12)	31 (27-43.5)	13 (11-15)

Table 4.1 Demographic and respiratory parameters of patients population during Volume Controlled Mode

4.2 Results

The tidal volume comparison, at the same Paw_{mean}, between VCM and HFPV is reported in table 4.2.

VT VCM (mL)	**VT HFPV** (mL)	**VT/Kg_{PBW} VCM** (mL/Kg_{PBW})	**VT/Kg HFPV** (mL/Kg_{PBW})
440	530	7.33	8.83
500	520	6.25	6.50
610	630	7.18	7.41
450	620	6.43	8.86
400	390	5.97	5.82
500	840	5.56	9.33
520	480	6.50	6.00
380	415	6.13	6.69
510	490	6.14	5.90
500	420	6.41	5.38

Table 4.2 Comparison of tidal volume and VT/Kg_{PBW} delivery, between VCM and HFPV at the same Paw_{mean}. In red are marked the patients that exceeded the upper safety volume limit.

In 30% of studied patients was detected that VT exceeded the upper safety limit of 8 mL/Kg_{PBW} as shown in table 4.2. In two cases the upper limit was 10% exceeded (8.83 and 8.86 mL/Kg_{PBW}), while in third case the increment was more important reaching 9.33 mL/Kg_{PBW}. In all three cases VT was immediately decreased to safety range by acting on flow knob.

The volume delivered for the predicted body weight during VCM presented a median and range values of 6.33 (5.55-7.33) mL/Kg_{PBW}, while in case of HFPV the corresponding values were 6.59 (5.38-9.33) mL/Kg_{PBW} (Table 4.3).

	Median	Min	Max	1st quartile	3rd quartile
VT VCM (mL)	500	380	610	440	510
VT HFPV(mL)	505	390	900	420	620
VT/Kg_{PBW}VCM (mL/Kg)	6,33	5,55	7,33	6,13	6,50
VT/Kg_{PBW}HFPV (mL/Kg)	6,59	5,38	9,33	5,90	8,83

Table. 4.3 The median, range and 1st - 3rs quartiles values of tidal volume and VT/KgPWB during VCM and HFPV

It is important to point out that during the transition from VCM to HFPV at the same mean airway pressure the tidal volume delivery can significantly change. Finally for a more intuitive comprehension the results are presented by box and whisker plot in figure 4.1

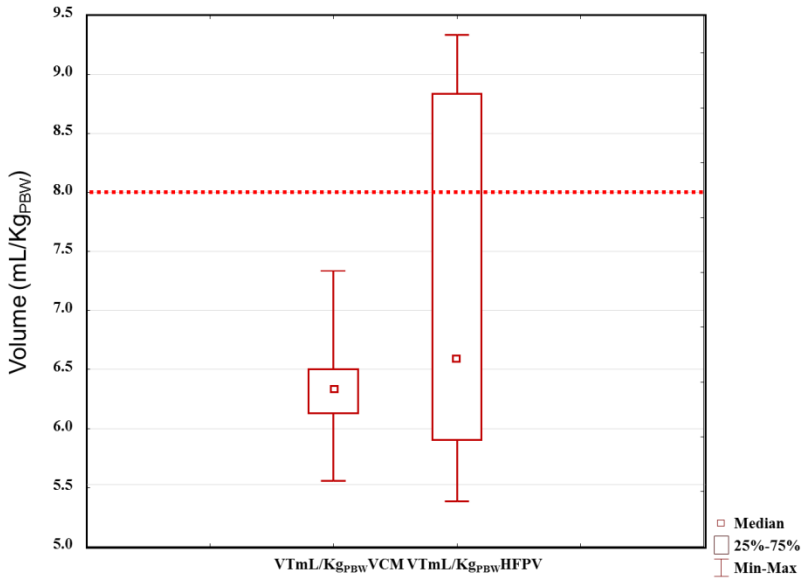

Fig 4.1 Tidal volume delivered (VTmL/Kg_{PBW}VCM and VTmL/Kg_{PBW}HFPV) during both ventilations are expressed as median, minimum, maximum and 1st 3rd quartiles. The red line represent the safety volume limit.

Once achieved the safety volume range, the ΔP_{TT} was estimated, and the pressure increment perturbation was applied. In table 4.4 are reported the comparison between the respiratory parameters before and after the application of ΔP_{TT} increment.

Patient	Rrs ($cmH_2O\ L^{-1}\ s$)	Rrs' ($cmH_2O\ L^{-1}\ s$)	Crs (mL/cmH_2O)	Crs' (mL/cmH_2O)	VT (mL/Kg_{PBW})	VT' (mL/Kg_{PBW})	ΔCrs (%)
1	12	11,5	25	31	6,5	7,9	24,0
2	18,2	17,8	40,3	41,8	6,5	7,5	3,7
3	15,6	14,9	44,2	49	7,41	8	10,9
4	18	18	55,8	52,6	7,1	7,7	-5,3
5	13	14	31	33	5,9	6,1	6,5
6	18	16,5	39	44	6,6	7,6	12,8
7	17	18,3	47,4	53,6	6	6,7	13,1
8	10,7	12	27	29	6,9	7,2	7,4
9	8,8	9,2	27,6	37	5,9	7,8	34,1
10	11	11,5	50,2	61,3	5,38	6,6	22,1
Median (1^{st}-3^{rd}IQT)	14,3 (11,2-17,8)	14,45 (11,6-17,5)	39,65 (28,5-46,6)	42,9* (34-51,7)	6,5 (5,9-6,8)	7,55# (6,8-7,7)	

Table 4.4 Comparison between the respiratory parameters before and after the application of ΔP_{TT} increment; Crs - Crs' and VT-VT' differed significantly * p = 0,016 and # p = 0,005 respectively. ΔCrs (%) represent compliance variation.

After the application of pressure perturbation, as a mini recruitment maneuver, the respiratory system compliance and delivered tidal volume varied significantly (p = 0,016 and 0,005 respectively) while the respiratory airway resistance remained constant. In all cases except one the ΔCrs% was positive (from 3,7 to 34,1%) suggesting an potential alveolar recruitment. The ΔCrs% increment greater than 10% was retained clinically significant considering the amount of pressure variation applied. Therefore the six patients can be identified as recruitment cases. On the other side, in only one patient ΔCrs% was negative suggesting a potential alveolar over-distention. An intermediate behavior characterized by the compliance increment lower than 10% occurred in three patients. In these cases the perturbation maneuver did not affected compliance.

For each of three aforementioned patient categories are reported below the most representative cases with corresponding curves and estimated respiratory parameters together with a brief clinical opinion.

4.2.1 Recruitment case

The initial respiratory parameters obtained before the ΔP_{TT} applications are reported in table 4.4 and figure 4.1. The VT is in a safety range and Crs is low as expected in a patient suffering from sepsis. The application of pressure increment produced a concomitant increase of tidal volume and compliance. In this case the pressure perturbation amounted of 6 cmH_2O with consequential poor Paw_{mean} increment, although the $VTmL/Kg_{PBW}$ moved from 5.9 to 7.8 $VTmL/Kg_{PBW}$.

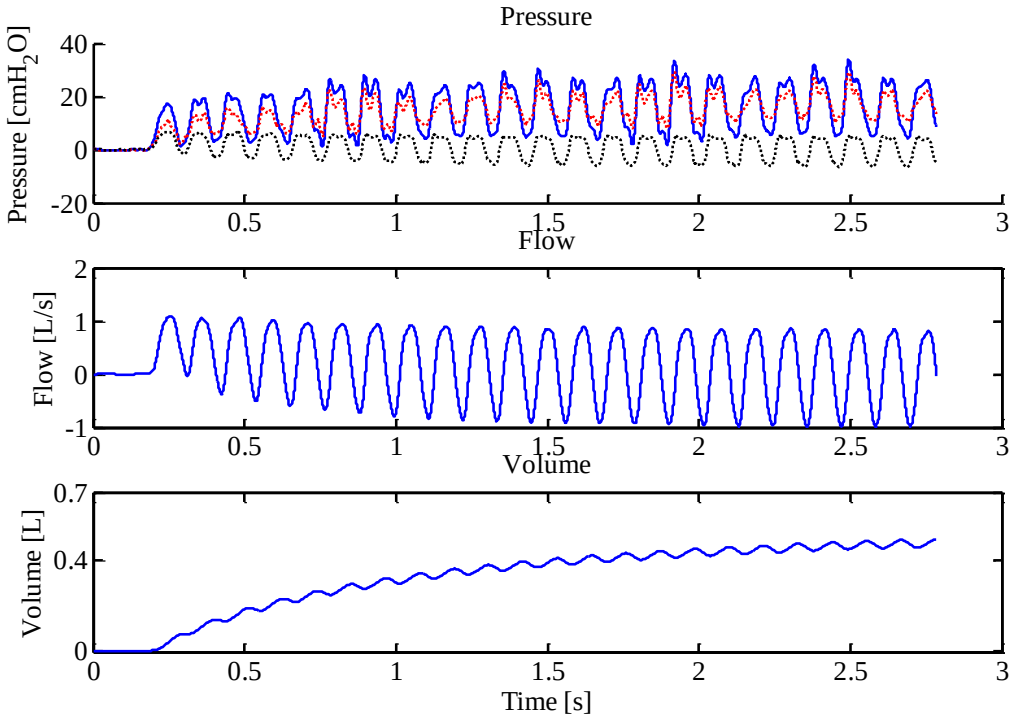

Figure 4.2 Recruitment case: pressures, flow and volume tracings during one inspiration recorded at the beginning of HFPV. In the top panel are depicted measured airway pressure (blue line), estimated tracheal pressure (red line) and estimated ΔP_{TT} (black line).

Rrs (cmH_2O/Ls^{-1})	Crs (mL/cmH_2O)	Paw_{mean} (cmH_2O)	Peak (cmH_2O)	VT (mL)	$VTmL/Kg_{PBW}$ (ml/Kg_{PBW})	ΔP_{TT} (cmH_2O)
8.8	27.6	9.1	34	490	5.9	6

Table 4.5 Recruitment case: respiratory mechanics parameter relative to figure 4.2 obtained at the beginning HFPV

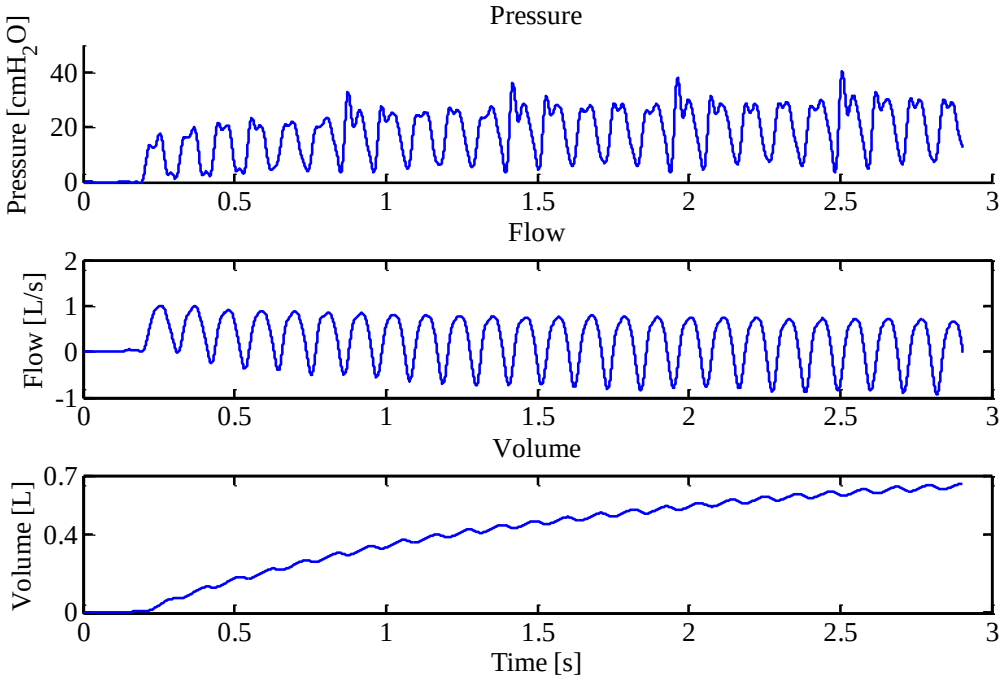

Figure 4.3 Recruitment case recorded after ΔP_{TT} increment. Airway pressure, flow and volume tracings during one inspiration

Rrs' (cmH_2O/Ls^{-1})	Crs' (mL/cmH_2O)	Paw_{mean}' (cmH_2O)	Peak'= Paw+ ΔP_{TT} (cmH_2O)	VT' (mL)	VT'mL/Kg_{PBW} (ml/Kg_{PBW})
9.2	37	9.6	40	650	7.8

Table 4.6 recruitment case recorded after ΔP_{TT} increment. Respiratory mechanics parameter relative to figure 4.3.

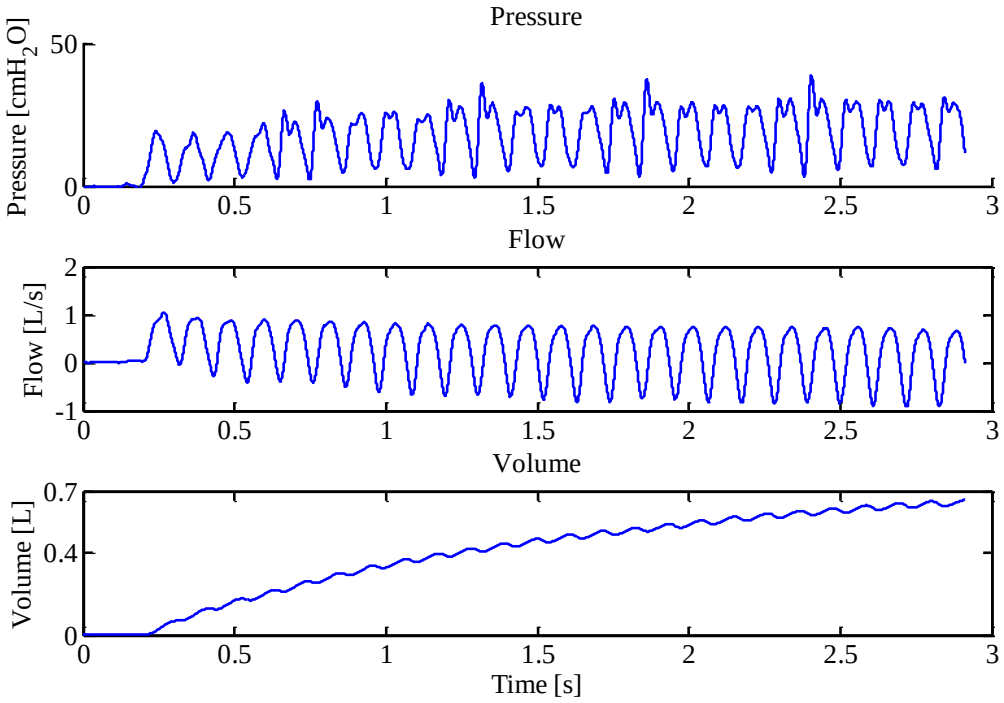

Figure 4.4 Recruitment case recorded after 12 hours. Airway pressure, flow and volume tracings during one inspiration

Rrs" (cmH_2O/Ls^{-1})	Crs" (mL/cmH_2O)	Paw_{mean}" (cmH_2O)	Peak" (cmH_2O)	VT" (mL)	VT"mL/Kg_{PBW} (ml/Kg_{PBW})
9.5	38	9.5	39	655	7.9

Table 4.7 Recruitment case recorded after 12 hours Airway pressure, flow and volume tracings during one inspiration.

4.2.2 Over-distension case

The respiratory parameters corresponding to initial condition are reported in table 4.8 and figure 4.5. The application of pressure increment produced a Crs decrement while VT increased. In this case, for safety reason, the ΔP_{TT} pressure increment was removed and the patient was ventilated with the previous HFPV setup until the end of treatment.

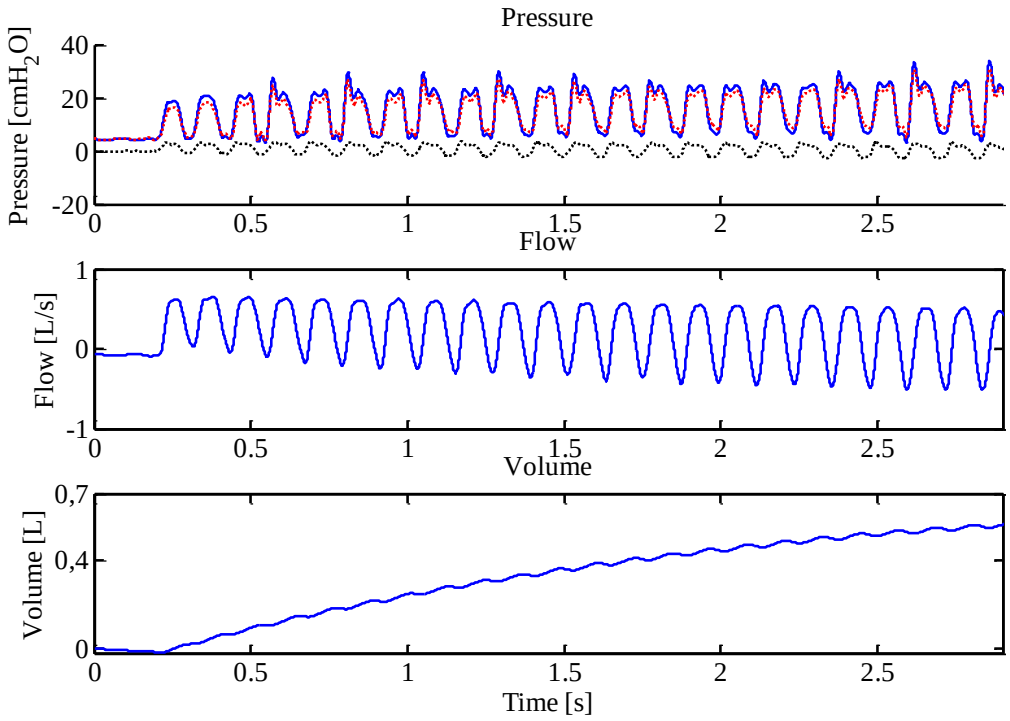

Figure 4.5 over-distension case: pressures, flow and volume tracings during one inspiration recorded at the beginning of HFPV. In the top panel are depicted measured airway pressure (blue line), estimated tracheal pressure (red line) and estimated ΔP_{TT} (black line).

Rrs (cmH_2O/Ls^{-1})	Crs (mL/cmH_2O)	Paw_{mean} (cmH_2O)	Peak (cmH_2O)	VT (mL)	$VTmL/Kg_{PBW}$ (ml/Kg_{PBW})	ΔP_{tube} (cmH_2O)
18	55.8	11	34	565	7.1	4

Table 4.8 Over-distension case: respiratory mechanics parameter relative to figure 4.5 obtained at the beginning HFPV.

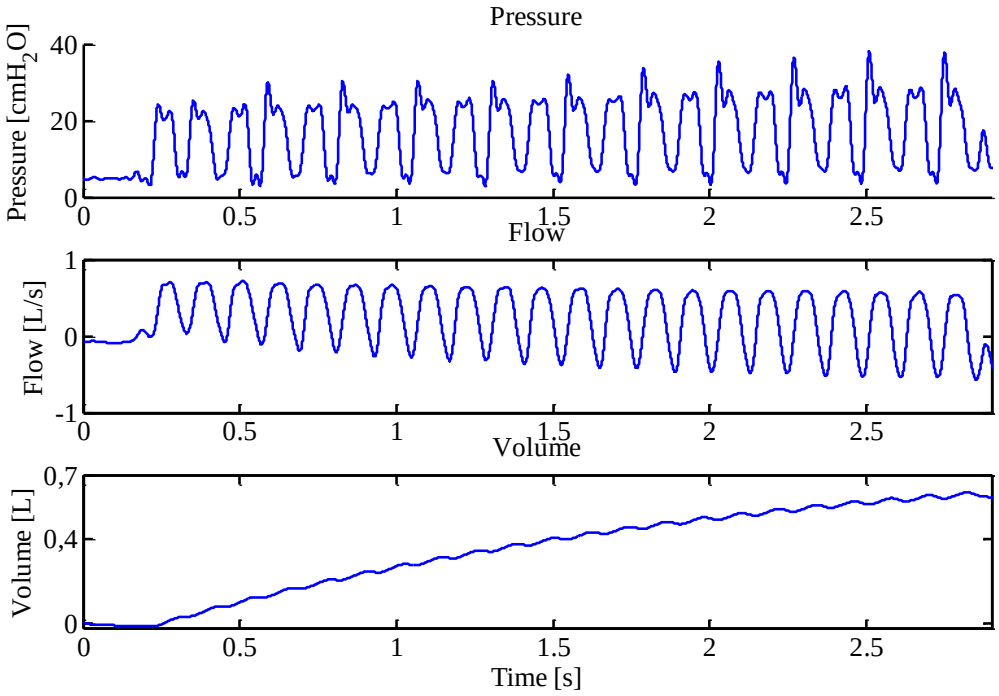

Figure 4.6 Over-distension case: airway pressure, flow and volume tracings during one inspiration recorded after ΔP_{TT} increment.

Rrs' (cmH_2O/Ls^{-1})	Crs' (mL/cmH_2O)	Paw_{mean}' (cmH_2O)	Peak'= Paw+ ΔP_{tube} (cmH_2O)	VT' (mL)	VT'mL/Kg_{PBW} (ml/Kg_{PBW})
18	52.6	12	38	615	7.7

Table 4.9 Over-distension case: respiratory mechanics parameter relative to figure 4.6, obtained after ΔP_{TT} pressure increment, during HFPV.

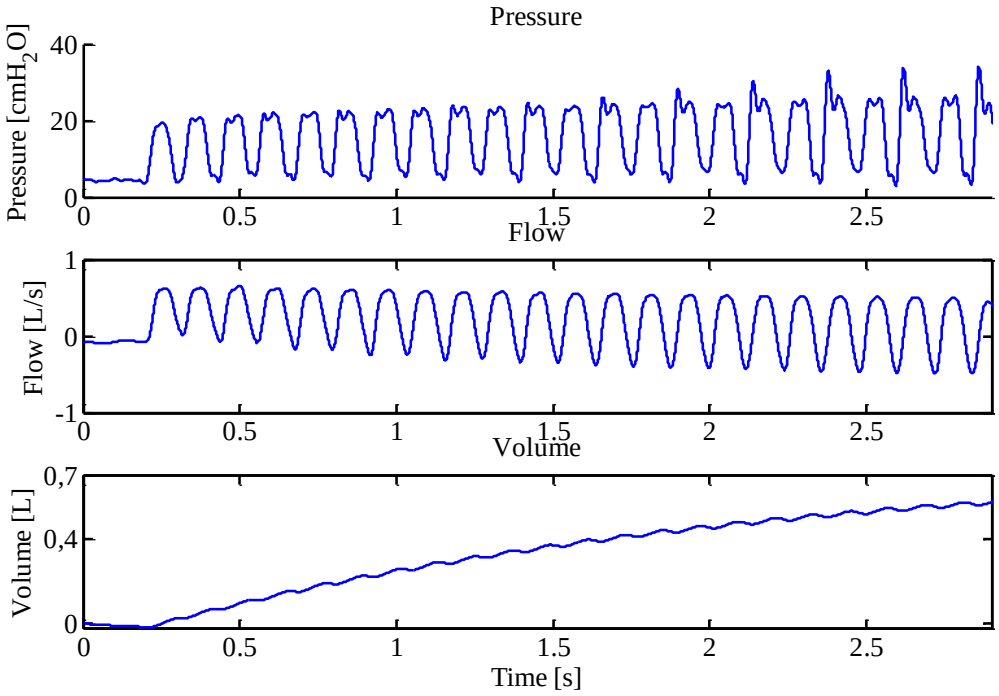

Figure 4.7 Over-distension case: airway pressure, flow and volume tracings during one inspiration recorded after 12 hours.

Rrs" (cmH_2O/Ls^{-1})	Crs" (mL/cmH_2O)	Paw_{mean}" (cmH_2O)	Peak" (cmH_2O)	VT" (mL)	VT"mL/Kg_{PBW} (ml/Kg_{PBW})
17.4	58	11	35	580	7.0

Table 4.10 Over-distension case: respiratory mechanics parameter relative to figure 4.7, obtained at the end of HFPV treatment.

4.2.3 Linear case

The respiratory parameters corresponding to initial condition are reported in table 4.11 and figure 4.8. The application of pressure perturbation produced a VT increment together with a small increase in Crs.

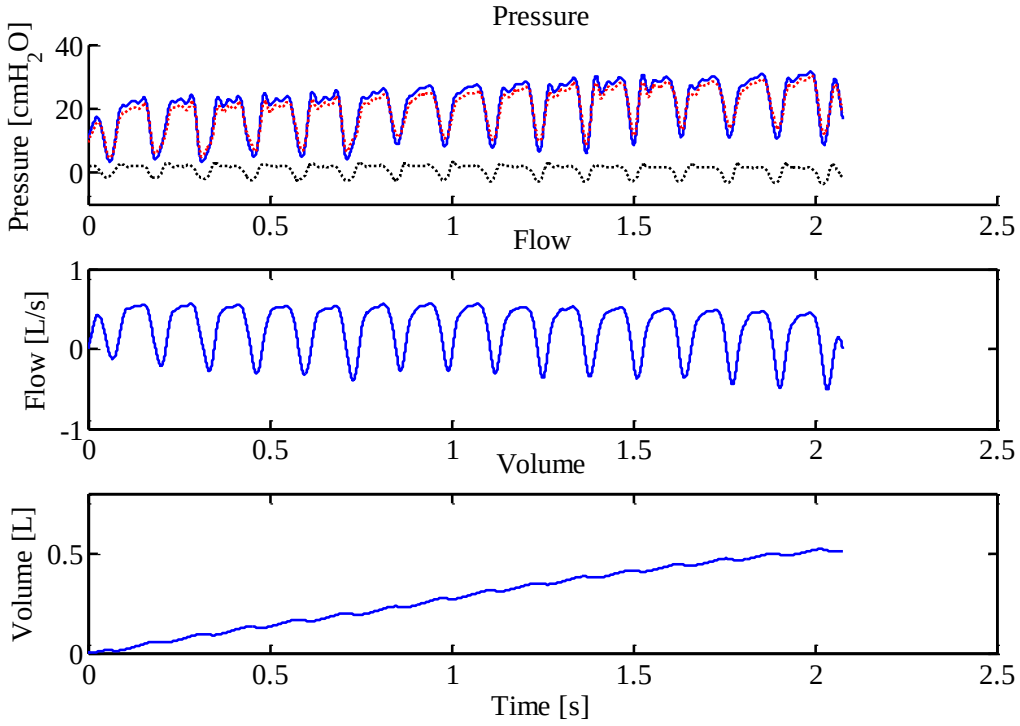

Figure 4.8 Linear case: pressures, flow and volume tracings during one inspiration recorded at the beginning of HFPV. In the top panel are depicted measured airway pressure (blue line), estimated tracheal pressure (red line) and estimated ΔP_{TT} (black line).

Rrs (cmH_2O/Ls^{-1})	Crs (mL/cmH_2O)	Paw_{mean} (cmH_2O)	Peak (cmH_2O)	VT (mL)	$VTmL/Kg_{PBW}$ (ml/Kg_{PBW})	ΔP_{TT} (cmH_2O)
18.2	40.3	14	32	520	6.5	4

Table 4.11 Linear case: respiratory mechanics parameter relative to figure 4.8 obtained at the beginning HFPV.

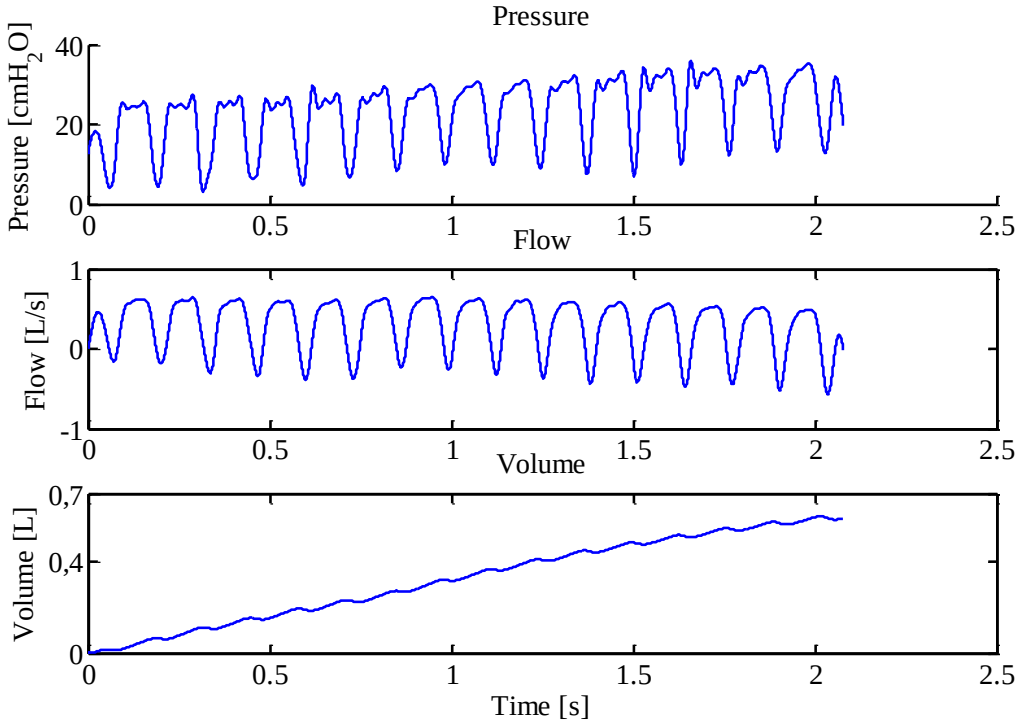

Figure 4.9 Linear case: airway pressure, flow and volume tracings during one inspiration recorded after ΔP_{TT} increment.

Rrs' (cmH_2O/Ls^{-1})	Crs' (mL/cmH_2O)	Paw_{mean}' (cmH_2O)	Peak'= Paw+ ΔP_{tube} (cmH_2O)	VT' (mL)	VT'mL/Kg_{PBW} (ml/Kg_{PBW})
17.8	41.8	15	36	600	7.5

Table 4.12 Linear case: respiratory mechanics parameter relative to figure 4.9, obtained after ΔP_{TT} pressure increment, during HFPV.

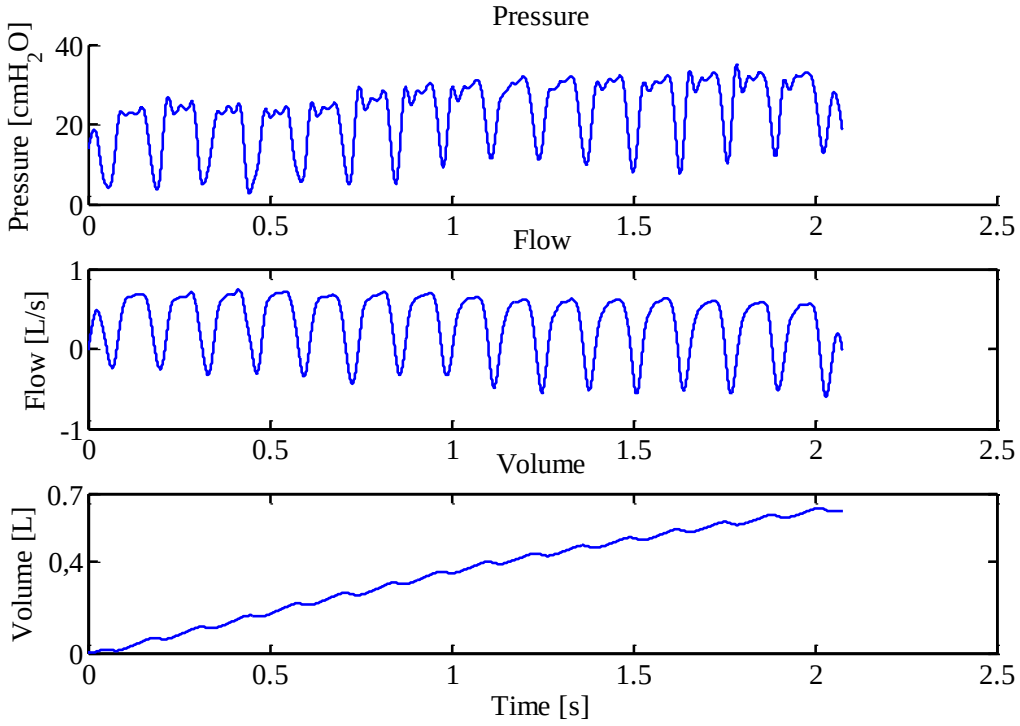

Figure 4.10 Linear case: airway pressure, flow and volume tracings during one inspiration recorded after 12 hours.

Rrs" (cmH_2O/Ls^{-1})	Crs" (mL/cmH_2O)	Paw_{mean}" (cmH_2O)	Peak" (cmH_2O)	VT" (mL)	VT"mL/Kg_{PBW} (ml/Kg_{PBW})
14.2	42	14	35	635	7.9

Table 4.13 Linear case: respiratory mechanics parameter relative to figure 4.10, obtained at the end of HFPV treatment.

4.3 Gas exchange analysis

Blood gas analysis were recorded before and during the HFPV treatment. In figure 4.11 PaO_2/FiO_2 ratio is reported in ten patients underwent "mini recruitment maneuver" performed at the beginning of HFPV trial. The reported samples are corresponding to ICU admission (initial observation), HFPV enrollment (after 12 hrs), four, eight and twelve hours of HFPV treatment, respectively. The data were compared with the mean (± SD) values of 35 patients (control group) obtained in the previous HFPV study [36] based on

constant Paw_{mean} as described in chapter 1. As expected gas exchange did not differ from initial observation and HFPV enrollment. The slopes of the mean values between ICU admission and HFPV enrollment were similar although our population presented lower initial values. Is important to point out, that during the following four hours, a different behavior should be described between the two considered populations. In control group the slope of PaO_2/FiO_2 was 10 hrs^{-1} while in mini-recruitment group was 12 hrs^{-1}. This slight but important increment should be considered clinically relevant because obtained in accordance with the protective ventilatory strategy. However these preliminary results should be confirmed in future study.

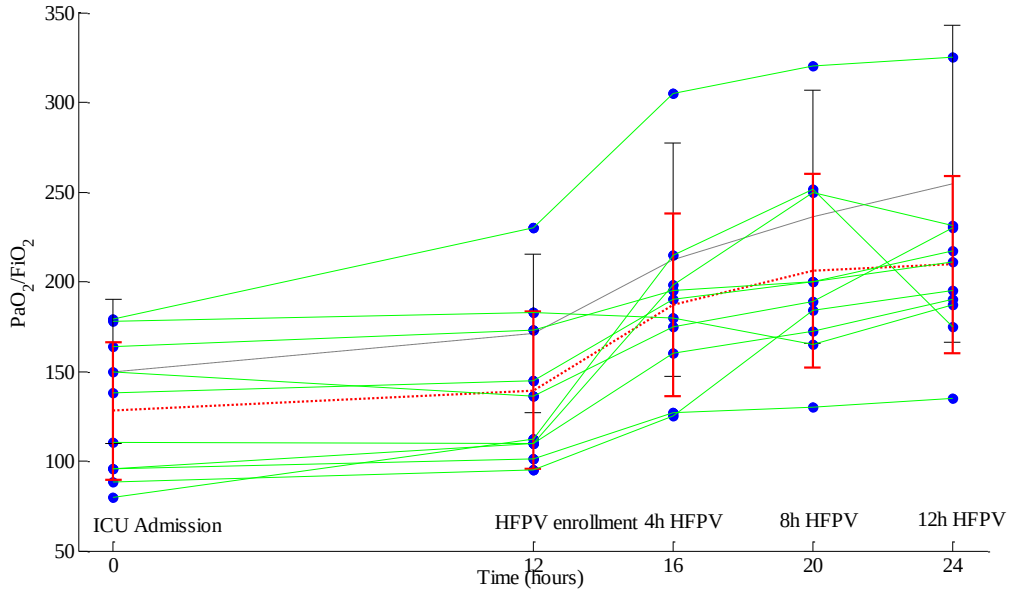

Figure 4.11 PaO_2/FiO_2 ratio corresponding to ICU admission (initial observation), HFPV enrollment (after 12 hrs), four, eight and twelve hours of HFPV treatment, respectively. Dotted lines represent the mean and 1SD values in each sampling moment, for case (red line) and mean±SD values (black line). of 35 patients, obtained in the previous HFPV study based on constant Paw_{mean} (control group) The exact PaO_2/FiO_2 values are represented with blue circles.

Chapter 5 – Discussion

The main result of this study is the discrepancy between VT delivery, at the same Paw_{mean}, during VCM and HFPV in 30% of studied populations (Table 4.2). In these patients the VT exceeded the upper safety limit of 8 mL/Kg_{PBW}. For this reason Paw_{mean} cannot be considered a reliable parameter of volume variations.

The "mini recruitment maneuver" was applied on 10 patients during the trial. The pressure increment in six of them (2 chest trauma, 3 sepsis and 1 pneumonia) resulted in transition from low to significantly higher values (≥10%) of Crs without overcoming the safety volume zone (Table 4.4). This behavior is characteristic for alveolar recruitment and could be described in pressure – volume (P-V) curve by translation from low inflation zone (Figure 4.2 and Table 4.5) to linear zone (Figure 4.3 and Table 4.6). In the five of six patients the etiology of the acute hypoxemia is not related to direct lung injury.

On the other hand, in one patient with stiff lungs (Figure 4.5 and Table 4.8) due to bilateral pneumonia the pressure increment produced an increase in VT and at the same time, a decrease in Crs, resulting an undesired over-distention (Figure 4.6 and Table 4.9).

Finally the other three patients (2 pneumonia and 1 neurogenic pulmonary edema) (Figure 4.8 and Table 4.11) presented an intermediate respiratory mechanics behavior corresponding to linear part of P-V curve. In this case a volume increment resulted in poor compliance variation (Figure 4.9 and Table 4.12) as expected in subjects suffering hypoxemia due to primitive lung lesions.

5.1 Interpretation of "mini recruitment maneuver" by pressure–volume curve model

The variations of respiratory mechanics should be physiopathologically understood by considering the pressure volume relationship during mechanical ventilation. The pressure-volume curve shows that the pressure-volume tracing (P-V) of the respiratory

system is not linear; rather, in general it is sigmoidal in shape with two extremities where Crs is smaller and a relatively linear intermediate zone in which Crs is greater. The three segments of the inspiratory arm of the curve are separated by lower inflexion point (LIP) and upper inflexion point (UIP) that allow us to identify the pressures at which recruitment and de-recruitment begin and end (figure 5.1). Accordingly, it has been postulated that tidal ventilation (VT) should occur in the central zone of the P-V tracing, between the two inflexion points. [72].

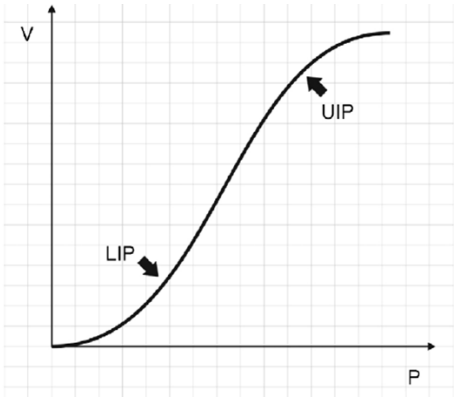

Figure 5.1 Inspiratory limb of a P-V curve. LIP and UIP represent lower and upper inflation point respectively. [72]

Several studies have demonstrated that the inspiratory limb of P-V curve is parallel to both aeration and recruitment curves. For inspiratory pressures between 0 cmH_2O and the inspiratory LIP, the increase in lung volume is mainly due to aeration of normally poorly aerated areas. When airway pressure increases above the LIP, recruitment starts. Therefore, the LIP reflects the onset of recruitment of non-aerated areas in the lung. It has been reported that the presence of an LIP in the curve indicates significant potential for recruitment. As detecting these potential could have important consequences for patient management, it is tempting to speculate that P-V curves could be useful tool at bedside. From the clinical point of view the elements of particular interest provided by P-V curve are the LIP, UIP, the inflation maximum curvature and total respiratory system compliance. At the beginning the P-V curve is flat and reflects very low compliance (LIP), the following segment is characterized by a steeper slope that represents the maximum

compliance (Crs_{max}). At the end of inflation (UIP) when the respiratory system is completely distended, the decrease in compliance suddenly approaches zero. Recruitment pressures have a Gaussian distribution that is responsible for the steeper part of the curve, with the inspiratory UIP reflecting the end of these massive recruitment. However, some recruitment takes place at pressures higher than this point. It is useful to detect the UIP to obtain an upper pressure ventilator limit to avoid overdistension, although some studies suggest that the UIP might indicate the end of alveolar recruitment and not necessarily the beginning of overdistension. The LIP occurs at the beginning of lung inflation, where alveoli are less distensible and require high insufflation pressures to reopen. The application of positive and expiratory pressure (PEEP) values chosen slightly above than LIP pressure value prevents end expiratory alveolar collapse and avoids shear stress trauma caused by periodic alveolar opening and closing. In the linear part of P-V curve the ratio between volume and pressure variations is almost constant. In these conditions tidal volume ventilation is desirable to minimize ventilatory induced lung injury.

It is important to point out that the P-V curve represents a dynamic phenomenon that reflects alveolar distension of open units and recruitment of previous closed lung units. As depicted in figure 5.2 there is a close correlation between the P-V curve and the radiologic images, confirming the clinical relevance of the viscoelastic respiratory system parameters estimation.

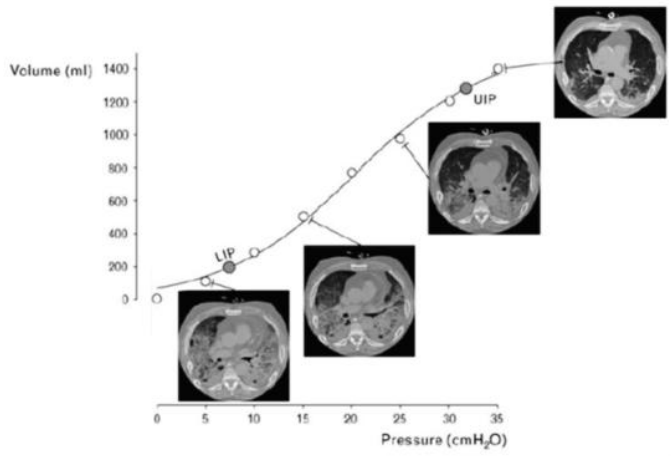

Figure 5.2 Computed tomographic scan images were obtained while tracing the curve in static conditions. Note that recruitment only starts when airway pressure is higher than the lower inflection point (LIP) of the inspiratory limb and continues up to the maximum pressure reached, even above the upper inflection point (UIP) modified from [73].

Our results suggest that is of paramount importance to use an appropriate acquisition and elaboration system during HFPV to avoid volutrauma. Moreover, a standardized and safe recruitment maneuver during HFPV is not available. The clinical studies reports that HFPV acts as pressure controlled logic promoting alveolar recruitment [36][71]. This phenomenon is particularly evident after at least 12 hours of continuous treatment[36].From a clinical point of view the possibility to early optimize the pressure volume relationship can improve the beneficial effect of HFPV, minimizing iatrogenic lung damage.

Nevertheless, it is important to point out that the choice of VT mL/Kg_{PBW} should not be "blind" but always is mandatory consider the heterogeneity of underlying lung injury typically present in these patients. In other words, it is essential that tidal volumes should be titrated based on Crs, in patients with Acute Lung Injury (ALI) and Acute Respiratory Distress Syndrome (ARDS).

Important study indicate that although some patients, such as those with poor Crs and high airway pressures, would benefit from very low tidal volume, others with less severe lung injury may require larger volumes to maintain ventilation and avoid alveolar collapse during conventional mechanical ventilation [74].

Deans et al. have demonstrated that the effect of changing tidal volume on mortality is dependent on starting pulmonary compliance (figure 5.4). The authors examined the pre-randomization compliance of patients in the ARMA trial that randomly assigned 861 mechanically ventilated patients with ARDS to receive initial VT of 6 or 12 mL/Kg. In this case the data analysis revealed that before randomization, tidal volume was titrated based on pulmonary compliance (figure 5.3) [74-75].

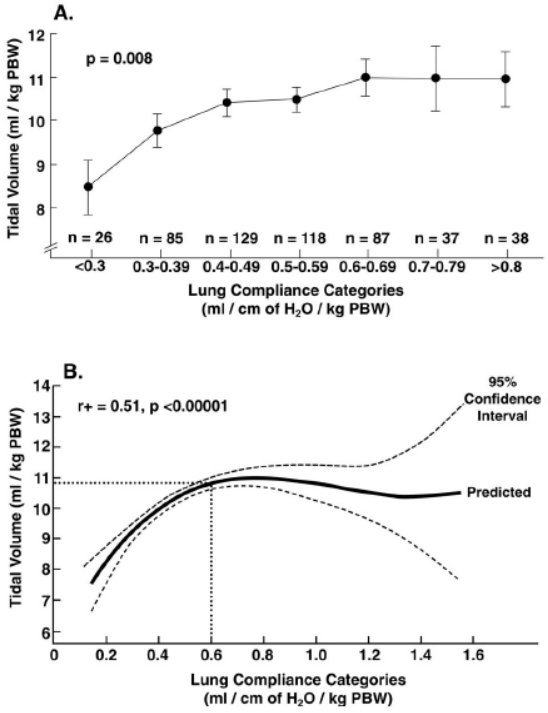

Figure 5.3 Relationship between pre-randomization pulmonary compliance and tidal volume. Panel A shows a significant relationship between tidal volume and lung compliance pre-randomization. Lower tidal volumes were administered to patients with less compliant lungs. Panel B, modeling of the relationship between compliance and tidal volume reveals that the best predictive relationship is biphasic. In patients with less compliant lungs, there is a direct linear relationship between compliance and tidal volume; however, in patients with more compliant lungs, there was no relationship between tidal volume and compliance. Tidal volume remained relatively constant over this range of pulmonary compliance. [74-75]

Interestingly, the mortality effect of changing tidal volume was significantly associated with pre-randomization lung compliance (p = 0.003 for interaction) (figure 5.4).

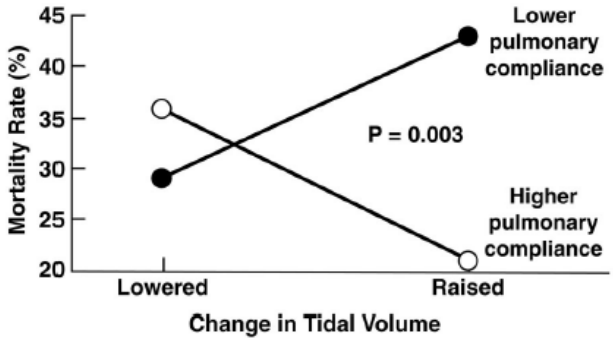

Figure 5.4 The effect of changing tidal volume on mortality is dependent on pulmonary compliance. There is a significant interaction between pulmonary compliance and mortality rate in the ARMA trial (p =0 .003). In patients with lower pulmonary compliance, raising tidal volume increased mortality compared with lowering tidal volume (*filled circles*; 42% vs. 29%). In contrast, in patients with higher pulmonary compliance, raising tidal volume decreased mortality compared with lowering tidal volume (*unfilled circles*; 21% vs. 37%) [74-75].

Patients with more compliant lungs did poorly if tidal volumes were lowered. In contrast, those with relatively less compliant lungs did well if tidal volumes were lowered. This finding is consistent with the philosophy that parameters of mechanical ventilation should be titrated based on surrogates of disease severity [76-80].

At the present time, the above mentioned clinical considerations are routinely used during conventional mechanical ventilation.

Unfortunately, these important recommendations cannot yet be applied in the sickest patients not responding to CMV.

Therefore, in order to comply with these important recommendations, and with the aim to early optimize HFPV treatment, an algorithm based on results of this study is proposed.

Chapter 6 – Proposed algorithm for the optimization of HFPV treatment

The algorithm based on the tidal volume (VT), viscoelastic respiratory system parameters (Crs, Rrs, Irs) and endotracheal tube pressure drop (ΔP_{TT}) estimated values is proposed. The decisional flow diagram of proposed algorithm is represented in Figure 6.1.

Ten minutes after the beginning HFPV at the same mean airway pressure as VCM the VT, Crs, Rrs, Irs and ΔP_{TT} values are estimated. In particular, VT and Crs are considered as starting point. If the measured VT is over the safety range of 6-8 mL/Kg of predicted body weight (PBW) the decrease of the working pressure is mandatory as well as to repeat the measure until the safety volume is reached.

If the patient presents a measured tidal volume in the safety range the "mini recruitment maneuver" should be considered. The effects of this pressure increment on the respiratory system are referred to measured initial conditions. To avoid arbitrary pressure increment we propose to use the previous defined ΔP_{TT} value by acting on pulsatile flow rate (F-knob) till a working peak pressure increases by ΔP_{TT} value. At this point, a novel values of VT', Crs', Rrs' and Irs', parameters are estimated and compared with the corresponding starting point values.

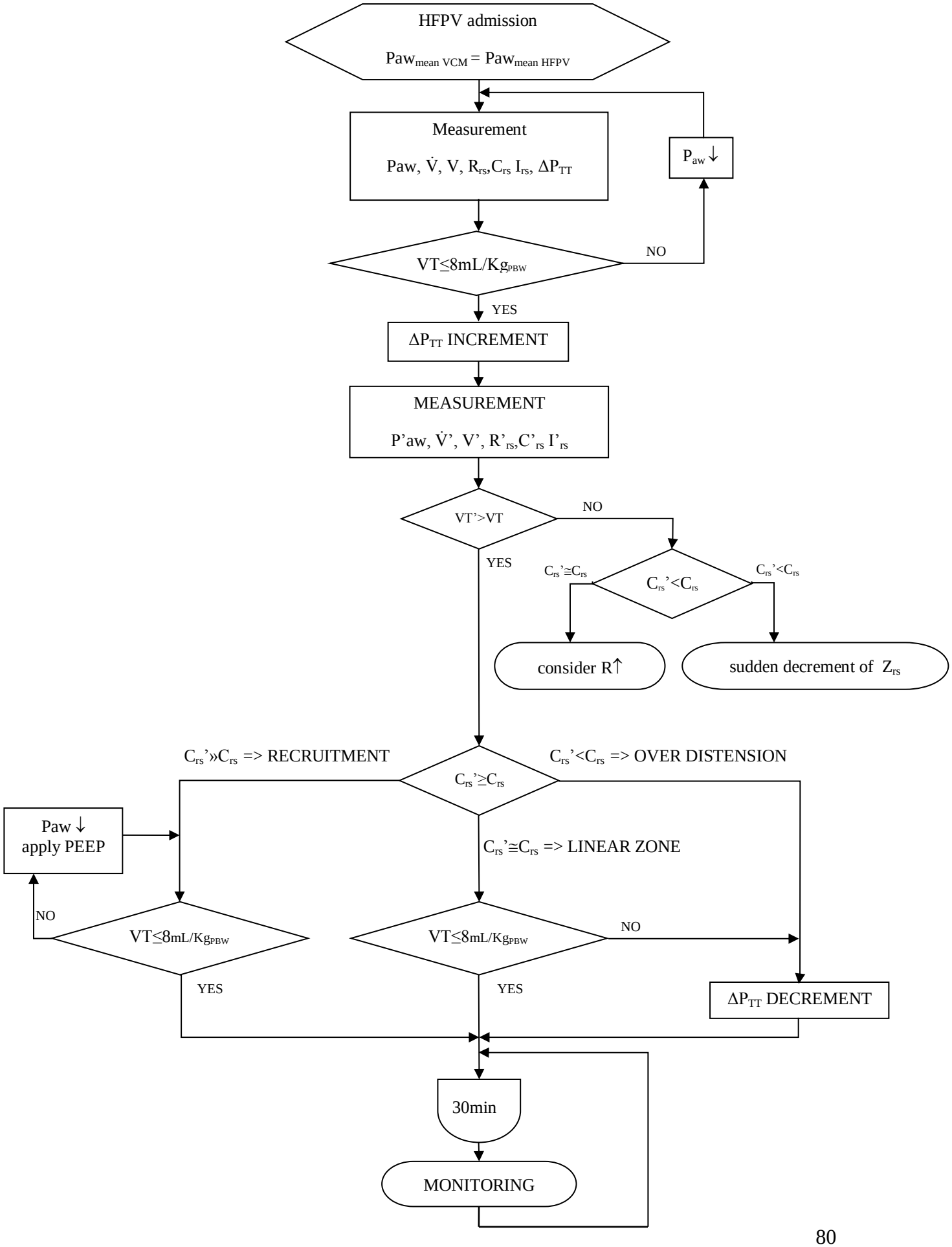

Figure 6.1 Flow diagram representation of the algorithm based on results of this study.

The following possibilities should be considered:

1. VT'> VT and Crs' > Crs. This case contemplates the alveolar recruitment effect due to pressure increment, theoretically described by shift from LIP to linear zone on the P-V curve (figure 6.2).

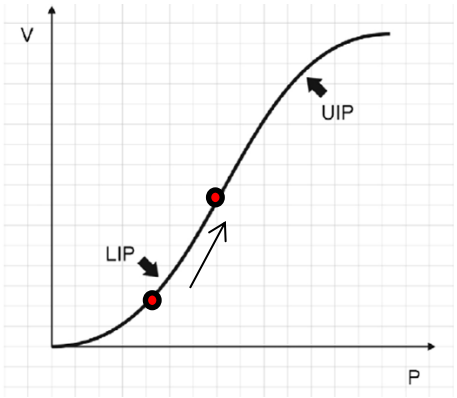

Figure 6.2.The arrow indicates the translation between lower and linear zone on pressure-volume curve (red circles)

2. VT'> VT and Crs' ≅ Crs. The pressure increment produces a VT rise without affecting respiratory system elastic properties. Thus the ratio between pressure and volume variations is almost constant and corresponds to the linear part of P-V curve (figure 6.3).

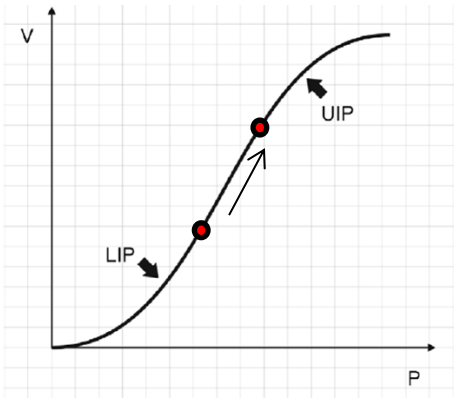

Figure 6.3. In the linear part of P-V curve (reed circles) the ratio between volume and pressure variations is constant as a consequence the slop represented by Crs is almost constant .

3. VT'> VT and Crs' < Crs. This is a typical example of lung overdistension. The pressure increment produces a sudden decrease in P-V curve slope due to the transition from linear to UIP zone (figure 6.4).

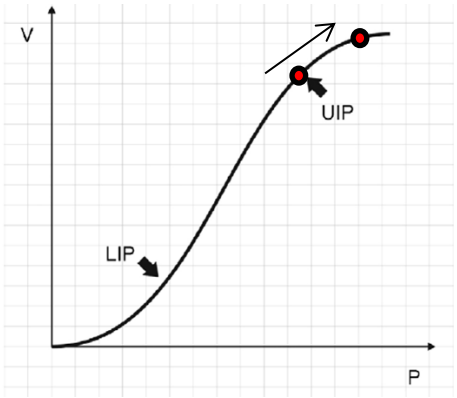

Figure 6.4. In the upper part of P-V curve (reed circles) the ratio between volume and pressure variations is not constant as a consequence the slop represented by Crs changes suddently .

4. VT'< VT and Crs' ≅ Crs. In this case VT decrement is not related to Crs and a resistive effect on volume should be advocated. The additional pressure applied is probably counterbalanced by the increment of resistive component.

5. VT'< VT and Crs' < Crs. This example describes a case of sudden increase in respiratory system impedance or a VDR-4® pressure power supplies limitation.

Once identified which of these possibilities is verified the following steps (see Figure 6.1 in which the algorithm is represented as a flow diagram) should be considered:

In case VT'> VT and Crs' > Crs consider if the VT value is 6-8 mL/Kg_{PBW} (depending on the lung pathology):

- If VT'> 8 mL/Kg_{PBW} the convective volume decrease by positive PEEP increment is mandatory. The approximated PEEP level should be calculated as:

PEEP = ΔVT/Crs' where ΔVT corresponds to a desired volume decrement in order to reach 6-8 mL/Kg_{PBW}. After the PEEP application a new measurement of the volume is necessary.

- If VT' is in the safety range (6-8 mL/Kg_{PBW}) gas exchange and a new respiratory mechanics measure should be considered after 30 minutes.

Also in case of VT'> VT and Crs' ≅ Crs a verification if VT' is in the safety range should be considered.

- If VT'>8 mL/Kg_{PBW} then a decrease of the working pressure toward the starting point level or a decrease of the convective volume by positive PEEP increment is appropriate.

- Otherwise, if VT' is in the safety range (6-8 mL/Kg_{PBW}), a new gas exchange and respiratory mechanics measure should be considered after 30 minutes.

When VT'> VT and Crs' < Crs an immediate decrease of the working pressure toward the starting point level is mandatory. A new gas exchange and respiratory mechanics measure should be considered after 30 minutes.

In the case of VT'< VT and Crs' ≅ Crs it is possible to consider patient or respiratory circuit resistance increment as bronchospasm or secretion inside endotracheal tube. Consider to use bronco-dilatation therapy and remove the secretion by suction.
Finally, when VT'< VT and Crs' < Crs a condition of selective bronchial intubation or hypertensive pneumothorax could be considered. Perform endotracheal tube repositioning and chest drain insertion, respectively.

6.1 Conclusion

At the present time the use of HFPV is increased, nevertheless the monitoring *state of art* is still based on mean airway pressure and gas exchange analysis. From the bench studies it is known that volume delivery and mean airway pressure do not change accordingly. For this reason a suitable acquisition system for measurement of pressure, flow and volume during HFPV was developed. Thereafter the acquisition prototype was

modified in order to be available to the bedside and suitable signal elaboration for estimation of respiratory mechanics (Rrs, Crs, Irs) and endotracheal tube pressure drop (ΔP_{TT}) was performed. The possibility to measure respiratory signals during HFPV and estimate corresponding parameters have opened a new horizon in clinical monitoring.

In conclusion, as a result of in vivo measurements, this thesis describes and provides for the first time the application of a decision support algorithm, based on the viscoelastic respiratory system properties during HFPV. The most representative examples were described suggesting the paramount importance of a proper monitor system during HFPV.

This algorithm represents the result of a pilot study performed in a small sample size population. Accordingly, we cannot exclude that the results could partially depend on different etiologies of lung injury. The decision support algorithm should be tested and optimized in future randomized study.

The clinical message of this study should be addressed bearing in mind all of the aforementioned limitations.

References

1. Cioffi WG, Graves TA, McManus WF, Pruitt BA Jr. “High Frequency Percussive Ventilation in patients with inhalation injury”, J Trauma 1989; 29:350-4
2. Cioffi WG Jr, Rue LW 3rd, Graves TA, McManus WF, Mason AD Jr, Pruitt BA Jr. “Prophylactic use of high frequency percussive ventilation in patients with inhalation injury”, Ann Surg 1991; 213:575-82
3. Rue LW 3rd, Cioffi WG, Mason AD, McManus WF, Pruitt BA Jr. “Improved survival of burned patients with inhalation injury”, Arch Surg 1993; 128:772-80
4. Mlcak RP. “Ventilation strategies for smoke inhalation”, J Resp Care Pract 1996; 103-6
5. Lentz CW, Peterson HD. “Smoke inhalation is a multilevel insult to the pulmonary system”, Curr Opin Crit Care 1996; 2:230-5
6. Barillo DJ, Dickerson EE, Cioffi WG, Mozingo DW, Pruitt BA Jr. “Pressure controlled ventilation for the long range aeromedical transport of patients with burns”, J Burn Care Rehabil 1997; 18:200-5
7. Reper P, Dankaert R, van Hille F, van Laeke P, Duinslaeger L, Vanderkelen A. “The usefulness of combined high frequency percussive ventilation during acute respiratory failure after smoke inhalation”, Burns 1998; 24:34-8
8. Crawford MR. “High frequency ventilation”, Anaesth Intensive Care 1986; 14: 281
9. Lunkenheimer PP, Keller H, Rafflenbeul W, Gref H, Dickhuth HH. “Application of transtracheal pressure oscillations as a modification of diffusion respiration”, Br J Anaesth 1972; 44:627
10. Heijman K, Heijman L, Jonzon A, Sedin G, Sjöstrand U, Widman B. “High frequency positive pressure ventilation during anaesthesia and routine surgery in man”, Acta Anaesth Scand 1972; 16:176-87
11. Bjerager K, Sjöstrand U, Wattwil M. “Long-term treatment of 2 patients with respiratory insufficiency with IPPV/PEEP and HFPV/PEEP”, Acta Anaesth Scand 1977; 64:55-68

12. Butler WJ, Bohn DJ, Bryan AC, Froese AB. “Ventilation by high frequency oscillation in humans”, Anaesth Analg 1980; 59:577-84
13. Schmid ER, Knopp TJ, Rehder K. “Intrapulmonary gas transport and perfusion during high frequency oscillation”, J Appl Physiol 1981; 51:1507-14
14. Chang HK. “Mechanisms of gas transport during ventilation by high frequency oscillation”, J Appl Physiol 1984; 56:553-63
15. Sykes MK. “High frequency ventilation” in Zorab JMS, “Lectures in anaesthesiology”, Oxford: Blackwell Scientific Publications, 1987:9-20
16. Standford TJ, Morganroth ML. “High frequency ventilation”, Chest 1989; 96:1380-9
17. Gerstmann DR, deLemos RA, Coalson JJ, Clark RH, Wiswell TE, Winter DC, Kuehl TJ, Meredith KS, Null DM Jr. “Influence of ventilatory technique on pulmonary baroinjury in baboons with hyaline membrane disease”, Pediatric Pulmonol 1988; 5:82-90
18. Froese AB. “High frequency ventilation: a critical assessment”, Crit Care:state of art 1984; 5:A3-51
19. Gioia FR. “ High frequency ventilation of the lungs” in Atkinson RS. "Recent advances in anaesthesia and analgesia”, London: Chirchill Livingstone; 1985: 62-78
20. Branson RD. “High frequency ventilators” in Branson et al, “Respiratory care equipment”, Philadelphia: Lippincott; 1995: 446-58
21. Product information. Percussionaire Corporation. Sandopoint, ID, USA,1997
22. Lucangelo U., Fontanesi L., Antonaglia V., Pellis T., Berlot G., Liquori G., Bird FM, Gullo A. “High Frequency Percussive Ventilation (HFPV) Principles and techinique” Minerva Anestesiol, 2003; 69:841-51
23. Lucangelo U. “High Frequency Percussive Ventilation” in Gullo, “Anaesthesia pain, intensive care and emergency medicine” APICE, Proceedings of the 15th postgraduate course in critical care medicine. Berlin: Springer – Verlag; 2001: 163-71
24. Pfenninger J, Minder C. Pressure-volume curves, static compliances and gas exchange in hyaline membrane disease during conventional mechanical and high-frequency ventilation. Intensive Care Med 1988; 14:364-72

25. Campbell PJ, Chilton HW, Garvey PA, Gupta JM. Volumetric diffusive respirator use in neonatal respiratory failure. J Paediatr Child Health 1991; 27:31-3
26. Soudon P. Mechanical ventilation by tracheostomy in neuromuscular disease: experience and evaluation. Eur Respir Rev 1993; 3:300-4
27. Hurst JM, Branson RD, DeHaven CB. The role of high-frequency ventilation in post-traumatic respiratory insufficiency. J Trauma 1987; 27:236-42
28. Natale JE, Pfeifle J, Homnick DN. Comparison of intrapulmonary percussive ventilation and chest physiotherapy. A pilot study in patients with cystic fibrosis. Chest 1994; 105:1789-93
29. Barrette RR, Hurst JM, Branson RD, Davis K Jr. A comparison of conventional mechanical hyperventilation with 2 forms of high frequency ventilation for the control of intracranial pressure in closed head injury. Respire Care 1987; 32:733-40
30. Hurst JM, Branson RD, Davis K Jr. High-frequency percussive ventilation in the management of elevated intracranial pressure. J Trauma 1988; 28:1363-7
31. Gallagher JT, Boysen PG, Davidson DD, Miller JR, Leven SB. High frequency percussive ventilation compared with mechanical ventilation. Crit Care Med 1989; 17:364-6
32. Allardet-Servent J, Bregeon F, Delpierre S, Steinberg JG, Payan MJ, Ravailhe S, Papazian L. High-frequency percussive ventilation attenuates lung injury in a rabbit model of gastric juice aspiration. Intensive Care Med 2008; 34:91-100
33. Lucangelo U, Zin WA, Antonaglia V, Gramaticopolo S, Maffessanti M, Liguori G, Cortale M, Gullo A. High-frequency percussive ventilation during surgical bronchial repair in a patient with one lung. Br J Anaesth 2006; 96:533-6
34. Lucangelo U, Antonaglia V, Zin WA, Confalonieri M, Borelli M, Columban M, Cassio S, Batticci I, Ferluga M, Cortale M, Berlot G. High-frequency percussive ventilation improves perioperatively clinical evolution in pulmonary resection. Crit Care Med 2009; 37:1663-9
35. Esan A, Hess DR, Raoof S, George L, Sessler CN. Severe hypoxemic respiratory failure: part 1--ventilatory strategies. Chest 2010; 137:1203-16
36. Lucangelo U, Zin WA, Fontanesi L, Antonaglia V, Peratoner A, Ferluga M, Marras E, Borelli M, Ciccolini M, Berlot G. “Early short-term application of high-

frequency percussive ventilation improves gas exchange in hypoxemic patients" Respiration 2012; 84:369-76

37. Mlcak R, Cortiella J, Desai M, Herndon D. "Lung compliance, airway resistance, and work of breathing in children after inhalation injury" J Burn Care Rehabil. 1997; 18(6):531-4
38. Lucangelo U, Antonaglia V, Zin WA, Fontanesi L, Peratoner A, Bird FM, Gullo A. "Effects of mechanical load on flow, volume and pressure delivered by high-frequency percussive ventilation" Respir Physiol Neurobiol. 2004; 142(1):81-91
39. Riscica F, Lucangelo U, Accardo A. "Development of an innovative instrument for the online characterization of high frequency percussive ventilators" Proceedings of the World Congress on Medical Physics and Biomedical Engineering, September 7-12, 2009, Munich, Germany. Berlin: Springer; 2009:480-3.
40. Shaw A, Gregory NL, Davis PD, Patel K. "Flow-volume integrator for respiratory studies" Med Biol Eng. 1976; 14(6):695-6
41. Dorkin HL, Lutchen KR, Jackson AC. "Human respiratory input impedance from 4 to 200 Hz: physiological and modeling considerations" J Appl Physiol. 1988; 64:823-31
42. Rossi A, Gottfried SB, Higgs BD, Zocchi L, Grassino A, Milic-Emili J. "Respiratory mechanics in mechanically ventilated patients with respiratory failure" J Appl Physiol. 1985; 58(6):1849-58
43. Bernasconi M, Ploysongsang Y, Gottfried SB, Milic-Emili J, Rossi A. "Respiratory compliance and resistance in mechanically ventilated patients with acute respiratory failure" Intensive Care Med. 1988; 14(5):547-53
44. Riscica F, Lucangelo U, Ferluga M, Accardo A. "In vitro measurements of respiratory mechanics during HFPV using a mechanical lung model" Physiological measurement. 2011; 32(6): 637-48
45. Kaczka DW, Barnas GM, Suki B, Lutchen KR. "Assessment of time-domain analyses for estimation of low-frequency respiratory mechanical properties and impedance spectra" Ann Biomed Eng. 1995; 23(2):135–51
46. Jackson EA, Coates AL, Gappa M, Stocks J. "In vitro assessment of infant pulmonary function equipment" Pediatr Pulmonol. 1995; 19:205–13

47. Hauschild M, Schmalisch G, Wauer RR. “Accuracy and reliability of commercial lung function diagnostic systems and respiratory monitors in newborn infants” Klin Padiatr. 1994; 206:167–74
48. Lucangelo U, Accardo A, Bernardi A, Ferluga M, Borelli M, Antonaglia V, Riscica F, Zin WA “Gas distribution in a two-compartment model ventilated in high-frequency percussive and pressure-controlled modes” Intensive Care Med. 2010; 36:2125–31
49. Bersten AD, Rutten AJ, Veding AE, Skowronski GA. “Additional work of breathing imposed by endotracheal tubes, breathing circuits, and intensive care ventilators” Crit Care Med. 1987; 17:671–7
50. Bolder PM, Healy TEJ, Bolder AR, Beatty PCW, Kay B. “The extra work of breathing through adult endotracheal tubes” Anesth Analg. 1986; 65:853–9
51. Rocco PRM, Zin WA. “Modelling the mechanical effects of tracheal tubes in normal subjects” Eur Respir J. 1995; 8:121–6
52. Conti G, De Blasi R A, Lappa A, Ferretti A, Antonelli M, Bufi M, Gasparetto A. “Evaluation of respiratory system resistance in mechanically ventilated patients: the role of the endotracheal tube” Intensive Care Med. 1994; 20:421–4
53. Zin WA, Pengelly LD, Milic-Emili J. “Active impedance of respiratory system in anesthetized cats” J Appl Physiol. 1982; 53:149–57
54. Rohrer F. “Der Stroemungswiderstand in den menschlichen atemwegen und der Einfluss der unregelmaessigen verzweigung des bronchialsystems auf den atmungsverlauf in verschiedenen lungenbezirken” Pfluegers Arch Gesamte Physiol. Menschen Tiere. 1915; 162:225–59
55. Rossi A, Gottfried S B, Higgs B D, Zocchi L, Grassino A, Milic-Emili J. “Respiratory mechanics in mechanically ventilated patients with respiratory failure” J Appl Physiol. 1985; 58:1849–58
56. Lorino AM, Beydon L, Mariette C, Dahan E, Lorino H. “A new correction technique for measuring respiratory impedance through endotracheal tube” Eur Respir J. 1996; 9:1079–86
57. Guttmann J, Eberhard L, Fabry B, Bertschmann W, Wolff G. “Continuous calculation of intratracheal pressure in tracheally intubated patients” Anesthesiology. 1993; 79:503–13

58. Jarreau PH, Louis B, Dassieu G, Desfrere L, Blanchard PW, Moriette G, Isabey D, Harf A. “Estimation of inspiratory pressure drop in neonatal and pediatric endotracheal tubes” J Appl Physiol. 1999; 87:36–46
59. Lofaso F, Louis B, Brochard L, Harf A, Isabey D. “Use of the Blasius resistance formula to estimate the effective diameter of endotracheal tubes” Am Rev Respir Dis. 1992; 146:974–9
60. Shumann S, Krappitz M, Moeller K, Hentschel R, Braun G, Guttmann J. “Pressure loss caused by pediatric endotracheal tubes during high frequency oscillation ventilation” Respir Physiol Neurobiol. 2008; 162:132–7
61. Ajčević M, Lucangelo U, Ferluga M, Zin WA, Accardo A. “In vitro estimation of pressure drop across tracheal tubes during high-frequency percussive ventilation” Physiological measurement. 2014; 35(2):177- 88.
62. Chang HK, Mortola JP. “Fluid dynamic factors in tracheal pressure measurement” J Appl Physiol. 1981; 51:218–25
63. Loring SH, Elliot EA, Drazen JM. “Kinetic energy loss and convective acceleration in respiratory resistance measurements” Lung. 1979; 156:33–42
64. Sullivan M, Paliotta J, Saklad M. “Endotracheal tube as a factor in measurement of respiratory mechanics” J Appl Physiol. 1976; 41:590–2
65. Gammon RB, Shin MS, Buchalter SE. “Pulmonary barotrauma in mechanical ventilation. Patterns and risk factors” Chest. 1992; 102:568–72
66. Khattree R, Naik DN. “Computational Methods in Biomedical Research” Boca Raton: Chapman and Hall. 2008
67. Rodarte JR, Rehder K. “Dynamics of respiration” in Macklem PT, Mead J, “Handbook of Physiology. The Respiratory System. Mechanics of Breathing”, Bethesda: The American Physiological Society, 1986:131–44
68. Guttmann J, Kessler V, Mols G, Hentschel R, Haberthuer C, Geiger K. “Continuous calculation of intratracheal pressure in the presence of pediatric endotracheal tubes” Crit Care Med. 2000; 28:1018–26
69. Peslin R, Fredberg JJ. “Oscillation mechanics of the respiratory system” in Macklem PT, J Mead J, “Handbook of Physiology. The Respiratory System. Mechanics of Breathing”, Bethesda: The American Physiological Society, 1986:145–78

70. De Campos T, et al. “Ventilation with lower tidal volumes as compared with traditional tidal volumes for acute lung injury and the acute respiratory distress syndrome. The Acute Respiratory Distress Syndrome Network.” N Engl J Med. 2000; 342(18):1301-8
71. Kunugiyama SK, Schulman CS. “High-frequency percussive ventilation using the VDR-4 ventilator: an effective strategy for patients with refractory hypoxemia” AACN Adv Crit Care. 2012; 23(4):370-80.
72. Correger E, Murias G, Chacon E, Estruga A, Sales B, Lopez-Aguilar J, Montanya J, Lucangelo U, Garcia-Esquirol O, Villagra A, Villar J, Kacmarek RM, Burgueño MJ, Blanch L. “Interpretation of ventilator curves in patients with acute respiratory failure” Med Intensiva. 2012; 36(4):294-306.
73. Albaiceta GM, Blanch L, Lucangelo U. “Static pressure-volume curves of the respiratory system: were they just a passing fad?” Curr Opin Crit Care. 2008; 14(1):80-6.
74. Deans KJ, Minneci PC, Cui X, Banks SM, Natanson C, Eichacker PQ. “Mechanical ventilation in ARDS: One size does not fit all*” Critical care medicine. 2005; 33(5):1141-1143.
75. Data provided to the Office of Human Research Protections from ARDSNetwork investigators from the ARMA trial for use at the June 9–11, 2003 consultants meeting. Available under the Freedom of Information Act. Requests should be sent to Public Health Service, Freedom of Information Office, Rm 17A46, 5600 Fishers Lane, Rockville, MD 20857
76. Gattinoni L, Caironi P, Carlesso E. “How to ventilate patients with acute lung injury and acute respiratory distress syndrome” Curr Opin Crit Care. 2005; 1:69–76
77. Marini JJ, Gattinoni L. “Ventilatory management of acute respiratory distress syndrome: A consensus of two” Crit Care Med. 2004; 1:250–255
78. Petrucci N, Iacovelli W. “Ventilation with smaller tidal volumes: A quantitative systematic review of randomized controlled trials” Anesth Analg 2004; 1:193–200
79. Tobin MJ. “Culmination of an era in research on the acute respiratory distress syndrome” N Engl J Med. 2000; 18:1360–1361
80. Ricard JD. “Are we really reducing tidal volume—And should we?” Am J Respir Crit Care Med. 2003; 10:1297–1298

Acknowledgements

I would like to thank all the people who accompanied, helped and supported me to achieve this goal and who smiled seeing a student with a white beard.

I apologize to those I forgot to mention.

Professor Agostino Accardo my tutor, who taught me to think like an engineer without forgetting to be a doctor.

Professor Walter Zin, my mentor, who encouraged me to continue even when "waves" seemed to be insurmountable.

My PhD colleague, Milos Ajcevic which has allowed me to enjoy the concept of interdisciplinarity for the first time.

Patients, physicians and nurses of the Intensive Care Unit that have allowed me to carry out this study.

And finally, to my family and especially to my beautiful daughter Livia, who is still patiently waiting that her daddy repairs a toy received a few years ago.